Université du Québec
Institut National de la Recherche Scientifique
Énergie Matériaux Télécommunications

Photonics-based real-time spectrogram analysis and processing of broadband waveforms

Par

Saikrishna Reddy Konatham

Thèse présentée pour l'obtention du grade de
doctorat, PhD
en Télécommunications

Jury d'évaluation

Examinateur externe	Prof. John Xiupu Zhang Concordia University, Montreal, Canada
Examinateur externe	Prof. Lam Anh Bui Central Queensland University, Melbourne, Australia
Examinateur interne	Prof. Tiago H. Falk INRS-EMT, Montreal, Canada
Directeur de recherche	Prof. José Azaña INRS-EMT, Montreal, Canada

Dedicated to my parents and teachers

Acknowledgments

I have been fortunate to work with several wonderful and unique individuals during my graduate studies at INRS, no wonder Quebec is one of the best place in the world to pursue photonics research. This dissertation is a direct result of their help and support in many ways.
First of all, I want to convey deepest gratitude to my supervisor, Prof. José Azaña for giving me opportunity to work with him, for his constant support and encouragement throughout my studies. He gave me lot of freedom and support in pursuing ideas and research, at the same time providing timely guidance whenever I tend to go off the track. Pursing graduate studies with Prof. Azaña as a supervisor is unique in many ways, he is as much a visionary as he is contemporary and the approach is as much theoretical as it is practical. I cherish working with him and the invaluable learning experience in the group.
I want to convey my special regards to Dr. Hugues Guillet de Chatellus whose ideas and work inspired me during the entire course of my studies and constitute a major part of this Thesis.

I thank my friend and mentor Dr. Reza Maram who guided me during the initial days in the lab, and gave me best advises. I thank Dr. Luis Romero Cortes, who inspired me with his work ethic and approach towards research. I am greatly indebted for his timely help in performing final and crucial experiments at COPL in Quebec city. He drove me all the way to Quebec city, along with lab equipment. I learn a lot working with him in the lab. I thank my friend Benjamin Crockett, who has been an invaluable support to me in the lab. I learnt a lot working with him, and we had great time working in the lab. I thank Prof. Sophie LaRochelle, Prof. Leslie Rusch and their group members at COPL, for giving access to their labs and hosting us at COPL. I would like to thank all the colleagues and close knit members at INRS-EMT with whom I directly interacted.

My sincere gratitude goes to the core committee for my Ph.D Thesis: Prof. John Xiupu Zhang, Concordia University, Montreal, Canada; Prof. Lam Anh Bui, Central Queensland University, Melbourne, Australia; and Prof. Tiago H. Falk, INRS-EMT, Montreal, Canada. Thank you for your time and efforts in reviewing my Thesis.

Coming from a sleepy village in a remote part of south India, all the way to other part of the globe to pursue PhD studies, would not have possible without the love, support and sacrifices of my parents, Biksham Reddy and Badramma. I am especially grateful to my uncle and aunt, Dr. Vidyasagar Reddy and Padmasagar Reddy who are my biggest support, and who made me feel home in the North American continent. I thank my friends and teachers in India who inspired me to pursue PhD.

Finally, I thank le Fonds Québécois de la Recherche sur la Nature et les Technologies (FQRNT), for providing the scholarship which allowed me to undertake this PhD research.

Résumé

La transformée de Fourier décompose un signal temporel en ses composantes spectrales de fréquence. En tant que telle, c'est une idée simple et pourtant élégante, et la pierre angulaire de l'analyse des signaux. Les spectres de fréquence de Fourier fournissent des informations indispensables à la caractérisation des signaux rencontrés dans une grande variété de domaines. Le calcul de la transformée de Fourier numérique est tellement omniprésent que son algorithme de calcul numérique, la transformée de Fourier rapide (TFR), est souvent considéré comme l'algorithme numérique le plus important pour la résolution de nombreux problèmes scientifiques et techniques. L'acquisition en temps réel du contenu spectral dynamique du monde physique est une exigence encore plus fondamentale et difficile. La transformée de Fourier à court terme (TFCT), en tant qu'outil d'analyse du signal, est le cheval de bataille de la représentation spectrale dynamique de Fourier. La représentation spectrale dynamique en temps réel ou l'analyse spectrale en temps réel (AS-TR) est un outil indispensable pour capturer les phénomènes transitoires rapides ou les événements fréquentiels rares ou de courte durée. Dans un tel scénario, les techniques d'analyse spectrale en temps réel doivent être capables de fonctionner de manière continue et sans interruption, sur toute la largeur de bande d'observation, afin de pouvoir capturer les spectres changeant dynamiquement.

Les formes d'onde de largeur GHz avec un contenu spectral dynamique se retrouvent dans tout le spectre électromagnétique, allant des micro-ondes au domaine optique, en passant par les ondes millimétriques et THz. Le AS-TR de ces formes d'onde à large bande et à grande vitesse, d'une durée de l'ordre de la nanoseconde ou de la sub-nanoseconde, sans interruption, est fondamental pour de nombreuses applications importantes, notamment les communications à large bande, les radars, la caractérisation ultra-rapide, la détection, la spectroscopie et la recherche en radioastronomie. Le AS-TR avec ces spécifications est un défi et dépasse les performances des instruments AS-TR basés sur la TFR numérique.

Dans cette Thèse, j'ai développé une architecture universelle de traitement du signal analogique qui est particulièrement adaptée à la AS-TR de formes d'onde temporelles à large bande et à grande vitesse, sans interruption. Le TFCT ou spectrogramme mappé dans le temps (SP-MT) proposé saisit le TFCT des signaux large bande entrants (par exemple, micro-ondes à optique) directement dans le domaine d'onde analogique temporel natif, fournissant un accès en temps réel au contenu spectral dynamique du signal large bande d'entrée, évitant complètement le besoin de convertisseurs analogique-numérique et d'algorithmes TFR intensifs en calcul. Le SP-MT comprend deux unités de traitement du signal de base, à savoir l'échantillonnage temporel et les unités de retard dispersif. Une mise en œuvre photonique du concept SP-MT a permis d'obtenir des performances AS-TR sans précédent pour des signaux micro-ondes d'une largeur de bande de GHz, répondant ainsi aux exigences critiques des applications mentionnées ci-dessus. L'architecture SP-MT proposée est universelle et peut être mise en œuvre dans d'autres domaines d'ondes. Plus important encore, l'approche SP-MT ouvre la voie à la mise en œuvre efficace en temps réel dans le domaine des

ondes analogiques de fonctionnalités de traitement du signal telles que l'analyse/synthèse temps-fréquence, le filtrage à fréquence variable dans le temps, la convolution/corrélation, le filtrage adapté, les banques de filtres, etc.

Mots-clés: transformée de Fourier à court terme (TFCT), Analyse spectrale en temps réel, Echantillonnage, Dispersion, Traitement du signal analogique.

Abstract

Fourier transform decomposes a temporal signal into its constituent frequency spectral components. As such it is a simple and yet elegant idea, and the cornerstone in signal analysis. The Fourier frequency spectra provide indispensable information in characterizing signals encountered in a wide variety of areas. The digital Fourier transform computation is so ubiquitous that, it's numerical computation algorithm, the fast Fourier transform (FFT) is often referred to as the most important numerical algorithm in solving many scientific and engineering problems. Real-time acquisition of dynamic spectral content from the physical world is even more fundamental and challenging requirement. The short-time Fourier transform (STFT), as a signal analysis tool, is the workhorse of dynamic Fourier spectral representation. Real-time dynamic spectral representation or the real-time spectral analysis (RT-SA) is an indispensable tool for capturing rapid transient phenomenon, or rare/short-lived frequency events. In such a scenario, the RT-SA techniques must be able to operate in a real-time continuous and gap-free fashion, over the entire bandwidth of observation, to be able capture the dynamically changing spectra.

GHz-bandwidth waveforms with dynamic spectral content are found across the electromagnetic spectrum, ranging from microwave to optical domain, including millimeter and THz waves. The continuous gap-free RT-SA of these high-speed broadband waveforms, with durations in the nanosecond/sub-nanosecond range, is fundamental to many important applications, including broadband communications, radar, ultra-fast characterization, sensing, spectroscopy, radio astronomy research. The RT-SA with these specifications is challenging, and beyond the performance of the state-of-the-art digital FFT based RT-SA instrumentation.

In this Thesis, I have developed a universal analog signal processing architecture that is particularly suitable for continuous gap-free RT-SA of high-speed broadband temporal waveforms. The proposed time-mapped STFT or time-mapped spectrogram (TM-SP), captures the STFT of the incoming broadband signals (e.g., microwave to optical) directly in native temporal analog wave domain, providing real-time access to the dynamic spectral content of the input broadband signal, completely avoiding the need for analog-to-digital converters and computationally intensive FFT algorithms. The TM-SP involves two basic signal processing units, namely temporal sampling and dispersive delay units. A photonic implementation of the TM-SP concept has enabled unprecedented RT-SA performance for GHz-bandwidth microwave signals, fulfilling critical requirements in the above mentioned applications. The proposed TM-SP architecture is universal, and can be implemented in other wave domains. Most importantly, the TM-SP approach paves the way for efficient real-time analog wave domain implementation of signal processing functionalities such as time-frequency analysis/synthesis, time-varying frequency filtering, convolution/correlation, matched filtering, filter-banks, etc.

Keywords: Short-time Fourier transform (STFT), Real-time spectral analysis, Sampling, Dispersion, Analog signal processing

Sommaire Récapitulatif

Un résumé de la thèse est présenté dans cette section. Je motive en présentant les objectifs majeurs de la Thèse, en fournissant une introduction à l'analyse spectrale de Fourier en temps réel et à ses défis d'implémentation actuels. Un nouveau schéma universel de traitement analogique est proposé pour surmonter les limitations des approches existantes de l'analyse spectrale de Fourier en temps réel. La description mathématique du schéma de traitement du signal proposé, appelé spectrogramme mappé dans le temps (SP-MT), est présentée et validée par des simulations numériques et des démonstrations expérimentales.

0.1 Introduction

Les techniques d'analyse spectrale en temps réel (AS-TR) sont largement utilisées pour l'analyse d'une grande variété de signaux rencontrés dans de nombreux problèmes scientifiques et d'ingénierie. Les techniques d'AS-TR sont des outils indispensables, notamment pour étudier les phénomènes transitoires rapides ou pour capturer les événements fréquentiels rares/à courte durée de vie lorsqu'ils se produisent dans le signal. À cette fin, l'analyse spectrale doit être effectuée en temps réel, en continu et sans interruption. Le terme "ininterrompu" signifie ici la capacité de mettre en œuvre l'analyse spectrale souhaitée sans temps d'arrêt dans l'acquisition et le traitement du signal d'intérêt. L'AS-TR est utile pour des signaux de nature très différentes, notamment les signaux audio [sr1], radiofréquence (RF) [sr2, sr3], et optique [sr4] etc.

Je m'intéresse principalement à l'analyse AS-TR de formes d'ondes temporelles à grande vitesse (c'est-à-dire à large bande) avec des largeurs de bande allant jusqu'à la gamme des GHz et au-delà. Les formes d'onde avec une largeur de bande se situe dans la gamme des GHz se retrouvent le plus souvent dans le spectre électromagnétique allant des micro-ondes aux fréquences optiques, en passant par les ondes millimétriques et les fréquences térahertz (THz). L'AS-TR des formes

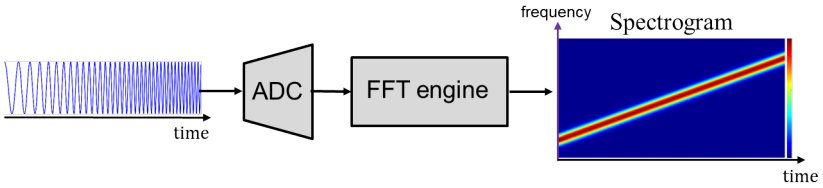

Fig. 1: Schéma d'un analyseur de spectre en temps réel (AS-TR) basé sur une approche numérique conventionnelle. Le signal temporel entrant est numérisé à l'aide d'un convertisseur analogique-numérique, puis le AS-TR est réalisé par le calcul en temps réel de la TFCT du signal à l'aide de transformées de Fourier rapides (TFR). Cela implique le calcul d'un grand nombre de TFR, généralement en temps réel et avec un fort chevauchement. ADC: analog to digital converter; FFT: Fast Fourier transform

d'onde temporelles à grande vitesse que l'on trouve dans ces domaines est fondamentale pour de nombreuses applications importantes, notamment la détection spectrale dans les communications à large bande [sr5, sr6]; l'alerte radar, la guerre électronique et les récepteurs de contre-mesures [sr7, sr8]; la caractérisation, la détection et la spectroscopie ultrarapides [sr9]; la recherche en radioastronomie [sr10, sr11], etc. Ces applications requièrent la capacité de réaliser des AS-TR sur des largeurs de bande instantanées bien au-delà de la gamme des GHz et, potentiellement, avec une résolution temporelle de seulement quelques nanosecondes ou même plus courte. De plus, ces applications exigent que l'analyse AS-TR soit effectuée en continu et sans interruption, sinon des informations critiques peuvent être perdues dans le processus d'analyse de la forme d'onde. L'approche conventionnelle de l'analyse et du traitement de Fourier de ces signaux implique l'échantillonnage et la numérisation de la forme d'onde analogique à l'aide d'un convertisseur analogique-numérique, suivis du calcul en temps réel de la transformée de Fourier à court terme (TFCT) ou du spectrogramme du signal d'intérêt dans le domaine numérique, comme le montre la Fig. 1. L'opération TFCT est effectuée en évaluant la transformée de Fourier discrète (TFD) du signal fenêtré temporellement, alors que la fenêtre est déplacée à travers le signal tout en assurant un chevauchement significatif entre les sections consécutives tronquées du signal [sr12]. Cela exige que le délai entre des fenêtres d'analyse temporelle consécutives soit beaucoup plus court que la durée de chacune de ces fenêtres. De plus, la durée temporelle de la fenêtre d'analyse détermine la résolution temporelle de la AS-TR. Le fenêtrage superposé est effectué pour garantir que l'analyse AS-TR est exempte de lacunes dans la résolution temporelle de l'analyse de Fourier dynamique effectuée. Le calcul numérique de la TFD est effectué à l'aide d'algorithmes de transformée de Fourier rapide (TFR) et, comme la TFD est appliquée à un signal fenêtré à fort chevauchement, un grand nombre d'opérations TFR rapides en temps réel sont nécessaires pour générer en temps réel la TFCT continue sans intervalle souhaitée. Les calculs de TFR sont effectués sur des moteurs de traitement

numérique du signal en temps réel [sr2, sr13] et la TFCT résultante est généralement affichée sous la forme d'une distribution temps-fréquence 2D.

Les approches AS-TR numériques sont confrontées à des contraintes fondamentales, par exemple en termes de compromis entre la vitesse de traitement et la consommation d'énergie [sr14, sr15]. Celles-ci deviennent particulièrement importantes lorsque la largeur de bande de fréquence de la forme d'onde analogique augmente juste au-dessus de quelques dizaines de MHz. À titre de référence, les instruments AS-TR basés sur le traitement des signaux numériques disponibles dans le commerce sont actuellement limités à des largeurs de bande de fréquence instantanées inférieures à quelques centaines de MHz, avec des résolutions temporelles de l'ordre de la microseconde, et à une vitesse de traitement maximale d'environ 2.6×10^6 TFR par seconde [sr16]. Ces limitations sont principalement associées aux contraintes de performance (vitesse) des engins de traitement des signaux numériques pour calculer la TFR de sections consécutives de la forme d'onde entrante numérisée en temps réel et de manière continue et sans interruption, c'est-à-dire sans aucune interruption dans la capture et le traitement du signal temporel entrant [sr13, sr15]. Les capacités des méthodes AS-TR disponibles basées sur les approches numériques sont donc insuffisantes pour atteindre les spécifications souhaitées dans une large gamme d'applications émergentes, comme indiqué ci-dessus, telles que la détection spectrale dans les systèmes de communication sans fil intelligents avancés [sr7], les radars et lidars à grande vitesse [sr6], les observations en radio-astronomie [sr10, sr11], l'imagerie biomédicale [sr17], etc. Ces applications requièrent la capacité d'effectuer une AS-TR continue et sans interstice sur des largeurs de bande instantanées bien au-delà de la gamme des GHz et, éventuellement, avec une résolution temporelle de quelques nanosecondes seulement, voire même plus courte.

Le développement du concept de transformée de Fourier en temps réel ou mappée dans le temps (TF-MT) [sr18, sr19] a représenté une étape fondamentale pour le calcul analogique en temps réel du spectre de Fourier des signaux du domaine temporel. Le TF-MT s'appuie sur la propagation des ondes dans un milieu dispersif de second ordre pour cartographier les informations spectrales de la forme d'onde entrante souhaitée dans le domaine temporel (voir Annexe B). Cependant, le concept TF-MT est limité uniquement à la mise en œuvre de la transformée de Fourier standard des formes d'onde pulsées limitées dans le temps [sr9, sr19]. En tant que telle, l'approche TF-MT ne convient pas à l'analyse AS-TR sans intervalle des signaux à large bande à haut débit. Des schémas alternatifs ont été démontrés pour le TF-MT de formes d'onde à large bande, par exemple, en incorporant

une modulation temporelle au signal analysé avant la dispersion [sr20, sr21], ou en exploitant les propriétés des boucles de rétroaction décalées en fréquence [sr22], mais seule l'analyse spectrale statique de formes d'onde tronquées dans le temps [sr20] ou de signaux strictement périodiques [sr22, sr23] a été rapportée par ces méthodes. Ainsi, la AS-TR continue et sans espace de formes d'onde arbitraires à large bande, avec des largeurs de bande de fréquence instantanée dépassant la gamme des GHz, reste très difficile. Aucune solution n'a été envisagée pour mettre en œuvre le puissant concept de cartographie fréquence-temps afin de permettre une analyse complète des spectres continus variant dans le temps.

0.2 Contributions originales

L'objectif principal de cette thèse est de concevoir, d'étudier et de démontrer expérimentalement une approche de traitement du signal analogique pour l'analyse spectrale en temps réel de formes d'onde à large bande, capable de fournir les spécifications de performance cibles suivantes :

- Bande passante instantanée en temps réel dans la gamme des GHz ou plus,
- Vitesses de traitement par transformée de Fourier dans la gamme des GHz,
- Résolutions temporelles de l'ordre de la nanoseconde,
- Analyse spectrale continue et sans interruption pour ne pas manquer d'événements rares.

Dans ce but, cette Thèse propose un nouveau schéma universel de traitement analogique qui permet de cartographier la TFCT complète d'un signal arbitraire entrant dans le domaine temporel. Ceci peut être interprété comme une extension du concept TF-TR mais pour une analyse et un traitement du signal temps-fréquence bidimensionnel complet. L'approche proposée implique un échantillonnage temporel du signal entrant suivi d'une quantité appropriée de dispersion chromatique de second ordre. Le principe exploite une interférence bien conçue entre des copies consécutivement échantillonnées et dispersées du signal d'entrée ; [AJ1]. Les principales contributions de ma thèse sont les suivantes :

- La proposition et étude théorique comprenant la dérivation de toutes les principales équations de conception d'un traitement de signal analogique universel pour l'analyse spectrale en temps

réel, basé sur un TFCT mappé dans le temps. Les conditions de conception de ce schéma pour effectuer une analyse TFCT mappée dans le temps du signal entrant seront dérivées et discutées dans cette Thèse.

- La validation numérique du concept proposé de TFCT mappé dans le temps et de ses principales spécifications et compromis de performance. L'analyse numérique de l'architecture de traitement du signal proposée est effectuée sur une implémentation photonique visant l'AS-TR de signaux micro-ondes à large bande.

- La démonstration expérimentale d'une TFCT à mappage temporelle basée sur la photonique pour l'AS-TR de signaux micro-ondes arbitraires à large bande, fournissant les spécifications de performance ciblées, telles que la bande passante instantanée et les vitesses de traitement dans la gamme des GHz, les résolutions temporelles dans la gamme des nanosecondes et le fonctionnement continu sans interruption.

- La proposition, évaluation théorique et démonstration expérimentale des capacités d'analyse et de traitement supplémentaires de la conception TFCT à mappage temporel, notamment les suivantes :

  – TFCT mappé dans le temps de formes d'onde optiques complexes (amplitude et phase).

  – Mise en œuvre photonique du concept de TFCT à échantillonnage passe-bande.

  – Filtrage à fréquence variable dans le temps de formes d'onde à large bande à l'aide de la TFCT mappée dans le temps.

0.3 Théorie du spectrogramme mappé dans le temps (SP-MT)

Comme l'illustre la Fig. 2, le concept proposé pour le SP-MT implique le traitement du signal entrant sous test, $s(t_1)e^{i\omega_0 t_1}$, avec une cascade de deux unités de traitement de signal standard, à savoir 1) une unité d'échantillonnage temporel, et 2) une unité de retardement temporel dépendant de la fréquence. Le signal temporel en bande de base testé, $s(t_1)$ est représenté sur l'axe horizontal, et son spectre, $S(\omega_1) = \mathrm{FT}(s(t_1))$ sur l'axe vertical, sur la Fig. 2. Ici, FT représente la transformée de Fourier. Le fonctionnement de chaque unité de traitement du signal sur le temporel du signal testé (SUT) entrant est décrit ci-dessous : Une unité d'échantillonnage temporel conventionnelle est utilisée pour moduler le SUT avec un train périodique d'impulsions courtes (voir Annexe A).

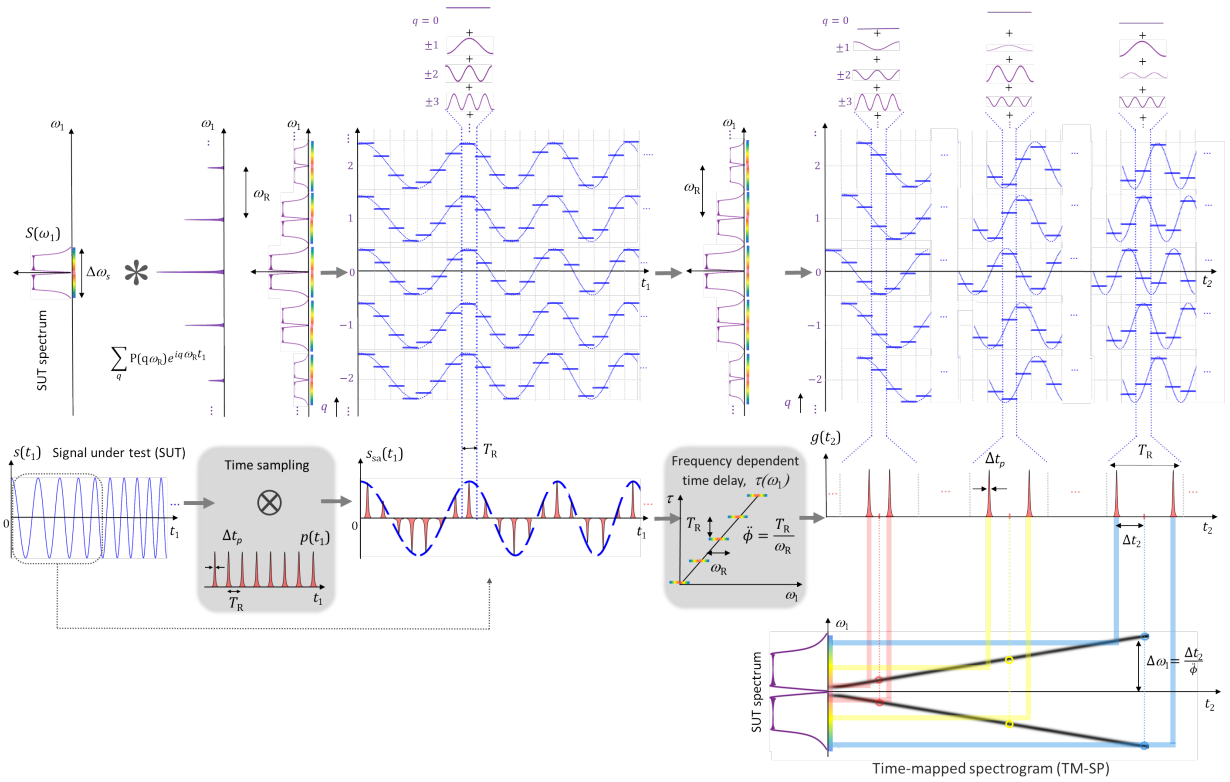

Fig. 2: Principe de base de la méthode SP-MT proposée. Le SP-MT implique un échantillonnage temporel du signal testé (SUT), $s(t_1)$, avec un train répétitif de courtes impulsions. L'échantillonnage temporel génère des copies décalées en fréquence du SUT d'entrée, tandis que chaque copie spectrale est décalée de $\omega_R = 2\pi/T_R$. L'unité de retard (dispersif) dépendant de la fréquence $\tau(\omega_1)$ introduit un retard relatif de T_R entre les copies spectrales décalées en fréquence (de ω_R). L'interférence entre les copies simultanément retardées et décalées en fréquence du SUT produit un modèle temporel $g(t_2)$ le long de chaque T_R, qui est proportionnel à la fenêtre temporelle FT du SUT, mettant en œuvre une cartographie temporelle continue de la TFCT ou SP complète du signal. Ici, le SUT est un signal à fréquence linéaire, d'où le FT fenêtré dans le temps composé de deux impulsions de durée finie, correspondant au spectre bilatéral d'une fonction sinusoïdale à fréquence unique, dans chaque période d'analyse de durée T_R. Comme la fréquence de la fonction sinusoïdale augmente dans le temps, le FT fenêtré change de période en période.

La Fig. 2 montre le train d'impulsions d'échantillonnage à l'intérieur de l'unité d'échantillonnage temporel. Le signal échantillonné à la sortie de cette unité peut être mathématiquement exprimé comme suit :

$$s_{sa}(t_1) = s(t_1)\sum_m p(t_1 - mT_R) \propto s(t_1)\sum_q P(q\omega_R)e^{iq\omega_R t_1} = \sum_q P(q\omega_R)s(t_1)e^{iq\omega_R t_1}, \qquad (1)$$

où $p(t_1)$ définit la forme temporelle de chaque impulsion individuelle dans la séquence d'échantillonnage, et T_R représente la période de répétition, c'est-à-dire que la fréquence de répétition de l'échantillonnage est $\omega_R = 2\pi/T_R$. où $\propto$ représente la proportionnalité, et $m, q = 0, \pm1, \pm2, ...$ Pour calculer cette équation, nous avons utilisé la représentation en série de Fourier d'un train d'impulsions d'échantillonnage périodique [sr24], où $P(\omega_1)$ est le spectre de fréquence du train d'impulsions

d'échantillonnage individuel, c'est-à-dire $P(\omega_1) = \mathrm{FT}(P(\omega_1))$. L'étendue spectrale de pleine largeur de $P(\omega_1)$ est $\sim \Delta\omega_p$. L'unité d'échantillonnage crée des copies spectrales du signal d'entrée qui sont décalées en fréquence de $q\omega_\mathrm{R}$, et pondérées par le coefficient de Fourier de l'impulsion d'échantillonnage correspondante $P(q\omega_\mathrm{R})$, comme le montre le tracé temps-fréquence 2D de la Fig. 2. Le critère de Nyquist garantit que chacune de ces copies du signal s'étend sur une largeur de bande de fréquence plus étroite que ω_R, évitant ainsi leur chevauchement spectral.

Le processus d'échantillonnage est suivi d'une unité dispersive qui cause un délai temporel dépendant de la fréquence tel qu'illustrée sur la Fig. 2. La forme d'onde temporelle à la sortie de l'unité de retard de dispersion peut alors être exprimée par $g(t_2)e^{i\omega_0 t_2}$, où $t_2 = t_1 - \Delta t_L$, et Δt_L est la latence du système. L'enveloppe complexe temporelle résultante de la forme d'onde de sortie est alors la suivante

$$\begin{aligned} g_2(t_2) &\propto \sum_q P(q\omega_\mathrm{R}) s(t_2 - q\Delta\tau) e^{iq\omega_\mathrm{R}(t_2 - q\Delta\tau)} \\ &= \sum_q P(q\omega_\mathrm{R}) s(t_2 - q\Delta\tau) e^{iq\omega_\mathrm{R} t_2} e^{(-iq^2\omega_\mathrm{R}\Delta\tau)}. \end{aligned} \tag{2}$$

L'équation ci-dessus 2 montre que la forme d'onde de sortie, $g(t_2)$ consiste en l'addition cohérente d'un ensemble de copies du SUT d'entrée qui sont simultanément décalées dans le temps (avec un retard relatif entre les copies consécutives de $\Delta\tau$) et en fréquence (avec un espacement de fréquence relatif entre les copies consécutives de ω_R), tout en étant pondéré en fonction du spectre de fréquence des impulsions d'échantillonnage, comme illustré sur la figure 2.

Lorsque le délai relatif entre les copies spectrales consécutives du SUT est égal à la période d'échantillonnage, c'est-à-dire $\Delta\tau = T_\mathrm{R}$, la pente du processus de retard dispersif (paramètre de dispersion) est alors la suivante

$$\mid \ddot{\phi} \mid = \frac{\Delta\tau}{\omega_\mathrm{R}} = \frac{{T_\mathrm{R}}^2}{2\pi} \tag{3}$$

Il est pratique d'évaluer l'Eq. 2 sur chacune des tranches de temps consécutives définies par $nT_\mathrm{R} - \frac{T_\mathrm{R}}{2} \leq t_2 < nT_\mathrm{R} + \frac{T_\mathrm{R}}{2}$, avec $n = 0, \pm1, \pm2, ...$ Dans le n itmè créneau temporel, la fonction $s(t_2)$ peut être approximée par $s(nT_\mathrm{R})$. La forme d'onde temporelle à la sortie de l'unité de retard dispersif le long du n itmè créneau temporel, $g_n(t_2 - nT_\mathrm{R})$, peut alors être exprimée comme suit :

$$g_n(t') \propto \sum_q P(q\omega_\mathrm{R}) s(nT_\mathrm{R} - qT_\mathrm{R}) e^{iq\omega_\mathrm{R} t'} = e^{in\omega_\mathrm{R} t'} \sum_{q'} P([n - q']\frac{T_\mathrm{R}}{\ddot{\phi}}) s(q'T_\mathrm{R}) e^{(i\omega_1 q' T_\mathrm{R})}, \tag{4}$$

où $t' = t_2 - nT_\mathrm{R}, q' = n - q$, et $\omega_1 = t'/\ddot{\phi}$. En définissant la "fonction de fenêtre temporelle" comme suit

$$h(t) = P(\omega_1 = -t'/\ddot{\phi}), \tag{5}$$

alors l'équation 4 peut être exprimée comme suit

$$g_n(t') \propto e^{in\omega_\mathrm{R}t'} \sum_{q'} h(q'T_\mathrm{R} - nT_\mathrm{R}) s(q'T_\mathrm{R}) e^{i\omega_1 q' T_\mathrm{R}}. \tag{6}$$

La somme dans l'Eq. 6 peut être interprétée comme la version discrétisée de la forme intégrale en temps continu correspondante, échantillonnée à $t_1 \leq t'T_\mathrm{R}$. En particulier, dans le créneau temporel d'analyse défini ($-T_\mathrm{R}/2 \leq t' \leq T_\mathrm{R}/2$), l'expression de l'équation 6 est alors équivalente à :

$$g_n(t') \propto \int_{-\infty}^{\infty} h(t_1 - nT_\mathrm{R}) s(t_1) e^{-i\omega_1 t_1}, \tag{7}$$

où, nous rappelons que $\omega_1 = t'/\ddot{\phi}$. Enfin, l'Eq. 7 implique une transformée de Fourier (FT), elle peut donc être réécrite comme suit :

$$g_n(t_2) \propto e^{in\omega_\mathrm{R}t_2} \times \mathrm{FT}(h(t_1 - nT_\mathrm{R}) s(t_1))_{\omega_1 = \frac{t_2 - nT_\mathrm{R}}{\ddot{\phi}}} = e^{in\omega_\mathrm{R}t_2} \times \mathrm{STFT}_s(nT_\mathrm{R}, \omega_1 = \frac{t_2 - nT_\mathrm{R}}{\ddot{\phi}}), \tag{8}$$

où nous avons utilisé la définition de la transformée de Fourier à court terme : [sr12] Le résultat de l'équation 8 montre qu'à l'exception d'un terme de phase linéaire supplémentaire $e^{in\omega_\mathrm{R}t_2}$, la forme d'onde temporelle à la sortie du système proposé, $g_n(t_2)$, lorsqu'elle est évaluée à chaque intervalle de temps $nT_\mathrm{R} - \frac{T_\mathrm{R}}{2} \leq t_2 < nT_\mathrm{R} + \frac{T_\mathrm{R}}{2}$, est proportionnelle à la transformée de Fourier à court terme de la forme d'onde analysée, $s(t_1)$, à savoir la FT d'une version fenêtrée dans le temps du SUT, avec la l'emplacement central de la fenêtre d'analyse temporelle, $h(t_1)$, s'étendant comme nT_R, avec $n = 0, \pm1, \pm2, ..., \pm\infty$. Ainsi, le long de la n itmè tranche de période d'échantillonnage, l'intensité de la forme d'onde temporelle de sortie est proportionnelle à une distribution SP ou temps-fréquence complète du SUT, c'est-à-dire $|g_n(t_2)|^2 \propto SP_s(nT_\mathrm{R}, \omega_1 = \frac{t_2 - nT_\mathrm{R}}{\ddot{\phi}})$. De cette manière, l'ensemble du spectre dynamique de l'objet testé est mis en correspondance avec le domaine temporel de sortie au cours de chaque période d'échantillonnage, nT_R, comme illustré au bas de la forme d'onde temporelle de sortie de la figure 2. Ici, le facteur de correspondance fréquence-temps dans le processus décrit ($\Delta\omega_1 \rightarrow \Delta t_2$) est défini par la pente du processus de retard dispersif, c'est-à-dire, $\Delta t_2/\Delta\omega_1 = \ddot{\phi} = T_\mathrm{R}/2\pi$.

Les résolutions temporelle et fréquentielle de l'approche TM-SP sont respectivement déterminées par la durée et la largeur de bande de fréquence de la fonction de fenêtre virtuelle, $h(t)$, dans le calcul STFT implémenté [sr12]. Comme défini dans l'équation 5, la fonction fenêtre $h(t)$ est proportionnelle au FT de l'impulsion d'échantillonnage, mise à l'échelle dans le domaine temporel par le facteur de dispersion $\ddot{\phi}$. Les résolutions temporelle et fréquentielle de la SP-MT sont alors estimées comme suit:

$$\text{Résolution temporelle: } \delta t_r \approx \delta t_h \approx |\ddot{\phi}| \times \Delta\omega_p \tag{9a}$$

$$\text{Résolution spectrale: } \delta\omega_r \approx \Delta t_p/|\ddot{\phi}| \tag{9b}$$

où, $\Delta\omega_p$ est la largeur totale à mi-hauteur (FWHM) du spectre de fréquence de l'impulsion d'échantillonnage individuelle, $P(\omega_1)$, et Δt_p est la FWHM de l'impulsion d'échantillonnage temporel, $p(t)$. En dérivant ces équations, nous avons également supposé qu'en première approximation, $\Delta t_p \approx 2\pi/\Delta\omega_p$. Les estimations de l'équation 9 indiquent que la résolution du spectre mappé dans le temps est directement déterminée par la largeur temporelle, Δt_p, des impulsions utilisées dans le processus d'échantillonnage. Par conséquent, chaque spectre de Fourier fenêtré (cartographié le long d'une durée T_R) est résolu dans le temps avec un nombre total de caractéristiques (ou points) donné par le rapport entre la période d'échantillonnage et la largeur d'impulsion, $M \approx T_\mathrm{R}/\Delta t_p$. En outre, si le SP-MT de sortie est capturé avec une largeur de temps accrue de $\Delta t_d > \Delta t_p$ en raison d'une largeur de bande de détection limitée, la résolution en fréquence du SP détecté sera réduite à $\delta\omega_{r,d} \approx \Delta t_d/|\ddot{\phi}|$. Néanmoins, il est important de mentionner que la résolution temporelle du SP obtenu ne dépend que des caractéristiques du spectre de l'impulsion d'échantillonnage telles qu'elles sont cartographiées dans le domaine temporel, selon l'estimation de l'équation 9(a), et qu'elle n'est donc pas affectée par la résolution du détecteur.

En introduisant la condition de dispersion principale, Eq. 3, dans l'expression de la résolution temporelle de l'équation 9(a), nous obtenons ce qui suit :

$$\delta t_r \approx \ddot{\phi} \times \Delta\omega_p = \frac{{T_\mathrm{R}}^2}{2\pi}\Delta\omega_p \approx \frac{T_\mathrm{R}}{\Delta t_p}T_\mathrm{R} \approx M \times T_\mathrm{R} \tag{10}$$

Cette dernière équation implique que la résolution temporelle de la SP-MT réalisée est environ M fois plus longue que la période d'échantillonnage, T_R. Cela implique que le même profil spectral devrait être capturé sur un nombre M de périodes consécutives le long de la forme d'onde temporelle

de sortie. La fenêtre temporelle utilisée pour le SP-MT (de durée δt_r) est généralement beaucoup plus longue que le décalage temporel entre les fenêtres d'analyse consécutives (T_{R}). Cela implique qu'il y a un chevauchement important des fenêtres d'analyse temporelles consécutives dans le calcul du SP-MT, ce qui garantit que l'AS-TR réalisé est exempt de lacunes, sans temps morts dans l'acquisition ou le calcul du FT. De plus, comme le spectre fenêtré et mappé dans le temps reste approximativement le même (c'est-à-dire qu'il se répète) sur un nombre M de périodes de représentation, il y a un sur-échantillonnage efficace de l'information SP-MT. Cette dernière caractéristique peut être exploitée pour assouplir les spécifications, par exemple la fréquence d'échantillonnage, de l'étape de détection visant à capturer la distribution temps-fréquence obtenue.

0.4 Simulations numériques d'un spectrogramme à mappage temporel basé sur la photonique

Un schéma pratique de SP-MT basé sur la photonique pour la AS-TR de formes d'onde à large bande est simulé numériquement. Les propriétés importantes du SP-MT, telles que les résolutions temporelle et fréquentielle, le fonctionnement continu sans espace, les fonctions de suréchantillonnage, sont toutes vérifiées par des simulations numériques.

La Fig. 3 illustre un schéma SP-MT basé sur la photonique pour le AS-TR de formes d'onde à large bande. Le signal entrant sous test (SUT) est modulé sur un train d'impulsions optiques picosecondes (avec une largeur temporelle FWHM d'amplitude de $\Delta t_p \sim 2$ ps et une fréquence de répétition de 10 GHz ou $T_{\mathrm{R}} = 100$ ps), en utilisant un modulateur Mach-Zehnder (MZM) électro-optique [sr4]. Le train d'impulsions optiques modulées par le MZM est ensuite propagé à travers une dispersion optique de second ordre [sr25]. La fibre optique dispersive introduit la quantité de dispersion requise par la condition de conception principale de l'équation suivante 3, $\ddot{\phi} = \frac{T_{\mathrm{R}}}{\omega_{\mathrm{R}}} = \frac{{T_{\mathrm{R}}}^2}{2\pi} = 10^4/2\pi$ ps^2/rad, sur toute la bande de fréquence des impulsions d'échantillonnage.

La Fig. 4(a) montre l'objet sous test hyperfréquence d'une durée de 50 ns, qui est composé d'une fréquence sinusoïdale croissante linéaire, avec une fréquence augmentant de 500 MHz à 4.5 GHz, et d'évènements isolées d'amplitude égale à celle de la composante de fréquence chirp, mais avec un contenu de fréquence et des durées temporelles variables, comme indiqué sur la Fig. 4(a). L'amplitude moyenne de la forme d'onde temporelle à la sortie du système SP-MT (c'est-à-dire la magnitude de la forme d'onde temporelle complexe de sortie), s'étendant également sur une durée

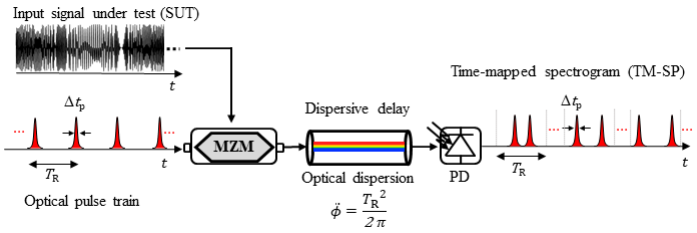

Fig. 3: Configuration de simulation pour l'analyse SP-MT des signaux micro-ondes à large bande basée sur la photonique. Le SUT hyperfréquence est modulé sur des impulsions optiques courtes en utilisant le MZM. Le SUT échantillonné est propagé à travers une ligne dispersive. La conversion optique-électrique est effectuée dans un photodétecteur de largeur de bande suffisante, de sorte que la largeur de l'impulsion de sortie est la même que celle des impulsions d'échantillonnage. MZM : modulateur Mach-Zehnder ; PD : photodétecteur.

totale de 50 ns, est illustrée à la Fig. 4(b). La Fig. 4(b) présente également un zoom sur différentes périodes d'analyse (chacune d'une durée de T_{R}) à des emplacements d'interférence spécifiques le long de la forme d'onde temporelle de sortie. Chaque période temporelle (T_{R}) est mise en correspondance avec l'axe de fréquence correspondant selon la loi de mise en correspondance fréquence-temps définie dans la Fig. 2, $\frac{\Delta t_2}{\Delta \omega_1} = \ddot{\phi}$.

La cartographie temporelle identifie clairement les composantes de fréquence de l'objet sous test, à savoir le terme d'oscillation de fréquence à augmentation linéaire (désigné par $\boldsymbol{c}$) et les interférences de fréquence isolées (désignées par $\boldsymbol{i}$) aux emplacements temporels prévus, à l'exception du terme d'interférence d'une durée de 100 ps centré à 2,5 GHz qui se produit à l'emplacement temporel de 45 ns (par rapport au début de la forme d'onde d'oscillation, $t = 0$). Ceci est prévu parce que la durée de 100 ps est à la limite de la période d'échantillonnage de Nyquist $T_{\mathrm{R}} = 100$ ps, de sorte que le processus d'échantillonnage ne peut pas capturer cet événement d'interférence. La détection des autres événements d'interférences est finalement limitée par la résolution temporelle de l'analyse SP-MT effectuée. Rappelons que les résolutions temporelles et fréquentielles (largeurs FWHM d'amplitude) peuvent être estimées à partir de l'équation 9 comme suit: résolution temporelle, $\delta t_r \sim 4.4$ ns, et résolution fréquentielle, $\delta \omega_r \sim 2\pi \times 200$ MHz, avec une fenêtre d'analyse temporelle de forme gaussienne $h(t)$. La Fig. 4(c) montre les distributions T-F récupérées correspondant à la composante linéaire de fréquence-chirp et aux interférences de fréquence du SUT aux emplacements de temps et de fréquence prescrits, validant ainsi le principe de fonctionnement théorique principal du SP-MT. Le spectre dynamique FT des signaux de largeur de bande GHz est calculé toutes les 100 ps, c'est-à-dire à une vitesse de 10×10^9 FT par seconde, avec une résolution temporelle de $\delta t_r \sim 4.4$ ns.

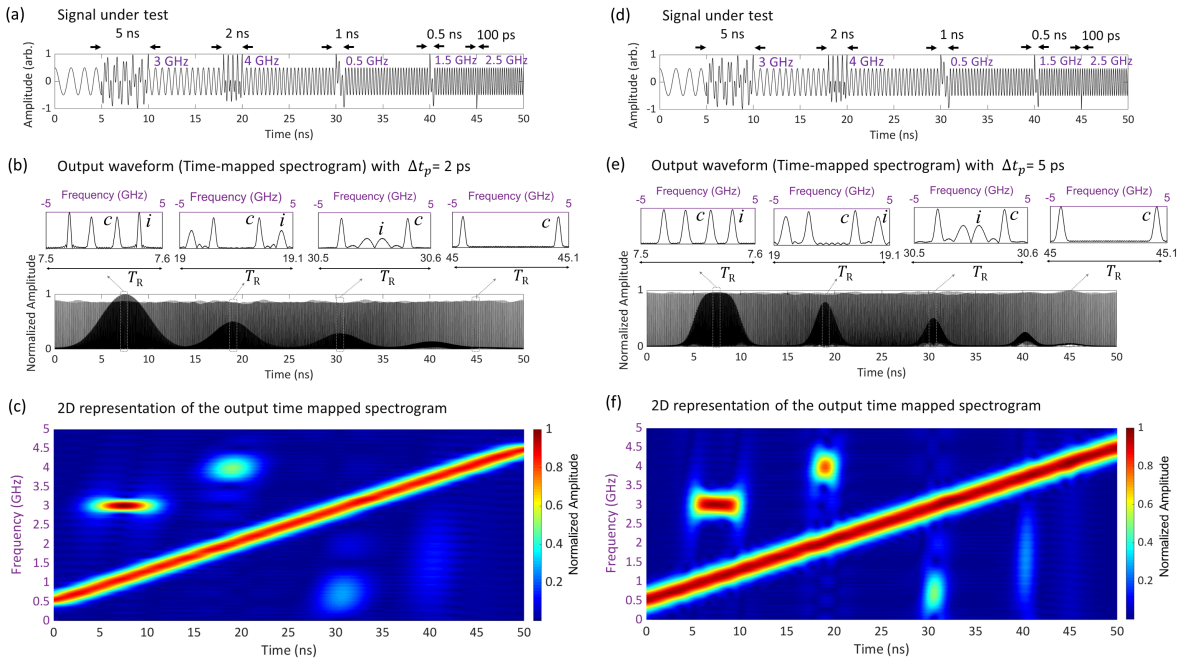

Fig. 4: Résultats de la simulation numérique d'un schéma SP-MT basé sur la photonique pour l'AS-TR de signaux micro-ondes à largeur de bande de GHz. (a) Trace temporelle d'un signal sous test (SUT), avec la largeur d'impulsion d'échantillonnage, $\Delta t_p = 2$ ps. (b) Amplitude moyenne de la forme d'onde temporelle à la sortie du système TM-SP. (c) Représentation 2D de la distribution d'énergie T-F conjointe du signal (SP) qui est récupérée à partir de la trace temporelle de sortie. (d) Trace temporelle du SUT à l'entrée du système SP-MT lorsque la largeur de l'impulsion d'échantillonnage, $\Delta t_p = 5$ ps. (e) Amplitude moyenne de la forme d'onde temporelle de sortie lorsque la largeur d'impulsion d'échantillonnage est augmentée à $\Delta t_p = 5$ ps. (f) Représentation en 2D de la distribution d'énergie T-F conjointe du signal (SP) qui est récupérée à partir de la trace temporelle de sortie représentée en (e).

0.4.1 Résolutions en temps et en fréquence et capacité de détection des interférences

Les résolutions temporelle et fréquentielle peuvent être personnalisées à volonté en ajustant simplement la largeur temporelle (ou fréquentielle) des impulsions d'échantillonnage. Par exemple, ceci peut être facilement réalisé en réglant la largeur de bande de fréquence d'un filtre linéaire passe-bande appliqué aux impulsions d'échantillonnages [sr4]. La Fig. 4(d) montre le même SUT d'entrée que celui présenté ci-dessus, maintenant échantillonné avec les impulsions d'échantillonnages ayant une largeur de temps FWHM accrue, $\Delta t_p = 5$ ps. La Fig. 4(e) montre l'amplitude moyenne de la forme d'onde temporelle de sortie lorsque la largeur de temps FWHM des impulsions d'échantillonnage est augmentée à $\Delta t_p = 5$ ps, pour le même SUT. Un zoom sur différentes périodes d'analyse (chacune d'une durée de T_{R}), autour de différents emplacements d'interférence, montre les spectres mappés dans le temps respectifs. Les résolutions modifiées (largeurs FWHM d'amplitude) estimées à partir de l'équation 9 sont : résolution temporelle $\delta t_r = 1.7$ ns, et résolution fréquentielle correspondante,

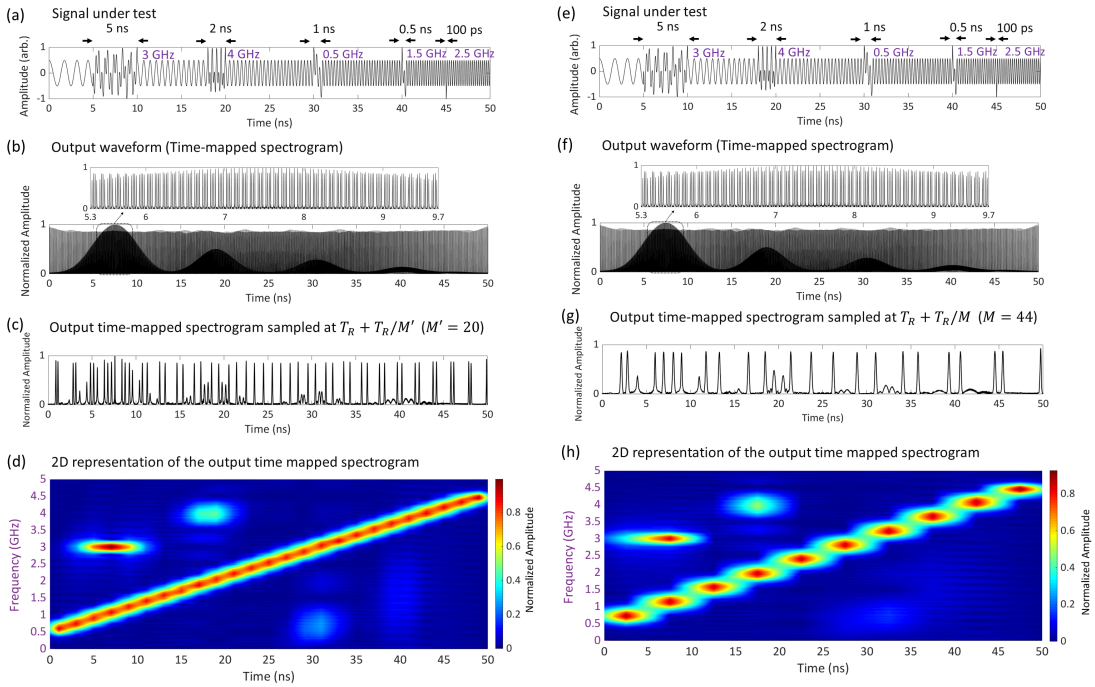

Fig. 5: Résultats de simulation numérique montrant la stratégie proposée pour assouplir le taux d'échantillonnage de détection en utilisant les caractéristiques de suréchantillonnage dans la méthode SP-MT. (a) Trace temporelle du SUT d'entrée (b) Forme d'onde temporelle de sortie (avec une largeur d'impulsion d'échantillonnage de $\Delta t_p = 2$ ps). L'encart montre la même forme d'onde sur une durée temporelle égale à $M = 44$ périodes d'analyse (durée totale de 4.4 ns). (c) La forme d'onde de sortie lorsqu'elle est échantillonnée à un taux réduit de 9.52 GHz, correspondant à une période d'échantillonnage de $T_{\mathrm{R}} + T_{\mathrm{R}}/20$. (d) Représentation 2D du SP qui est récupéré à partir de la sortie en (c). (e) SUT d'entrée temporel. (f) La forme d'onde de sortie (avec une largeur d'impulsion d'échantillonnage de $\Delta t_p = 2$ ps). (g) La forme d'onde de sortie lorsqu'elle est échantillonnée à un taux réduit de 9.77 GHz, correspondant à une période d'échantillonnage de $T_{\mathrm{R}} + T_{\mathrm{R}}/44$. (h) Représentation 2D du SP qui est récupéré à partir de la trace temporelle de sortie en (e).

$\delta\omega_r = 2\pi \times 500$ MHz. La Fig. 4(f) montre la représentation 2D de la distribution d'énergie T-F conjointe du signal (SP) qui est récupérée à partir de la trace temporelle de sortie. Cette analyse confirme que la durée réduite de la fenêtre d'analyse temporelle permet de mieux intercepter les interférences plus courtes (c'est-à-dire avec une valeur d'amplitude accrue, par rapport au cas de résolution de 4,4 ns), mais avec la détérioration connexe attendue de la résolution en fréquence. Le changement de l'amplitude relative des interférences capturées peut être clairement observé en comparant la Fig. 4(c) et la Fig. 4(f), en raison de la résolution temporelle améliorée dans le dernier cas.

0.4.2 Fonctionnement sans discontinuité et taux d'échantillonnage de détection réduit de la SP-MT

Comme indiqué dans l'équation 10, le FT fenêtré dans le temps reste approximativement le même (c'est-à-dire qu'il se répète) sur un nombre M ($M \approx 44$ dans cet exemple) de périodes d'analyse de la PS calculée (chaque période d'analyse ayant une durée T_{R}). Cette caractéristique permet de garantir que le FT fenêtré dans le temps est calculé de manière hautement chevauchée, sans qu'il ne manque aucun intervalle dans l'analyse effectuée, ce qui garantit un fonctionnement continu sans intervalle.

Cette fonctionnalité est confirmée par l'exemple de simulation présenté à la Fig. 5. L'objet sous test d'entrée et les paramètres d'analyse sont les mêmes que ceux utilisés dans les Fig. 4(a)-(c). La section zoomée de la forme d'onde temporelle de sortie dans l'encart de la Fig. 5(b) montre les spectres mappés dans le temps sur une durée égale à $M = 44$ périodes d'analyse (durée totale de 4,4 ns). Alors que le signal de Fréqunce linéaire est répété sur $M = 44$ périodes d'analyse dans les spectres mappés, sans être affecté par la forme de la fenêtre d'analyse temporelle $h(t)$, la composante d'interférence d'une durée de 5 ns est cependant relativement pondérée par la forme de la fenêtre d'analyse. La Fig. 5(b) montre clairement que la fenêtre temporelle, $h(t)$ est beaucoup plus longue que le décalage temporel entre les fenêtres d'analyse consécutives (T_{R}), cartographiant le FT dynamique du SUT sans manquer aucun intervalle entre les calculs TM-SP consécutifs. Cette caractéristique permet de garantir que la RT-SA réalisée est exempte de lacunes. Ces caractéristiques répétitives dans le calcul du FT peuvent être interprétées comme un suréchantillonnage de l'information récupérée, qui peut à son tour être exploité dans la détection ou le traitement de la distribution de PS obtenue.

L'une de ces stratégies consiste à tirer parti de ces caractéristiques répétitives pour assouplir les exigences en matière de taux d'échantillonnage de la détection: [AJ2]. Les exigences en matière de taux d'échantillonnage de détection peuvent être considérablement assouplies en tirant parti des caractéristiques répétitives dans le SP-MT de sortie. Par exemple, dans la Fig. 5(c), le SP-MT de sortie est échantillonné avec une période de $T_{\mathrm{R}} + T_{\mathrm{R}}/M'$, où $M' \leq M$ (c'est-à-dire, à une fréquence d'échantillonnage légèrement inférieure à la largeur de bande de Nyquist de l'objet sous test), de sorte que M' échantillons distincts sont capturés sur la durée de $M' \times T_{\mathrm{R}}$ ($\leq \delta t_r = 4.4$ ns), comprenant l'information SP complète. La Fig. 5(c) présente les résultats, lorsque le SP mappé dans le temps de sortie est échantillonné avec $T_{\mathrm{R}} + T_{\mathrm{R}}/M'$, où $M' = 20$ et $M' \leq M$. Elle montre les

interférences et la composante Fréqunce linéaire du SP-MT sous-échantillonné. La Fig. 5(d) montre le SP récupéré, mettant clairement en correspondance les composantes de fréquence attendues du SUT avec la résolution temps-fréquence prédite. Le SP-MT sous-échantillonné de la Fig. 5(d) permet toujours de capturer des événements rapides dont la durée est même inférieure d'un ordre de grandeur à la résolution temporelle de l'analyse SP (jusqu'à $\sim$ 500 ps contre une résolution temporelle de 5 ns). Enfin, la figure 5(f) montre la sortie SP-MT pour $M' = 44$ (c'est-à-dire à une fréquence d'échantillonnage de 9,77 GHz, légèrement inférieure à la largeur de bande de Nyquist du SUT), de sorte que 44 échantillons distincts sont capturés sur la durée d'une résolution temporelle, comprenant les informations SP complètes.

Ces résultats de simulation montrent que la mise en œuvre de la SP-MT basée sur la photonique est adaptée à l'AS-TR de formes d'onde à large bande, et capable de fournir les spécifications de performance visées. Les propriétés importantes du SP-MT, telles que les résolutions temporelle et fréquentielle, le fonctionnement continu sans espace, les fonctions de suréchantillonnage, sont toutes vérifiées par ces simulations numériques.

0.5 Évaluation expérimentale d'un spectrogramme temporel basé sur la photonique

Cette section présente les résultats de la démonstration expérimentale d'un SP-MT basé sur la photonique pour l'analyse spectrale en temps réel (AS-TR) de signaux micro-ondes arbitraires à large bande. Les expériences visent à atteindre les spécifications de performance ciblées [AJ1], telles qu'une bande passante instantanée et des vitesses de traitement de GHz ou plus, des résolutions temporelles de l'ordre de la nanoseconde ou plus courtes, et un fonctionnement continu et sans interruption.

Le montage expérimental de la SP-MT à base de photonique pour l'AS-TR de signaux micro-ondes arbitraires à large bande est illustré à la figure 6. Les signaux micro-ondes testés (SUT) définis par l'utilisateur et utilisés pour tester le SP-MT à base de photonique sont tous générés par un générateur électronique de formes d'onde arbitraires et modulés par des impulsions d'échantillonnages optiques générées par un laser à verrouillage de mode. Les impulsions optiques ont une forme temporelle gaussienne avec une largeur temporelle FWHM d'intensité de $\Delta t_p \approx 7$ ps (largeur de bande de fréquence FWHM limitée par transformation correspondante $\Delta\omega_p \approx 2\pi \times 60$ GHz), et une période

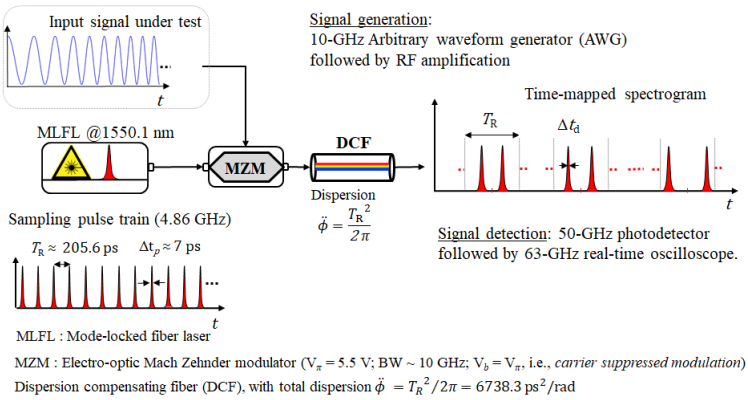

Fig. 6: Schéma du montage expérimental pour l'AS-TR sans interstice de signaux micro-ondes de largeur de bande GHz basé sur l'analyse de spectrogrammes mappés dans le temps. Le signal micro-ondes sous test (SUT) est échantillonné avec un train d'impulsions optiques picosecondes généré par un laser à fibre à verrouillage de mode, dans un modulateur Mach-Zehnder (MZM). Les échantillons optiques sont propagés à travers une fibre à compensation de dispersion (DCF) avec une dispersion totale de $\ddot{\phi}$, et le SP-MT de sortie est capturé dans un oscilloscope en temps réel après photodétection.

de répétition $T_{\mathrm{R}} \approx 205.76$ps (fréquence d'échantillonnage = 4.86 GHz). L'échantillonnage temporel des SUT micro-ondes est réalisé à l'aide d'un modulateur Mach-Zehnder (MZM) électro-optique de 40 GHz. Le taux d'échantillonnage de 4.86 GHz permet d'analyser les objets sous test micro-ondes avec une largeur de bande de fréquence complète allant jusqu'à $\sim$ 4.86 GHz (critère de Nyquist). Par la suite, dans les deux plateformes évaluées, les impulsions optiques modulées sont propagées linéairement à travers une fibre à compensation de dispersion (DCF), qui fournit une dispersion de second ordre de ~ 6825 ps^{2}rad^{-1}, soit environ 1.3% de la quantité idéale de dispersion de l'équation 3, $\ddot{\phi} = {T_{\mathrm{R}}}^2/2\pi = 6738.2$ ps^{2}rad^{-1}, sur toute la largeur de bande de fréquence des impulsions d'échantillonnage. La perte totale du DCF utilisé dans les expériences est de $\sim$ 28 dB, ce qui est compensé en utilisant un amplificateur d'impulsions optiques (Pritel EDFA) avant la photodétection. La forme d'onde non répétitive de sortie est capturée avec un photodétecteur à largeur de bande de 50 GHz relié à un oscilloscope en temps réel à largeur de bande de 63 GHz (Keysight DSAZ634A), sans moyennage.

La Fig. 7 présente l'analyse d'un signal hyperfréquence d'une duvée de 2-μs avec une fréquence instantanée $\omega_{RF}(t_1)$, augmentant linéairement de 500 MHz à 2 GHz, Fig. 7(b). Le tracé de la Fig. 7(c) montre la tension de la forme d'onde temporelle électrique de sortie qui est directement capturée sur l'oscilloscope en temps réel. La forme d'onde temporelle de sortie mesurée le long de chaque créneau de durée T_{R} (période d'échantillonnage) est mise en correspondance avec l'axe de fréquence équivalent à l'aide de la loi de mise en correspondance définie, $\Delta t_2 \leftarrow \Delta\omega_1\ddot{\phi}$. Le spectre instantané

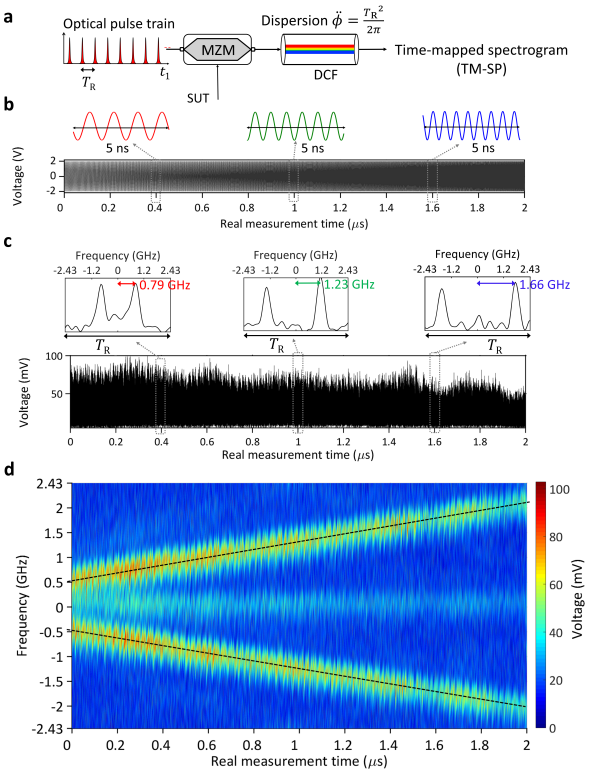

Fig. 7: Résultats expérimentaux de l'analyse de spectrogrammes mappés dans le temps d'une modulation de fréquence linéaire. (a) Schéma de la configuration expérimentale. (b) Trace temporelle du signal micro-ondes testé (SUT) (c) Forme d'onde temporelle de sortie (signal de tension) qui est directement capturée dans un oscilloscope en temps réel. Les graphiques en médaillon montrent un zoom de la forme d'onde de sortie autour de trois tranches de temps différentes, chacune s'étendant sur une période d'analyse ($T_{\mathrm{R}} = 205.6$ ps). Le spectre instantané du signal d'entrée à tout instant donné est constitué de 2 impulsions individuelles, correspondant à la fréquence du signal, $\pm\omega_{\mathrm{RF}}(t_1)$ augmentant linéairement avec le temps. (d) montre une représentation 2D de la distribution d'énergie temps-fréquence conjointe du signal (spectrogramme) qui est directement récupérée à partir de la trace temporelle de sortie.

du SUT d'entrée à tout instant donné est constitué de 2 impulsions individuelles, correspondant à la fréquence instantanée du signal, $\pm\omega_{RF}(t_1)$ augmentant linéairement avec le temps. La Fig. 7(d) montre la représentation 2D de la distribution d'énergie temps-fréquence conjointe du signal (spectrogramme) qui est directement récupérée à partir de la trace temporelle de sortie.

Comme prévu, le spectrogramme récupéré expérimentalement suit la courbe de fréquence linéaire théorique du SUT d'entrée (lignes grises pointillées). Les déviations de la distribution 2D le long de l'axe vertical des fréquences, par rapport à la fluctuation linéaire théorique des fréquences, observées sur la Fig. 7(d) sont attribuées à la gigue temporelle finie des impulsions optiques picosecondes utilisées pour l'échantillonnage temporel. Il est important de souligner qu'aucune remise à l'échelle n'a été appliquée pour représenter l'axe temporel dans le tracé temps-fréquence 2D de la Fig. 7(d), ce qui indique que la forme d'onde de sortie fournit le spectrogramme du signal d'entrée purement

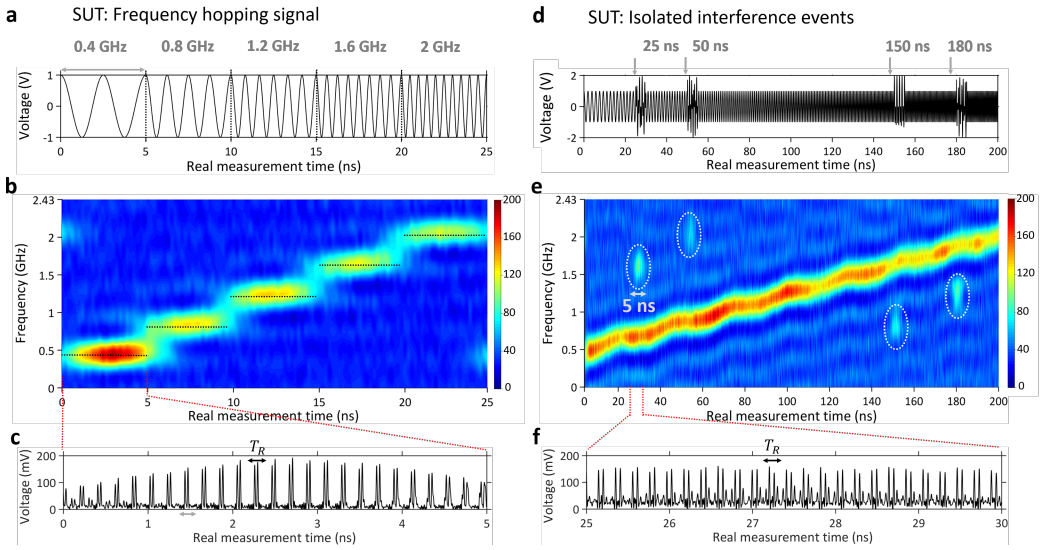

Fig. 8: Capacité de la méthode SP-MT à capturer des transitoires de fréquence de durée nanoseconde (a) Trace temporelle d'un signal hyperfréquence testé (SUT) consistant en une séquence rapide de sauts de fréquence. (b) Distribution du spectrogramme 2D directement récupérée à partir de la trace temporelle mesurée à la sortie du schéma SP-MT basé sur la photonique. (c) Zoom de la forme d'onde temporelle de sortie sur la fenêtre temporelle de 5 ns. (d) Trace temporelle d'un SUT hyperfréquence composé d'un saut de fréquence linéaire et de transitoires de fréquence parasites. (e) Distribution du spectrogramme 2D qui est directement récupérée de la trace temporelle mesurée à la sortie du dispositif SP-MT. (f) Zoom de la trace temporelle de sortie sur la fenêtre temporelle de 5 ns.

en temps réel. Plus précisément, le signal changeant FT est calculé toutes les $T_{\mathrm{R}} \approx 205.76$ ps, c'est-à-dire à une vitesse de 4.86×10^9 FT par seconde, ce qui surpasse considérablement les instruments actuels. Pour une référence comparative, un analyseur de spectre RF en temps réel de pointe basé sur un DSP, le Keysight N9040B-RT2, fournit un maximum de 292 969 transformées de Fourier discrètes par seconde. Les résultats de la Fig. 7 confirment la capacité de la configuration démontrée à fournir un AS-TR sans interruption des formes d'onde avec une largeur de bande de fréquence instantanée approchant 5-GHz, au-delà des capacités des plateformes électroniques actuelles basées sur le DSP.

0.5.1 Application pour le suivi des événements de courte durée (nanoseconde)

Le TM-SP basé sur la photonique est particulièrement intéressant pour le suivi en temps réel d'événements courts de durée nanoseconde dans le spectre large bande. Cette capacité du SP-MT est démontrée par les résultats expérimentaux présentés à la Fig. 8. Les objets soumis à l'analyse comprennent des événements aléatoires ou isolés rapides et des transitoires de fréquence dont la durée peut atteindre 5 ns. Cette capacité dépasse les performances des schémas AS-TR actuels basés sur le DSP, qui sont généralement limités à une interception avec une probabilité de 100 %

des caractéristiques du signal avec des durées d'au moins une microseconde. La Fig. 8(a) montre la trace temporelle d'une séquence rapide de sauts de fréquence micro-ondes conçue spécialement pour tester les performances de la configuration SP-MT. En particulier, le SUT consiste en des segments de 5 ns de long avec une fréquence augmentant linéairement, de 0,4 GHz à 2 GHz. La Fig. 8(b) montre la distribution du spectrogramme 2D directement récupérée à partir de la trace temporelle mesurée à la sortie de la configuration SP-MT, révélant la séquence de saut conçue dans le plan temps-fréquence. La Fig. 8(c) montre un zoom de la forme d'onde temporelle de sortie sur la fenêtre temporelle de 5 ns correspondant à la présence de la tonalité de 0,4 GHz. Ce tracé révèle que le spectre mappé dans le temps de cet événement est produit de manière répétitive sur cette fenêtre de 5 ns à chaque période d'échantillonnage (c'est-à-dire environ 25 fois), ce qui garantit que l'événement est intercepté avec une probabilité de 100%.

À titre d'exemple, les figures 8(d) et (e) montrent les résultats (trace temporelle d'entrée et spectrogramme récupéré, respectivement) de l'analyse d'un signal micro-ondes composé d'un chirp de fréquence linéairement croissante, ainsi que de transitoires de fréquence interférents isolés aléatoires, chacun ayant une durée de 5 ns. La Fig. 8(f) montre également un zoom de la trace temporelle de sortie sur la fenêtre temporelle de 5 ns correspondant à l'événement d'interférence de 1.6 GHz, révélant à nouveau les caractéristiques de suréchantillonnage de l'AS-TR réalisé. Ces résultats confirment clairement que la plateforme SP-MT basée sur la photonique permet d'intercepter le contenu fréquentiel de n'importe quel événement de signal aléatoire ou isolé en temps réel, tant que cela se produit sur une durée proche de la résolution temporelle de l'analyse de spectrogramme effectuée, ~ 2.54 ns dans la configuration expérimentale rapportée.

0.6 Démonstration expérimentale des caractéristiques supplémentaires de la SP-MT

Cette section présente quelques autres caractéristiques importantes de la SP-MT qui sont particulièrement avantageuses pour l'AS-TR et le traitement des formes d'onde à large bande.

0.6.1 Analyse de spectrogrammes en temps réel de formes d'onde optiques complexes

Comme indiqué dans la section 0.3, le concept SP-MT est applicable à des formes d'onde temporelles complexes générales, avec des profils temporels d'amplitudes et de phases arbitraires. Pour démontrer la capacité de la SP-MT à analyser des formes d'ondes complexes, des résultats expérimentaux sur l'application du concept SP-MT pour l'observation en temps réel de l'évolution spectrale dynamique d'un champ optique modulé en phase à changement rapide sont présentés [AC1].

Le montage expérimental pour l'AS-TR de formes d'ondes optiques complexes (spécifiquement, modulées en phase) est illustré sur la figure 9(a). Cette expérience est conçue pour suivre l'évolution dynamique du spectre d'un champ optique modulé en phase qui change rapidement. Le SUT optique est généré par la modulation de phase d'impulsions optiques verrouillées en modes (ayant une intensité FWHM $\Delta t_p \sim 7$ ps, une fréquence de répétition (échantillonnage) de 4.86 GHz et une fréquence centrale optique = 193. 5 THz), en utilisant un modulateur de phase électro-optique ($V_\pi = 3.2$ V) piloté par un signal sinusoïdal d'une longueur de 1.6-μs, d'une fréquence $f_m = 500$ MHz, avec une amplitude crête à crête augmentant de 0 à 5.5 V (signal de modulation représenté sur la Fig. 9(a)). Le signal à la sortie du modulateur de phase peut être interprété comme une forme d'onde optique d'amplitude uniforme modulée en phase (SUT) qui est échantillonnée par le train d'impulsions à verrouillage de mode, avec une période d'échantillonnage $T_\mathrm{R} = 205.6$ ps. Le signal échantillonné est ensuite propagé à travers une fibre à compensation de dispersion (DCF), avec une dispersion totale $\ddot{\phi} = {T_\mathrm{R}}^2/2\pi = 6738.3$ ps^{2}rad^{-1}. La forme d'onde de sortie unique est capturée avec un photodétecteur de 50 GHz connecté à un oscilloscope en temps réel, sans moyennage. La forme d'onde temporelle de sortie mesurée le long de chaque intervalle de temps de T_R (période d'échantillonnage) est simplement mise en correspondance avec l'axe de fréquence équivalent à l'aide de la loi de mise en correspondance définie, $\Delta\omega_1 \rightarrow \Delta t_2/\ddot{\phi}$; ceci produit la représentation 2D de la distribution d'énergie temps-fréquence conjointe du signal (SP) qui est illustrée sur la Fig. 9(b). Le SP récupéré révèle l'évolution des bandes latérales spectrales optiques qui sont induites par le processus de modulation de phase électro-optique, purement en temps réel. Le spectre optique mappé dans le temps à différents emplacements temporels est également représenté sur le côté droit de la Fig. 9(b).

En particulier, la tension linéairement croissante appliquée au modulateur de phase électro-optique génère de nouvelles bandes latérales à changement rapide à la sortie du modulateur de

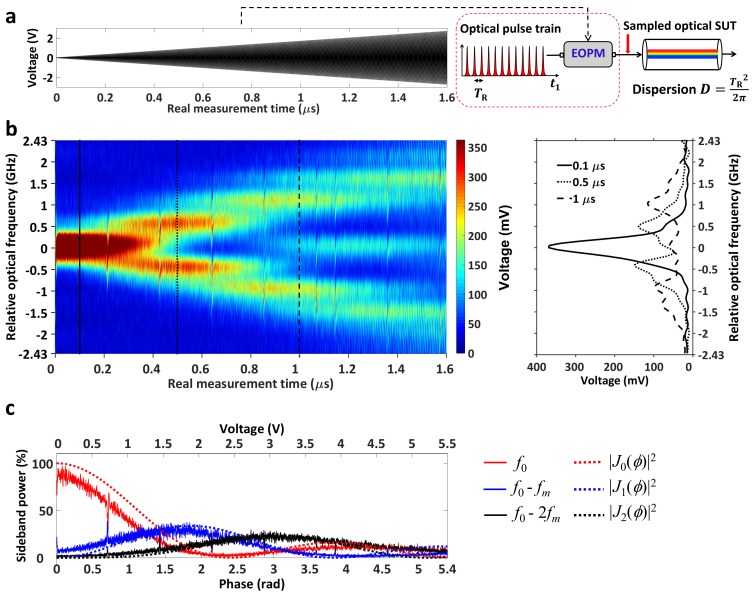

Fig. 9: Résultats expérimentaux sur l'analyse SP en temps réel d'un signal optique modulé en phase. (a) Signal de modulation de test, avec une amplitude linéairement croissante, appliqué à un champ optique à travers un modulateur de phase électro-optique. (b) Représentation 2D de la distribution d'énergie temps-fréquence conjointe du signal (SP) qui est directement récupérée à partir de la trace temporelle de sortie mesurée. (c) Puissance relative de chacune des 3 bandes latérales spectrales principales mesurées en fonction de la tension de modulation crête à crête linéairement croissante (et du déphasage électro-optique correspondant).

phase à $f_0 \pm f_m, f_0 \pm 2f_m$...etc. [sr26], autour de la fréquence porteuse des impulsions optiques d'entrée, f_0. La ligne dispersive suivante cartographie les spectres optiques instantanés générés le long de l'axe du temps en temps réel, selon la théorie de l'analyse des spectrogrammes mappés dans le temps. Le spectre changeant de la forme d'onde optique modulée est capturé à chaque période d'échantillonnage, $T_{\mathrm{R}} = 205.7$ ps, c'est-à-dire à un taux de 4.86×10^9 spectres par seconde, plusieurs ordres de grandeur au-delà des capacités des méthodes actuelles d'analyse du spectre optique. De plus, les spectres changeants sont chacun mesurés avec une résolution de ∼425 MHz. La figure 9(c) montre que la puissance relative de la bande latérale est représentée en fonction de la tension de modulation appliquée qui augmente linéairement (et du déphasage électro-optique correspondant). Les puissances relatives des bandes latérales suivent en fait les fonctions de Bessel qui régissent le processus de modulation d'un modulateur de phase électro-optique [sr26]. Ces résultats fournissent une observation expérimentale directe de la performance dynamique du modulateur de phase électro-optique évalué d'une manière qui ne serait pas possible autrement. Ces résultats montrent que le concept SP-MT en général peut être appliqué pour l'AS-TR de formes d'onde complexes. Cette capacité ouvre des possibilités supplémentaires importantes pour l'analyse spectrale et le traitement en temps réel des champs optiques.

0.6.2 Analyse spectrale en temps réel de formes d'ondes hautes fréquences par échantillonnage passe-bande

Dans le schéma SP-MT, l'extension maximale de la fréquence du SUT est limitée par la fréquence de répétition de l'unité d'échantillonnage à impulsions courtes, conformément au critère de Nyquist [sr24]. Lorsque la fréquence porteuse (ou centrale) du SUT augmente, le critère de Nyquist peut entraîner des exigences de taux d'échantillonnage trop élevées. Les AS-TR basés sur les méthodes numériques conventionnelles s'appuient sur la conversion vers le bas de ces formes d'ondes hautes fréquences en bande de base pour leur détection et utilisent des mélangeurs multi-étages encombrants et des oscillateurs locaux accordables [sr2].

Cependant, l'AS-TR des formes d'ondes hautes fréquences basé sur la conception SP-MT présente de nouvelles opportunités pour éviter les étapes de conversion vers le bas qui utilisent des mélangeurs et des oscillateurs locaux [AC2]. L'extrémité avant du schéma SP-MT est constituée d'une unité d'échantillonnage temporel de base ; par conséquent, la théorie de l'échantillonnage passe-bande [sr27] peut être utilisée pour échantillonner directement les formes d'onde haute fréquence en dessous du taux de Nyquist sans perdre aucune des informations du signal d'entrée, tout en évitant le besoin d'étages de conversion vers le bas. Dans les expériences de preuve de concept rapportées ici, j'ai démontré l'AS-TR d'impulsions micro-ondes de l'ordre de la nanoseconde avec un contenu spectral allant jusqu'à 10 GHz, correspondant à une largeur de bande globale de 20 GHz, par échantillonnage passe-bande à un taux de Nyquist nettement inférieur (< 5 GHz).

La Fig. 10(a) montre le montage expérimental pour l'AS-TR de formes d'onde haute fréquence utilisant le concept SP-MT combiné à l'échantillonnage passe-bande. L'objet sous test est une impulsion temporelle de forme sinc, avec une largeur de bande totale de 3dB $B \sim$1 GHz, Fig. 10(b), convertie à une fréquence porteuse $f_c = 4.86$ GHz par mélange avec une tonalité RF générée par un synthétiseur RF. La fréquence la plus élevée du signal converti dans ce premier exemple est alors $f_{max} \sim 4.86 + 0.5 = 5.36$ GHz. Le SUT est échantillonné à l'aide d'impulsions optiques provenant d'un laser à verrouillage de mode (largeur d'impulsion FWHM de l'intensité $\Delta t_p \sim 7$ ps) dans un modulateur Mach-Zehnder (MZM) électro-optique. Le critère de Nyquist établit une fréquence d'échantillonnage minimale requise de $2f_{max} = 10.72$ GHz. Cependant, selon la théorie de l'échantillonnage passe-bande, si elle est correctement conçue, la fréquence d'échantillonnage peut être aussi basse que $B = 1$ GHz (c'est-à-dire la largeur de bande d'information), pour une reconstruction complète de la forme d'onde en bande de base. Néanmoins, il est important de se

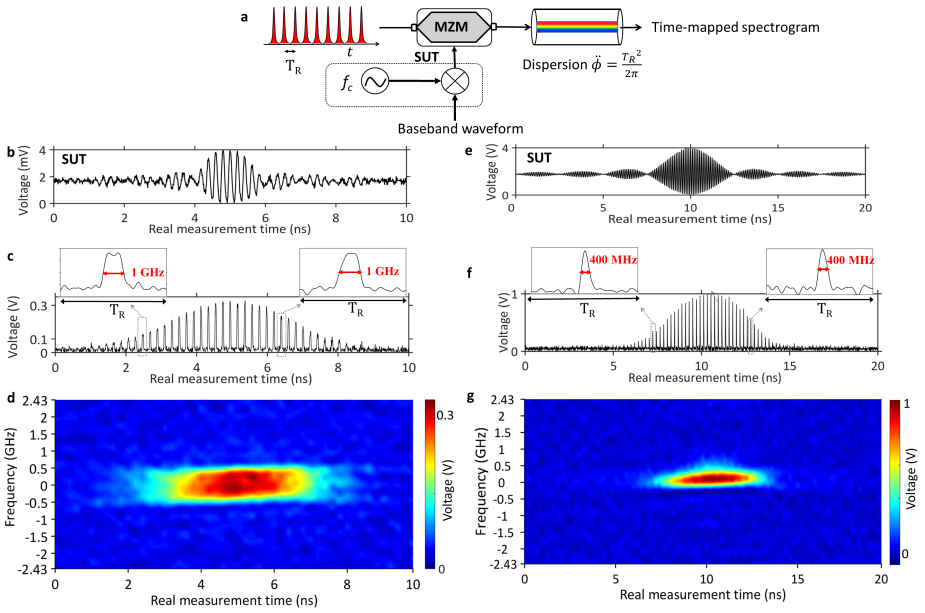

Fig. 10: AS-TR de formes d'onde à haute fréquence utilisant le concept SP-MT et l'échantillonnage passe-bande (a) Montage expérimental pour l'AS-TR de formes d'onde haute fréquence utilisant le concept SP-MT et l'échantillonnage passe-bande (b) Signal testé (SUT) : Une impulsion sincère de 2 ns modulée sur une tonalité de 4.86 GHz. (c) Trace unique de l'oscilloscope en temps réel à la sortie, montrant la cartographie du spectre en bande de base de forme carrée du SUT, le long de chaque intervalle de temps d'une durée de T_{R} (205.7 ps) (d) Représentation T-F conjointe en 2D du signal en bande de base SP, récupérée en remettant à l'échelle la trace temporelle de sortie le long de chaque période d'analyse consécutive dans l'axe de fréquence correspondant (axe vertical), montrant uniquement le côté positif des fréquences. (e) SUT: Une impulsion sincère de 5 ns modulée sur 9.72 GHz. (f) Forme d'onde temporelle de sortie montrant la cartographie des spectres en bande de base à résolution limitée du SUT. (g) Représentation conjointe 2D de la TF du SP.

rappeler que la fréquence d'échantillonnage détermine également la résolution temporelle et la quantité de dispersion nécessaire dans le schéma SP-MT, c'est-à-dire qu'une fréquence d'échantillonnage plus faible entraîne une résolution temporelle plus longue et nécessite une plus grande quantité de dispersion, comme décrit dans les chapitres précédents. Par conséquent, le taux d'échantillonnage choisi est fixé à $f_R = 4.86$ GHz (période d'échantillonnage correspondante $T_{\mathrm{R}} = 205.6$ ps). Après la dispersion, les copies retardées et décalées en fréquence du SUT d'entrée interfèrent les unes avec les autres, ce qui donne une forme d'onde temporelle qui suit la transformée de Fourier fenêtrée, c'est-à-dire le spectrogramme, du SUT à chaque période d'échantillonnage consécutive (avec une durée de $T_{\mathrm{R}} = 205.6$ ps). À la sortie, le zoom sur différentes périodes d'analyse (chacune d'une durée de T_{R}), comme indiqué dans les inserts de la Fig. 10(c), révèle la cartographie temporelle prédite du contenu spectral de la bande de base carrée convertie vers le bas du SUT, autour de la fréquence zéro. La Fig. 10(d) montre la représentation 2D de la distribution d'énergie T-F du SUT (le spectrogramme) qui est cartographiée directement à partir de la trace mesurée en temps réel. La Fig. 10(e) montre un autre exemple d'analyse d'un SUT haute fréquence, une impulsion

sinc de 400 MHz de largeur de bande totale, d'une durée de 5 ns, modulée sur une onde porteuse de 9.72 GHz. Les résultats ci-dessus démontrent une méthode permettant d'éviter les étapes de conversion vers le bas avant d'effectuer un AS-TR, en utilisant l'approche SP-MT combinée à un échantillonnage passe-bande. Cette méthode devrait s'avérer très utile pour les applications AS-TR de signaux hyperfréquences à large bande avec des fréquences porteuses élevées, comme celles que l'on trouve dans les environnements sans fil réels.

0.6.3 Filtrage à fréquence variable dans le temps de formes d'onde à large bande

Le filtrage des fréquences variables dans le temps est nécessaire pour un large éventail d'applications, notamment l'atténuation des interférences non stationnaires dans les radars [sr28, sr29], la radio cognitive [sr30, sr31], et les applications de communication à spectre étalé [sr32, sr33]. Je présente ici le concept de filtrage à fréquence variable dans le temps basé sur l'approche SP-MT, et je discute des résultats de simulation du filtrage à fréquence variable dans le temps basé sur la photonique pour les signaux micro-ondes à large bande, offrant des vitesses d'accord inférieures à GHz.

La figure 11 illustre le concept du filtrage à fréquence variable dans le temps proposé pour les signaux micro-ondes non stationnaires. Le signal micro-ondes testé (SUT) est d'abord échantillonné avec des impulsions courtes (largeur d'impulsion individuelle Δt_p, et fréquence de répétition $\omega_{\mathrm{R}} = 2\pi/T_{\mathrm{R}}$), suivies d'une dispersion chromatique (retard de groupe) de second ordre ($\ddot{\phi}$). À la sortie de l'élément dispersif $\ddot{\phi}$, la transformée de Fourier à court terme (TFCT) du SUT est cartographiée le long de l'axe temporel à la vitesse du signal, avec chaque spectre de Fourier consécutif cartographié dans chaque période d'analyse de durée T_{R}, lorsque le retard dispersif satisfait à $\ddot{\phi} = T_{\mathrm{R}}^2/2\pi$. La distribution d'énergie T-F 2D du SUT représentée sur la Fig. 11 est simplement obtenue en remettant à l'échelle la trace temporelle le long de chaque T_{R} dans l'axe de fréquence correspondant selon la loi de correspondance fréquence-temps définie (déterminée par le coefficient de dispersion). La résolution temporelle du spectrogramme généré est de $\delta t_r \approx \ddot{\phi} \times \Delta\omega_p$, tandis que la résolution fréquentielle est l'inverse de cette résolution temporelle, donnée par $\delta\omega_r \approx \Delta t_p/\ddot{\phi}$; ces résolutions ne sont alors contraintes que par le principe d'incertitude de la transformée de Fourier. Un modèle de modulation temporelle prédéfini est généré et utilisé pour moduler le spectrogramme de sortie mappé dans le temps après le premier élément dispersif, mettant en œuvre le filtre de fréquence variable dans le temps souhaité. Le motif de modulation peut être conçu pour mettre en œuvre l'opération de filtrage souhaitée par l'utilisateur sur la distribution d'énergie T-F. Comme la distribution T-F

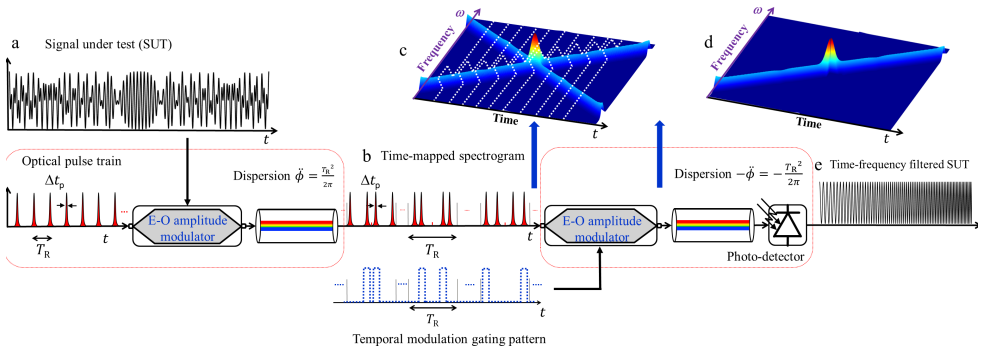

Fig. 11: Fonctionnement du filtrage à la volée de signaux micro-ondes à large bande à fréquence variable dans le temps. (a) Signal micro-ondes testé, composé de deux composantes de chirp linéaires. (b) TFCT mappé dans le temps ou le spectrogramme complet (c) La distribution d'énergie T-F. Notez que seules les fréquences positives sont représentées. Les lignes pointillées montrent le modèle de déclenchement de la modulation temporelle conçu pour filtrer l'une des composantes de chirp dans le domaine temps-fréquence. (d) La distribution d'énergie T-F après l'application du motif de déclenchement de modulation temporelle. (e) Le signal de sortie filtré composé d'une seule composante de chirp.

est maintenant accessible avec une résolution temporelle de δt_r, le motif de modulation temporelle peut modifier la distribution T-F du signal à une vitesse d'accord maximale correspondante de $1/\delta t_r$. Le signal filtré T-F est récupéré par propagation à travers une ligne à retard dispersive avec la dispersion exactement opposée à celle de l'entrée, $-\ddot{\phi}$. Enfin, un filtrage passe-bas, agissant comme un détecteur d'enveloppe, peut être utilisé pour extraire l'enveloppe du signal filtré T-F.

0.7 Conclusions

Cette thèse présente la théorie du spectrogramme mappé dans le temps (SP-MT) - un cadre universel de traitement des signaux analogiques permettant de mapper la transformée de Fourier à court terme (TFCT) complète d'une forme d'onde arbitraire entrante le long du domaine temporel par le biais de l'échantillonnage temporel et du retard dispersif. Le SP-MT capture la TFCT complète des signaux à grande vitesse (par exemple, micro-ondes à optique) en temps réel et directement dans le domaine d'onde analogique, évitant le besoin d'algorithmes de transformée de Fourier rapide (TFR) exigeants en calcul. Les principaux compromis de conception, les spécifications de performance et certaines caractéristiques uniques offertes par l'architecture SP-MT ont été discutés. Par exemple, nous avons constaté que les résolutions temporelle et fréquentielle de l'analyse TFCT effectuée sont liées à la largeur d'impulsion d'échantillonnage et qu'il est donc facile de les régler en modifiant la largeur d'impulsion d'échantillonnage. La cartographie temporelle répétée de l'information TFCT - une caractéristique unique du SP-MT - a également été découverte et étudiée en détail.

Des simulations numériques d'une plateforme photonique pratique pour la mise en œuvre du SP-MT, visant à l'AS-TR continu sans interstices de formes d'ondes à larges bandes, ont été réalisées. Les compromis de conception tels que les résolutions de temps et de fréquence, et les caractéristiques uniques telles que le fonctionnement continu sans espace, le mappage répété de l'information TFCT, ont tous été vérifiés par des simulations numériques. L'implémentation photonique de la SP-MT est particulièrement attrayante pour l'AS-TR continu de signaux micro-ondes d'une largeur de bande de GHz, offrant des vitesses de traitement de transformée de Fourier de l'ordre du GHz et des résolutions temporelles de l'ordre de la nanoseconde.

Une TM-SP basée sur la photonique a ensuite été démontrée expérimentalement en utilisant les composants disponibles sur le marché, permettant un AS-TR continu et sans interstice de formes d'onde micro-ondes d'une largeur de GHz. Le SP-MT basé sur la photonique a atteint des spécifications de performance AS-TR sans précédent, à savoir

- Bande passante instantanée en temps réel ~ 5 GHz,
- Vitesse de traitement des transformées de Fourier de $\sim 5 \times 10^9$ transformées de Fourier par seconde,
- Résolutions temporelles ~ 2 ns,
- Interception de signaux rapides aléatoires d'une durée de l'ordre de la nanoseconde, grâce à une analyse spectrale continue sans interruption.

Ces spécifications de performance répondent aux exigences critiques de l'AS-TR pour une large gamme d'applications, dans les domaines des communications, du radar, de la radioastronomie, de l'instrumentation biomédicale et autres. Plus important encore, l'architecture universelle du SP-MT est bien adaptée à l'analyse et au traitement des formes d'onde dans d'autres régions de fréquences du spectre électromagnétique. De plus, les spécifications de performance de la SP-MT basée sur la photonique réalisée dans ce projet de doctorat peuvent facilement être améliorées en utilisant les derniers développements sur les lasers à verrouillage de mode ayant des taux de répétition de centaines de GHz [sr34], auxquels s'ajoutent des technologies de modulation temporelle offrant des performances similaires en termes de largeur de bande [sr35] et des techniques d'échantillonnage temporel tout optique pour les mesures de la forme d'onde de sortie [sr36], ce qui offre la possibilité de réaliser des AS-TR à largeur de bande inférieure à THz avec des vitesses de traitement par transformée de Fourier de l'ordre du THz.

Enfin, certaines caractéristiques importantes de la SP-MT, particulièrement avantageuses pour l'AS-TR et le traitement des formes d'onde à large bande, ont été présentées. L'AS-TR des champs d'ondes optiques complexes basée sur la SP-MT pourrait être très utile pour étudier les phénomènes complexes ultra-rapides dans les systèmes laser [sr9]. Le concept d'échantillonnage passe-bande utilisé dans le SP-MT élimine le besoin d'étages de mélange encombrants tout en convertissant les formes d'ondes hautes fréquences en bande de base, ce qui simplifie grandement l'architecture AS-TR. Le filtrage temps-fréquence à la volée des formes d'onde à large bande basé sur le SP-MT permet une manipulation temps-fréquence en temps réel, ultra-rapide et définie par l'utilisateur des formes d'onde à large bande dans le domaine des ondes analogiques natives.

Références

[sr1] L. R. Rabiner and R. W. Schafer, *Introduction to Digital Speech Processing (Foundations and Trends in Signal Processing)* (NOW, 2007).

[sr2] "Tektronix, "Fundamentals of real-time spectrum analysis," 2020. [online] available:," https://www.tek.com/primer/fundamentals-real-time-spectrum-analysis.

[sr3] P. Berger, Y. Attal, M. Schwarz *et al.*, "RF spectrum analyzer for pulsed signals: Ultra-wide instantaneous bandwidth, high sensitivity, and high time-resolution," Journal of Lightwave Technology **34**, 4658–4663 (2016).

[sr4] A. Weiner, *Ultrafast Optics* (Wiley Publishing, 2009).

[sr5] H. Sun, A. Nallanathan, C. Wang, and Y. Chen, "Wideband spectrum sensing for cognitive radio networks: a survey," IEEE Wireless Communications **20**, 74–81 (2013).

[sr6] X. Zou, B. Lu, W. Pan *et al.*, "Photonics for microwave measurements," Laser & Photonics Reviews **10**, 711–734 (2016).

[sr7] J. B.-Y. Cheng, Chi-Hao; Tsui, *Digital Techniques for Wideband Receivers*, IET Radar Sonar Navigation and Avionics Series (SciTech Publishing, 2016), 3rd ed.

[sr8] A. De Martino, *Introduction to modern EW systems*, Electronic warfare library (Artech House, 2018), second edition ed.

[sr9] A. Mahjoubfar, D. V. Churkin, S. Barland *et al.*, "Time stretch and its applications," Nature Photonics **11**, 341–351 (2017).

[sr10] R. M. Monroe, "Gigahertz bandwidth and nanosecond timescales: New frontiers in radio astronomy through peak performance signal processing," Dissertation (Ph.D.), California Institute of Technology.

[sr11] D. C. Price, J. Kocz, M. Bailes, and L. J. Greenhill, "Introduction to the special issue on digital signal processing in radio astronomy," Journal of Astronomical Instrumentation **05**, 1602002 (2016).

[sr12] L. Cohen, *Time frequency analysis: Theory and applications*, Prentice-Hall signal processing series (Prentice Hall PTR, 1995), 1st ed.

[sr13] U. Meye-Baese, *Fourier Transforms, in Digital Signal Processing with Field Programmable Gate Arrays* (Springer Berlin Heidelberg, 2014).

[sr14] B. Murmann, "ADC performance survey 1997-2020, 2020. [online] available:," http://web.stanford.edu/murmann/adcsurvey.html.

[sr15] S. M. Kuo, B. H. Lee, and W. Tian, *Real-Time Digital Signal Processing: Fundamentals, Implementations and Applications* (Wiley, 2013), 3rd ed.

[sr16] Tektronix, "Real-time spectrum analyzers RSA7100A/B, 2020. [online] available:," https://www.tek.com/spectrum-analyzer/rsa7100b-realtime-spectrum-analyzer.

[sr17] M. Burla, X. Wang, M. Li, L. Chrostowski, and J. Azaña, "Wideband dynamic microwave frequency identification system using a low-power ultracompact silicon photonic chip," Nature Communications **7**, 13004 (2016).

[sr18] T. Jannson, "Real-time fourier transformation in dispersive optical fibers," Opt. Lett. **8**, 232–234 (1983).

[sr19] J. Azana and M. A. Muriel, "Real-time optical spectrum analysis based on the time-space duality in chirped fiber gratings," IEEE Journal of Quantum Electronics **36**, 517–526 (2000).

[sr20] R. E. Saperstein, D. Panasenko, and Y. Fainman, "Demonstration of a microwave spectrum analyzer based on time-domain optical processing in fiber," Opt. Lett. **29**, 501–503 (2004).

[sr21] S. Tainta, M. J. Erro, M. J. Garde, and M. A. Muriel, "Temporal self-imaging effect for periodically modulated trains of pulses," Opt. Express **22**, 15251–15266 (2014).

[sr22] H. G. de Chatellus, L. R. Cortés, and J. A. na, "Optical real-time fourier transformation with kilohertz resolutions," Optica **3**, 1–8 (2016).

[sr23] Q. Xie and C. Shu, "Reconfigurable envelope generation of optical pulse train based on discrete fourier transform," IEEE Photonics Technology Letters **30**, 242–245 (2018).

[sr24] A. V. Oppenheim and G. C. Verghese, *Signals, Systems and Inference*, Prentice Hall Signal Processing Series (Prentice Hall, 2015), 1st ed.

[sr25] G. A. Agrawal, *Nonlinear Fiber Optics* (Academic Press, 2013), 5th ed.

[sr26] A. Yariv and P. Yeh, *Photonics: Optical Electronics in Modern Communications* (Oxford University Press, 2007), 6th ed.

[sr27] R. Vaughan, N. Scott, and D. White, "The theory of bandpass sampling," IEEE Transactions on Signal Processing **39**, 1973–1984 (1991).

[sr28] V. C. Chen, *Time-Frequency Transforms for Radar Imaging and Signal Analysis*, Artech House radar library (Artech House, 2002), 1st ed.

[sr29] S. Neemat, O. Krasnov, and A. Yarovoy, "An interference mitigation technique for FMCW radar using beat-frequencies interpolation in the STFT domain," IEEE Transactions on Microwave Theory and Techniques **67**, 1207–1220 (2019).

[sr30] S. Haykin, "Cognitive radio: Brain-empowered wireless communications," IEEE Journal on Selected Areas in Communications **23**, 201–220 (2005).

[sr31] S. Lach, M. Amin, and A. Lindsey, "Broadband interference excision for software-radio spread-spectrum communications using time-frequency distribution synthesis," IEEE Journal on Selected Areas in Communications **17**, 704–714 (1999).

[sr32] S. Barbarossa and A. Scaglione, "Adaptive time-varying cancellation of wideband interferences in spread-spectrum communications based on time-frequency distributions," IEEE Transactions on Signal Processing **47**, 957–965 (1999).

[sr33] X. Ouyang and M. Amin, "Short-time fourier transform receiver for nonstationary interference excision in direct sequence spread spectrum communications," IEEE Transactions on Signal Processing **49**, 851–863 (2001).

[sr34] A. L. Gaeta, M. Lipson, and T. J. Kippenberg, "Photonic-chip-based frequency combs," Nature Photonics **13**, 158–169 (2019).

[sr35] M. Burla, C. Hoessbacher, W. Heni *et al.*, "500 GHz plasmonic mach-zehnder modulator enabling sub-THz microwave photonics," APL Photonics **4**, 056106 (2019).

[sr36] P. Andrekson and M. Westlund, "Nonlinear optical fiber based high resolution all-optical waveform sampling," Laser & Photonics Reviews **1**, 231–248 (2007).

Contents

List of Figures

List of Tables

Chapter 1

Introduction

This chapter reviews some preliminary concepts in signal processing that form the central part of the Thesis. Motivation for the dynamic Fourier spectral analysis, and various existing methods for real-time computation of the dynamic Fourier spectrum are discussed. The goals of the Thesis are established with the aim of overcoming some of the key performance limitations of the existing real-time Fourier spectral analysis methods. The original contributions by the author are briefly presented and the structure of the Thesis is outlined.

1.1 Fourier spectral analysis

The frequency spectrum representation is extensively used in the analysis and design of information processing systems, where many useful and important features are more easily characterized in the frequency domain rather than in the temporal domain. The Fourier transform (FT) is the fundamental mathematical tool that establishes the link between these two domains [1, 2]. The basic FT integral provides the frequency domain representation of a given time-domain signal. Methods based on FT play a key role in all areas of engineering and science.

Jean-Baptiste-Joseph Fourier introduced the FT as a mathematical tool in the early nineteenth century while studying the heat transfer phenomenon [3, 4], but his mathematical tool turned out to be more fundamental and embedded in nature than he perhaps realized. The basic idea of FT is that any complex wave-like signal that fluctuates over time or space, can be broken down into a sum of the familiar, regular, sine waves. The Fourier transform (FT) of a time domain signal $s(t)$

is defined as [1]

$$S(\omega) = \mathrm{FT}(s(t)) = \int_{-\infty}^{+\infty} s(t) e^{-j\omega t}\, dt, \tag{1.1}$$

and is called the analysis equation of $s(t)$. Here, $s(t)$ represents how the signal under analysis fluctuates over time. It is multiplied by a complex exponential with an angular frequency 'ω', and integrated over the entire duration of $s(t)$. Here e is the mathematical constant known as Euler number and $j = \sqrt{-1}$. The term $S(\omega)$ is the Fourier's coefficient at an angular frequency 'ω'and gives the magnitude (maximum height of the wave above and below zero) and relative phase (how much of a wave's cycle has been completed relative to a fixed point) of the specific sine-wave component of the signal under analysis. The signal, $s(t)$, is then said to be represented in the Fourier transform domain, $S(\omega)$. The transform $S(\omega)$ in Eq. 1.1 is finite and converges, if $s(t)$ has finite energy, i.e., if it is square integrable, so that

$$\int_{-\infty}^{+\infty} |s(t)|^2\, dt < \infty \tag{1.2}$$

A set of conditions, known as Dirichlet conditions can be derived from the above Eq. 1.2, that guarantee the existence of the FT of a signal [1]. Specifically, absolutely integrable signals that are continuous or have a finite number of discontinuities have FTs. Like-wise, the inverse Fourier transform (IFT) integral is used to transform the Fourier domain signal, $S(\omega)$ back to the native signal domain as

$$s(t) = \mathrm{IFT}(S(\omega)) = \frac{1}{2\pi} \int_{-\infty}^{+\infty} S(\omega) e^{j\omega t}\, d\omega, \tag{1.3}$$

and is referred to as the synthesis equation. Here, the Fourier's coefficients at angular frequencies 'ω', $S(\omega)$ are multiplied by the complex exponentials at angular frequencies 'ω', and integrated over all the angular frequency range to construct the original signal $s(t)$ back in the native signal domain.

Comparing with the analysis equation in Eq. 1.1, the synthesis equation in Eq. 1.3 has an additional 2π in the denominator, because we have defined the transform in the "angular" frequency domain in Eq. 1.3. Otherwise, except for the sign of the complex exponential, the analysis equation in Eq. 1.1 and the synthesis equation in Eq. 1.3 are similar and often used interchangeably in practice. The FT concept is so ubiquitous and embedded in nature that evolution dictated the

human eyes and ears to perform the Fourier decomposition subconsciously, to interpret sound and light waves [5]. A deeper insight into the FT properties and the relationship between time-domain and frequency-domain description of signals can be found in [1].

In the signal and system analysis framework, a class of systems that satisfy the properties of linearity (superposition) and time invariance are called linear time-invariant (LTI) systems. The Fourier decomposition of a signal of interest into a sum of complex exponential signal components is particularly useful in the analysis of LTI systems [1, 6, 7]. This is significant because many physical phenomena as well as man-made processes can be modeled as LTI systems [1, 7]. The response of an LTI system to a linear sum of complex exponentials at the input is again a linear sum of complex exponentials of the same frequencies, but with a change in the amplitude and/or phase of the complex exponentials. These amplitude and/or phase changes that are induced by the LTI system on the complex exponentials are characteristic to the LTI system, and referred to as the frequency response of that system under analysis. Since FT decomposes any arbitrary signal into a sum of complex exponentials weighted by its Fourier coefficients, the response of an LTI system to an arbitrary input signal can be thought of as modification of the Fourier coefficients of the input signal according to the frequency response of LTI system. This simple yet profound result makes the FT as an indispensable tool for the analysis and synthesis of LTI systems [6, 7].

1.1.1 The discrete Fourier transform (DFT)

The FT analysis is usually and most conveniently performed on a digital signal processor, which could be a general purpose computer or dedicated digital hardware [8]. In such a scenario, the discrete-time sequence representation $s[n]$ of the continuous-time signal $s(t_1)$ is used. The discrete-time sequence $s[n]$ is often obtained from the sampled version of the continuous-time signal $s_{sp}(t_1)$. The sampling process and related mathematical derivations in both temporal and FT domain are essential and play a major role in the current Thesis context. These derivations are discussed in greater detail in the Appendix A.

Sampling of the continuous-time signal $s(t_1)$ with a temporal periodic signal $r_1(t_1)$ at a periodic interval of every T_{R}, produces the sampled version of the signal $s_{sp}(t_1)$. In the case of ideal impulse sampling, the discrete-time sequence $s[n] = s_{sp}(t_1) = s(nT_{\mathrm{R}})$ (see Eq. A.3 in Appendix A). For the purpose of FT analysis of the discrete-time sequences, an analysis equation can be derived similar

to the equation Eq. 1.1 and is referred to as the discrete Fourier transform (DFT). Like-wise, a synthesis equation similar to Eq. 1.3 can be derived and is referred to as the inverse discrete Fourier transform (IDFT).

Let the discrete-time sequence $s[n]$ of length N be the discrete-time approximation of the continuous-time signal $s(t_1)$. The N-point DFT of the finite-duration sequence $s[n]$ is given by [8–10]

$$S[k] = \text{DFT}(s[n]) = \sum_{n=0}^{N-1} s[n]e^{-j2\pi kn/N}, \qquad k = 0, 1, 2, ...N-1 \tag{1.4}$$

This is referred to as the analysis equation, where the sampled spectrum $S[k]$ at a discrete-frequency $2\pi k/N$ is obtained by multiplying the discrete-time sequence $s[n]$ by a complex exponential of frequency $-2\pi k/N$ and summing over the length N. The synthesis equation for the inverse-DFT (IDFT) is given by

$$s[n] = \text{IDFT}(S[k]) = \frac{1}{N}\sum_{k=0}^{N-1} S[k]e^{j2\pi kn/N}, \qquad n = 0, 1, 2, ...N-1 \tag{1.5}$$

where the n^{th} discrete-time sample $s[n]$ is constructed back by adding all the discrete Fourier coefficients $S[k]$ that are multiplied by the corresponding complex exponentials at frequencies $2\pi k/N$. The DFT and IDFT pair is a computationally convenient tool for converting back and forth to the Fourier domain of the discrete-time signals, and play a key role in digital signal processing (DSP) applications, such as frequency spectral analysis, convolution, correlation, linear filtering, etc [8, 9]. From the DFT analysis formula in Eq. 1.4, computing each of the DFT coefficient $S[k]$ involves N complex multiplications, and $N-1$ complex additions. Consequently, computing $S[k]$ at all N values require N^2 complex multiplications and $N^2 - N$ complex additions, i.e., an operation count of order $\mathcal{O}(N^2)$. This calculation is inefficient because it does not exploit the symmetry and periodicity properties of complex exponentials. Moreover, the operation count increases rapidly as the length of the signal N increases.

The DFT/IDFT pair have become a key tool in DSP applications mainly because of the existence of computationally efficient algorithms, known as the fast Fourier transform (FFT) algorithms, for evaluating the DFT. The FFT algorithms take advantage of the inherent symmetry and periodicity of the DFT coefficients in Eq. 1.4, and employ divide and concur strategies to reduce the operation

count of the DFT computation from $\mathcal{O}(N^2)$ to $\mathcal{O}(Nlog_2N)$ [8,9]. This reduction in operation count is particularly significant as the length N increases. Even though Fourier derived the FT analysis method in the early nineteenth century, its general applicability to solving scientific problems in an efficient manner was greatly limited until the year 1965 when Cooley and Tukey proposed the FFT algorithm for computation of the DFT coefficients of finite length sequences [11,12]. The divide and concur strategy involved in the FFT algorithm can be traced back to Carl Friedrich Gauss as early as 1805 - even before the publication of Fourier's work on harmonic functions [13,14]. The availability of electronic digital computers in the 1960's made computer calculation of transforms a reality. The FFT algorithm reduced the time required for computing the transform by orders of magnitude, being perfectly suited for implementation on the then emerging electronic digital computers. This accelerated the development of discrete-time signal and system analysis techniques, opening the era of DSP and digital communication techniques [8–10, 15]. The interested reader is addressed to [9, 10] for a detailed description of the computation strategies utilized by the FFT algorithms and the resulting performance trade-offs.

Many applications of FT analysis enabled by the FFT have emerged in a wide variety of fields [8, 16, 17]. Various modifications/improvisations of the Cooley and Tukey's original FFT algorithm have been published [18–21], and this is still an active area of research. The FFT methods are extensively used in tackling modern scientific and engineering problems, and they are included in the Nature magazine's "Ten computer codes that transformed science" [22, 23].

1.2 Joint time-frequency representation

The FT as discussed in the previous section decomposes the signal of interest into a sum of pure sinusoids of different frequencies that are weighted by the corresponding Fourier coefficients, resulting in the frequency spectrum of the signal. Though simple, the FT is not always the best tool to analyze "real-life signals" which often exhibit a frequency spectral content that changes with time [24, 25]. Such signals with a changing spectral content are called non-stationary signals, the most common example being music or speech signals, where the harmonic content of the acoustic signal changes for different notes i.e., along the time domain [26]. The conventional FT provides the Fourier spectral information (magnitude and phase) averaged over the entire signal's temporal duration, such that it

misses the details on the times of occurrence of the dynamically varying frequency spectral content of the signal under analysis. The joint time-frequency (T-F) transforms were developed for the purpose of characterizing time-varying frequency content of the non-stationary signals [24, 25, 27]. The joint T-F transforms map the signal onto a two-dimensional (2D) distribution as a function of the time and frequency variables simultaneously. A 2D T-F representation provides a direct insight into the non-stationary signal's time-varying frequency spectrum while enabling a dynamic manipulation of this changing spectrum.

Dennis Gabor, best known as the father of holography (for which he won the Nobel Prize in 1971), is credited for the original proposal of a joint T-F analysis in his seminal paper on "Theory of communication" [28]. He realized that the FT definition, as defined in Eq. 1.1 though mathematically elegant, is only a theoretical abstraction and it assumes the waveforms to have been in existence since infinite past and until infinite future, an assumption that is far from a real-life scenario [28,29]. In the FT definition from Eq. 1.1, a "time" domain signal is represented in terms of the "frequency" domain spectrum, which are two mutually exclusive domains. The term "frequency" in the strict mathematical sense implies then an infinite duration signal. The static FT, as defined in Eq. 1.1 does not provide information on the time of occurrence of the signal's frequency content. The purpose of a joint T-F analysis is to overcome this critical limitation of the static FT: a T-F distribution provides a comprehensive dynamic representation of the signal's frequency spectrum as it changes along the time domain. The joint T-F representations are widely used for analyzing the transient phenomenon or changing frequency content [30–32]. A classic example applications of T-F techniques are in speech signal processing tasks, such as speech coding, synthesis, and pattern recognition [26, 33]. In biomedical signal processing, T-F techniques are extensively used for the analysis of non-stationary signals from electrocardiogram, Electroencephalography [32]. The joint T-F analysis is also a useful tool in radar signal processing functionalities such as, radar back-scattering and feature extraction, imaging of moving targets, etc. [30, 34]. Spread spectrum communication system receivers employ T-F techniques for interference rejection [32]. Joint T-F distributions also find applications in array signal processing, e.g., estimating direction of arrival by a sensor array - an important problem in radar, sonar, seismology [32]. Particularly, joint T-F analysis involving high-speed and broadband waveforms is challenging and increasingly desired in emerging applications such as radar, high-speed communications, radio astronomy, ultra-fast optical

pulse characterization [34–38]. Recently, T-F techniques even played a major role in detecting the frequency chirp that lead to the discovery of gravitational waves [39].

1.2.1 Short-time Fourier transform (STFT)

Many different techniques have been developed over the years for a joint T-F signal analysis [24,30, 31]. Among these, the short-time Fourier transform (STFT) or the spectrogram (squared magnitude of the STFT) remains as the workhorse of T-F signal analysis and processing. As illustrated in Fig. 1.1(a), the STFT can be calculated as the FT of a time truncated (or windowed) version of the signal under test (SUT), as the center of the window function is being shifted along the time domain. By examining the frequency content of the signal as the time window is moved, a 2D T-F distribution called the spectrogram is generated. The spectrogram provides information on the frequency content of the signal at different time instances. Mathematically, the STFT of a time-varying signal, $s(t)$, is defined as follows [40]:

$$X(\tau,\omega) = \mathrm{FT}(h(t-\tau)s(t)) = \int_{-\infty}^{+\infty} h(t-\tau)s(t)e^{-j\omega t}\,dt \tag{1.6}$$

Here ω holds for the radial frequency variable, τ is the time-delay parameter that defines the STFT analysis time variable and typically extends over the entire duration of the SUT. The FT holds for Fourier transform, and $h(t)$ is a time-limited weight function that serves as the "temporal analysis window". The spectrogram (SP) of the signal is then calculated as $\mathrm{SP}_s(\tau,\omega) =\mid X(\tau,\omega) \mid^2$. The SP is often represented as a 2D T-F distribution such as the one shown in Fig. 1.1(b). In practical STFT system, the window function $h(t)$ has finite duration in time, so the STFT integral in Eq. 1.6 always converges, unlike the FT integral discussed in Eq. 1.2.

The choice of the window function $h(t)$ plays a major role in the STFT analysis. In the T-F analysis, the smallest feature that can be separately analyzed in each of the two involved domains (time and frequency) determines the analysis "resolution" in the respective domain. The time resolution of the STFT distribution obtained in Eq. 1.6 is then dictated by the duration of the temporal window used in the analysis, $h(t)$, whereas the corresponding frequency resolution is given by the inverse of this time resolution [25,40]. The uncertainty principle of the FT imposes that these two resolutions cannot be arbitrarily sharp, but rather, they are inversely related [25, 40, 41]. Some

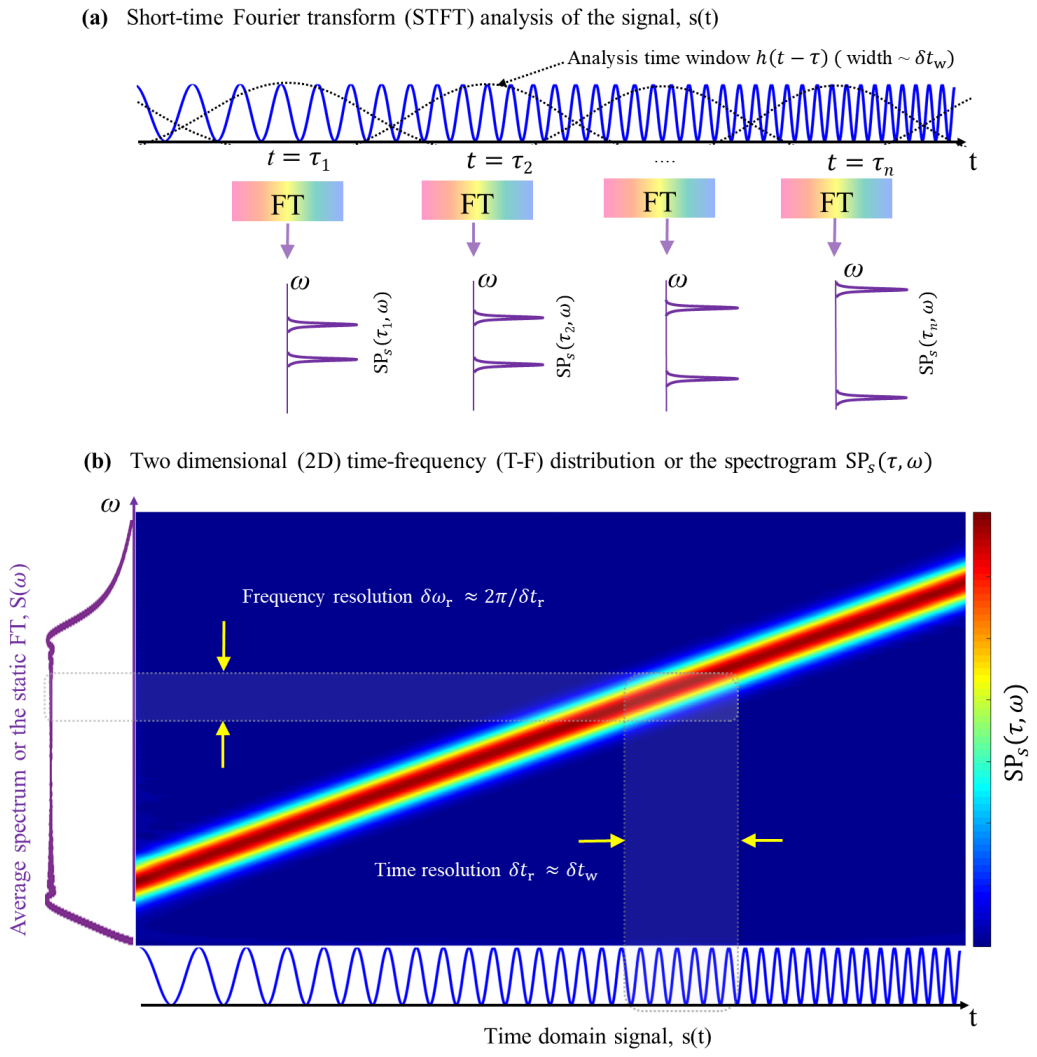

Fig. 1.1: The concept of STFT analysis of temporal signal and its 2D time-frequency representation. (a) The signal under test (SUT), $s(t)$ is temporally windowed by a window function, $h(t)$, and the Fourier transform (FT) is computed to obtain the short-time Fourier transform (STFT) of the SUT (see definition of STFT in Eq. 1.6). The square magnitude of STFT gives the spectrogram (SP). (b) 2D time-frequency representation of the spectrogram of the SUT. The color map of the 2D spectrogram represents magnitude of the windowed FT, at respective time and frequency locations. Here the SUT is a linearly increasing frequency chirp, hence the maximum amplitude of the 2D color map along the temporal axis moves from low frequency to high frequency.

typical examples of window functions include Gaussian window, Kaiser window, Hamming window, Hann window etc. The Gaussian window is of particular interest in the context of this Thesis work, because the window function in the STFT analysis proposed in this Thesis is directly related to the shape of the sampling pulses. The Gaussian shaped sampling pulses are easy to generate in practice as will be discussed in the experimental demonstration in Chapter 4. The Gaussian function in the

time and frequency domain can be defined as

$$p(t) = p_0 e^{t^2/2T_0^2} \tag{1.7a}$$

$$P(\omega) = P_0 e^{-T_0^2\omega^2/2} \tag{1.7b}$$

where T_0 is the $1/e$ width in the time domain; p_0 and P_0 are maximum amplitudes in the time and frequency domain respectively. The duration (in time or frequency) of the window function is often conveniently measured as the full width at the half maximum (FWHM) amplitude, and for the Gaussian function defined in the Eq. 1.7, the time FWHM = $\sqrt{8ln2}T_0$ and frequency FWHM=$\sqrt{8ln2}/T_0$. So the time-bandwidth product in FWHM amplitude for the Gaussian pulse in Eq. 1.7 = $8ln2$.

1.2.2 STFT analysis using DFT

The STFT is usually performed in the digital domain, hence it is useful to define the discrete-time representation of the continuous STFT integral defined in the Eq. 1.6. Initially, we represent the continuous time signal, $s(t)$ and the window function, $h(t)$ by its discrete-time versions $s[n]$ and $h[n]$ respectively, after properly sampling under Nyquist criterion. Let this sequence sampling period be 'T_{R}', so that $t = nT_{\mathrm{R}}$. Now, the STFT distribution in Eq. 1.6 has to be properly sampled by applying the Nyquist criterion both in the time and frequency domains, to avoid aliasing. The characteristics of the temporal window, '$h(t)$', i.e., its temporal width 'T', and the full frequency spectral width 'W'play a key role in the Nyquist sampling of the continuous STFT distribution, $X(\tau, \omega)$ [40]. In the discrete case, the temporal window width 'T' and spectral width 'W'are normalized by sequence sampling period 'T_{R}'. Note that these temporal and spectral widths can not be arbitrarily sharp, but rather, they are bound by the "uncertainty principle" [28,42]. Now the question is how many time and frequency samples are required to uniquely represent the distribution, $X(\tau, \omega)$. From the Eq. 1.6, for a fixed ω, the Fourier transform of the windowing function is a low pass filter of full frequency bandwidth 'W'. Then the corresponding Nquist sampling rate is $1/W$. The continuous time variable τ in Eq. 1.6 can then be replaced by $\tau = m/W = mD$, i.e., time shifting of the temporal window must be an integer multiple of the sampling rate, $m/W = mD$.

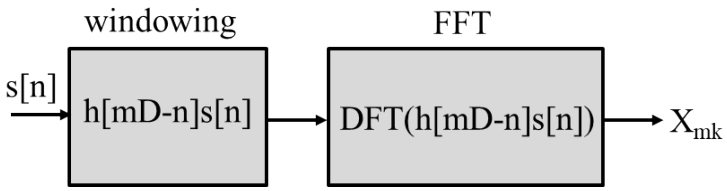

Fig. 1.2: Digital STFT analysis using the DFT. The SUT, $s[n]$ is temporally windowed with a time shifting window $h[mD-n]$, where D is the sampling period.The DFT operation is performed on the windowed SUT, as the window location moves along the time (see Eq. 1.9). The DFT operation is performed using the fast Fourier transform (FFT) algorithm on a digital signal processor.

Likewise, from Eq. 1.6, for a fixed τ, $X(\tau,\omega)$ is a continuous frequency spectrum, with a temporal duration dictated by '$h(t)$', i.e., 'T'. Nyquist sampling dictates that the frequency sampling must be at the rate of at least $1/T$. Then, the continuous frequency variable $\omega = k2\pi/T$, where k is an integer. Under these Nyquist conditions in the time and frequency domain, the continuous STFT $X(\tau,\omega)$ can be represented by its discrete version $X_{mk} = X[mD, k2\pi/T]$ without significant information loss. Then, the Nyquist sampled STFT in Eq. 1.6 can be expressed as

$$X_{mk} = X[mD, k2\pi/T] = \sum_{n=0}^{T-1} h[mD-n]s[n]e^{-j2\pi nk/T} \tag{1.8}$$

This is the analysis equation for discrete computation of STFT. Properly sampled in the time and frequency domain, the discrete STFT in the above Eq. 1.8 can be computed using the DFT. From the definition of the DFT in Eq. 1.4, the discrete STFT in the Eq. 1.8 can be expressed as

$$X_{mk} = DFT(h[mD-n]s[n]) \tag{1.9}$$

From the above discrete STFT analysis equation Eq. 1.9, computing the discrete STFT coefficients X_{mk} involve computing a T point DFT, as the window function $h[m]$ advances D samples each time. Then, during the analysis, each sample of the input sequence, $s[n]$ generates $\frac{T}{D} = TW$ samples of the output STFT, X_{mk}. The digital DFT based STFT analysis framework is summarized in the Fig. 1.2. The T point DFT in the STFT analysis is generally computed using the FFT algorithms on the DSP hardware. Moreover, as the sampling speed and bandwidth of the input sequence $s[n]$ increases, the digital STFT computation requires large number of high-speed FFTs, as the temporal windowing

is typically applied in a highly overlapping manner to avoid loosing the transient information of incoming sequence.

1.3 Real-time Fourier spectral analysis

Real-time Fourier spectral analysis (RT-SA) techniques are extensively used for analysis of a wide variety of signals encountered in many scientific and engineering problems, whenever one is interested in gaining access to the incoming signal's dynamically changing spectral content as it varies along the time domain. Moreover, RT-SA techniques are indispensable tools to study rapid transient phenomena or to capture rare/short-lived frequency events as they occur along the signal. Towards this aim, the spectral analysis needs to be performed in a real-time, continuous and gap-free manner. The term "gap-free" here means the capability to implement the desired spectral analysis with no dead times in the acquisition and processing of the signal of interest. RT-SA is useful for signals of very different nature, across the entire electromagnetic spectrum, including audio signals, radio-frequency to optical signals etc. [2, 26, 32, 43–50].

The focus of this Thesis is on RT-SA of high-speed (i.e., broadband) temporal waveforms with bandwidths into and above the GHz range. RT-SA analysis of these waveforms has gained increased interest in recent years, but it remains extremely challenging, as discussed below. GHz-bandwidth waveforms are most typically found in the electromagnetic spectrum that ranges from the microwave to the optical domain, also including millimeter and THz waves [38, 49, 51–54]. RT-SA of the high-speed temporal waveforms found in these domains is fundamental to many important applications, including broadband communications and radar technologies [36, 53, 55, 56] ultra-fast characterization, sensing and spectroscopy [52] and radio astronomy research [38], etc. These applications require the capability to perform RT-SA over instantaneous bandwidths well into the GHz range and eventually, with a temporal resolution of only a few nanoseconds or even shorter. Moreover, these applications require the RT-SA to be performed in a continuous and gap-free manner; otherwise critical information may be lost in the waveform analysis process.

Specific emerging application examples that require high-speed broadband RT-SA tools are:

- *Spectral sensing of advanced intelligent wireless environments*: In the wireless environment, the limited radio-frequency (RF) spectrum is a valuable and tightly regulated resource, lead-

ing to spectrum scarcity. Cognitive radio concepts [57], i.e., opportunistic or time sharing spectrum access as and when it is available, are becoming extremely important. The ability to independently detect spectral opportunities (spectrum sensing), is the most critical component of cognitive radio networks. Wide-band spectrum sensing methods over several GHz bandwidths through conventional methods involving analog-to-digital converters (ADC) could lead to unaffordably high sampling rates and impractical FT processing speeds. Hence revolutionary wide-band spectrum sensing techniques become increasingly important [57].

- *Radar*: Radar warning, electronic warfare and countermeasure receivers require GHz range instantaneous bandwidths to intercept ultra-wide-band pulses and estimate their characteristics, such as frequency, power, pulse width, etc., in a real-time fashion. In such a sensitive and mission-critical scenario, real-time FT processing needs to be performed over the entire GHz instantaneous bandwidth [53–56, 58].

- *Radio-astronomy* In radio-astronomical instrumentation, RT-SA techniques play a key role in detecting fast/rare transients of duration as short as a few nanoseconds or even shorter, occurring over a broad range of frequencies [38, 59].

- *Interference detection/mitigation*: The RT-SA methods that gain real-time access to the incoming high-speed signal's full 2D time-frequency distribution is extremely important, especially for detecting and mitigating RF interferences in the crowded wireless environments often found in the above discussed application scenarios [38, 53–58].

Analog high-speed broadband (microwave/optical) signals with transient events or time-varying frequencies are typically encountered in the above mentioned applications. The most conventional approach for Fourier analysis and processing of these signals involve sampling and digitizing the analog waveform using an analog-to-digital converter (ADC). The mathematical derivations involved in the sampling process is described in the Appendix A. As illustrated in Fig. 1.3, the STFT is then performed on the signal of interest in the digital domain. The signal processing involved in the STFT operation is discussed in the Section 1.2.2. The STFT computes the temporally windowed signal's DFT, as the window is being moved across the signal while ensuring a significant overlap between the consecutive truncated sections of the signal. This requires that the time delay between

consecutive temporal analysis windows is much shorter than the duration of each of these windows. Moreover, the temporal duration of the analysis window determines the temporal resolution of the RT-SA. The overlapped windowing is performed to ensure that the RT-SA is gap-free within the time resolution of the conducted dynamic Fourier analysis. Since the FFT is applied on a highly overlapped windowed signal, a large number of real-time high-speed FFT operations are required to generate the desired STFT. The FFT computations are performed on DSP engines [43, 50] and the resulting STFT is usually displayed as a 2D T-F distribution.

The digital RT-SA approaches face fundamental constraints, e.g., in terms of the processing speed and energy consumption trade-offs [60, 61], which become particularly significant as the frequency bandwidth of the analog waveform increases just above a few tens of MHz. It is challenging for digital RT-SA methods to provide a real-time dynamic Fourier analysis of the signal under test at a speed above the MHz range (i.e., equivalent to a computation of 1 million FTs per second). To give a reference, state-of-the-art commercially available DSP-based RT-SA instrumentation is presently limited to operation on instantaneous frequency bandwidths below a few hundreds of MHz, with temporal resolutions in the microsecond range, and at a maximum processing speed of about 2.6×10^6 FFTs per second [50]. These limitations are mainly associated with the performance (speed) constraints of DSP engines in computing the FFT of consecutive sections of the digitized incoming waveform in real time and in a continuous and gap-free fashion, i.e., without any gap in capturing and processing the incoming temporal signal [61]. The capabilities of available DSP-based RT-SA methods are thus insufficient to achieve the desired specifications across a wide range of emerging applications, as discussed above, such as spectral sensing in advanced intelligent wireless communication systems [53],high-speed Radar and Lidar [54], radio-astronomy observations [38,59], biomedical imaging [49] etc. These applications require the capability to perform continuous and gap-free RT-SA over instantaneous bandwidths well into the GHz range and eventually, with a temporal resolution of only a few nanoseconds or even shorter.

1.4 Analog approaches for real-time spectral analysis

Several analog signal processing methods have been explored towards high-performance broadband RT-SA [44–49]. Analog signal processing solutions are based on an implementation of the desired

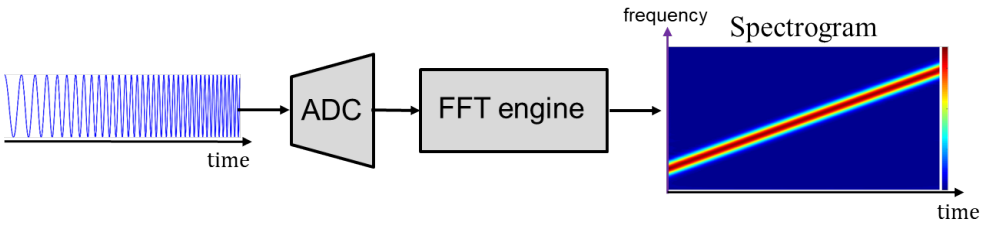

Fig. 1.3: Schematic of a conventional digital real-time spectrum analyzer (RT-SA). The incoming SUT is digitized using an ADC, and then real-time STFT analysis is performed on the digitized SUT. It involves computing large number of FFTs, usually in a highly overlapping real-time fashion.

functionality (e.g., RT-SA) directly on the signal under test (the input temporal waveform) in its original wave domain, thus avoiding the need for an ADC process. An analog-wave processing based approach that is of particular interest involves mapping the desired spectral information of the incoming waveform onto the space or time domain, so that this spectral information can then be visualized and/or processed in a direct and more efficient fashion. Standard optical spectral analysis is based on transferring the waveform frequency spectrum into the spatial domain [36]. A similar strategy has been used for the spectral decomposition of microwave signals using leaky-wave antennas [62] or after conversion into the optical domain [44–46]. An STFT analysis based on this method would require simultaneous detection of the spatially separated signal spectral components at a high speed [63]. In practice, this is an extremely challenging procedure, limited by the slow speed of detectors and difficult to scale for the analysis of even relatively simple signals. The optical spectral analysis methods based on spatial decomposition offer typical measurement update rates in the kHz range [36], thus being only suited for characterization of static or slowly-varying spectra. A time-frequency energy distribution of a broadband waveform can still be achieved through spectral analysis of consecutive time-gated sections of the waveform of interest [35, 37]. This approach is restricted to the analysis of time-limited (e.g., pulsed) repetitive waveforms and it is inherently slow.

Alternatively, a set of approaches have been developed in which the desired spectrum information is mapped along the time domain [52, 64]. This is an extremely powerful idea but so far it has been restricted to the analysis of static or periodic temporal waveforms. In the following subsections, I provide a brief overview of some of the main schemes reported for frequency-to-time mapping and their key design limitations and trade-offs.

1.4.1 Real time spectral analysis using time-mapped Fourier transform

The development of the real-time or time-mapped Fourier transform (TM-FT) concept [64–67] has represented a fundamental milestone for the real-time analog wave computation of the Fourier spectrum of time domain signals. The TM-FT relies on wave propagation in a dispersive medium, which is characterized by a dispersion relation, i.e., an equation relating frequency of a wave, ω to its propagation constant, β [68].If the frequency of the wave linearly depends on its propagation constant, then all the frequencies experience the same group delay, τ_g as the wave propagates through the medium and the wave is undistorted at the output. If the propagation constant is quadratically related to the frequency of the wave, then the group delay, τ_g varies linearly with frequency, ω, as depicted in the Fig. 1.4, and the medium is called second-order dispersive medium. In such a medium, different frequency components of a wave travel at different velocities, leading to a distortion of the output waveform- a phenomenon known as group-velocity (or chromatic) dispersion (GVD) [68]. The GVD is characterized by the second-order dispersion coefficient (dispersion accumulated per unit propagation distance), $\beta_2 = \frac{d\tau_g}{d\omega}$, which is usually given in units of ps^2/km (normalized to fiber length in km)for typical fiber optical cables. The total dispersion accumulated after propagation of a distance z is then defined as total dispersion $\ddot{\phi}_{\text{TM-FT}} = \beta_2 z$ [68]. As illustrated in the Fig. 1.4, when an input temporal waveform with a pulse width, Δt_s, and spectral bandwidth, $\Delta\omega_s$ is propagated through a second-order dispersive medium, such that the total dispersion satisfies the temporal Fraunhofer condition (see Appendix B), i.e., when the magnitude of the dispersion coefficient $\ddot{\phi}_{\text{TM-FT}}$ is much larger than the square of the input temporal waveform duration, Δt_s [64, 67], the average power of the output temporal waveform is proportional to the energy density spectrum (square magnitude of the Fourier transform) of the input waveform complex envelope evaluated at $\omega = t/\ddot{\phi}_{\text{TM-FT}}$. In the example case depicted in the Fig. 1.4, the input waveform energy density spectrum "full spectral width", $\Delta\omega_s$, is mapped on to the output temporal domain, with a frequency-to-time mapping law $t \leftarrow \omega \times \ddot{\phi}_{\text{TM-FT}}$. Detailed mathematical derivations pertaining to the TM-FT operation are provided in the Appendix B.

The TM-FT approach allows one to capture and/or process broadband spectral information through available time-domain instrumentation, at speeds orders of magnitude beyond the capabilities of any other known Fourier analysis method. This concept has been the enabler of many

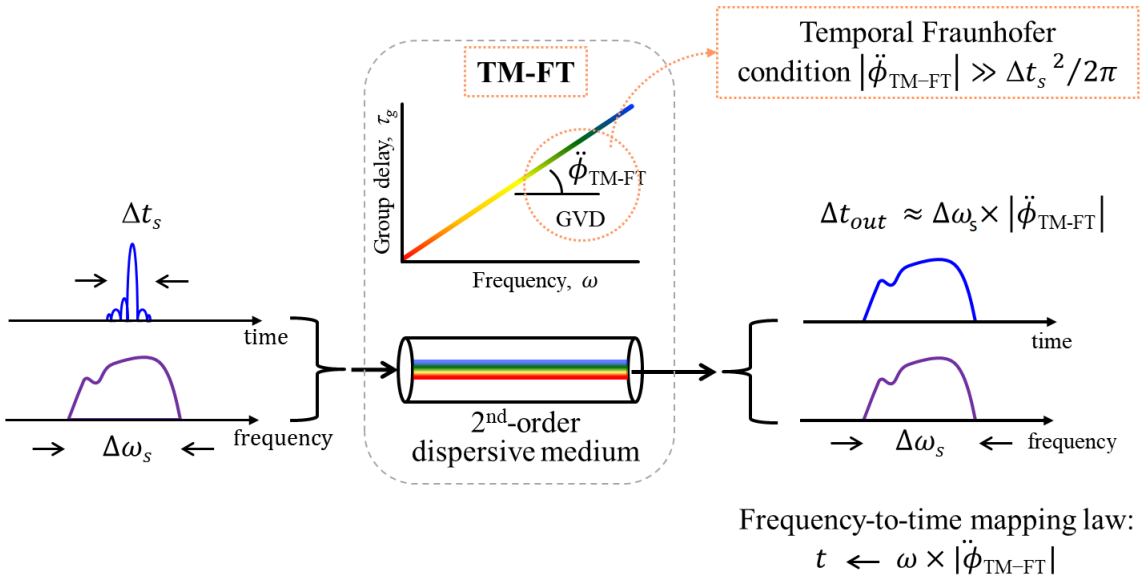

Fig. 1.4: The concept of Time-mapped Fourier transform (TM-FT). The TM-FT is based on the use of linear chromatic (or group-velocity) dispersion to directly map the incoming wave spectrum along the output time axis (frequency-to-time mapping). See Appendix B

important new applications, such as for real-time spectroscopy [69,70], interferometry or reflectometry [71,72] using light waves, dynamic optical imaging of rapidly changing events [73,74], temporal magnification and compression of broadband optical or RF waveforms for enhanced detection or generation tasks [75–81], etc.

As illustrated in Fig. 1.5(a), the TM-FT concept is still constrained only to implement the standard FT of time-limited pulsed waveforms. The TM-FT of a time-limited signal with a duration Δt_s requires stretching the signal with a group-velocity dispersion larger than $|\ddot{\phi}_{\text{TM-FT}}| > \Delta t_s{}^2$. As a result, the input signal is temporally stretched to an output duration $\Delta t_{out} \approx |\ddot{\phi}_{\text{TM-FT}}| \times \Delta\omega_s > \Delta t_s \times TBP$, where $\Delta\omega_s$ is the full frequency bandwidth of the input signal, and the time-bandwidth product $TBP \approx \Delta t_s \times \Delta\omega_s$ defines the required number of resolvable points in the spectrum analysis. Thus, in the case of a continuous incoming signal, such as the one shown in Fig. 1.5(b), the signal first needs to be truncated along the time domain, ensuring a sufficient spacing among the consecutive truncated signal sections such that to avoid any temporal overlapping among the corresponding time-mapped Fourier transforms at the output of the dispersive line. The signal portions in between the truncated sections will be lost in the Fourier analysis process. Specifically, for each analyzed signal portion with a duration Δt_s, one misses the signal information over the rest

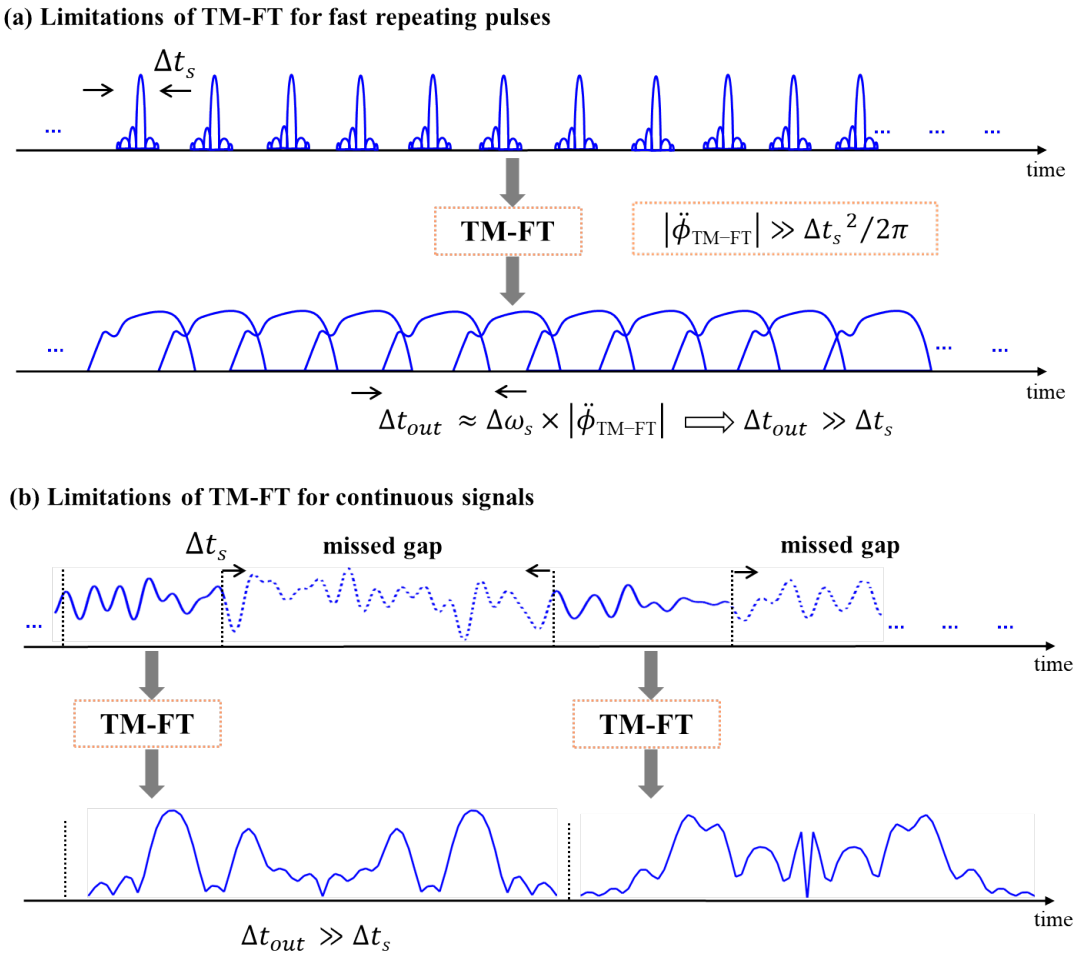

Fig. 1.5: The limitations of the TM-FT (a) TM-FT of a fast repeating temporal pulses, each of duration, Δt_s. The TM-FT maps the energy density spectrum of the input pulse to the output time axis. The output time-mapped spectrum occupies a duration, $\Delta t_{out} = \Delta\omega_s \times |\ddot{\phi}_{\text{TM-FT}}|$, much longer than the duration of the pulse at the input, Δt_s. This constraint leads to the output mapped spectral information overlapping for fast repeating pulses. Hence, the TM-FT is constrained to implement static FT of well-separated pulse-like waveforms, e.g., picosecond optical pulses spaced by at least a few nanoseconds. (b) The TM-FT analysis of continuous signals require the signals to be truncated, as the output mapped spectrum occupies a time duration much longer than the input. Hence most of the signal is missed in gaps.

of an entire section longer than $\Delta t_{out} > \Delta t_s \times TBP$. As a result, the percentage of lost information can be estimated to be at least $[(TBP-1)/TBP] \times 100$. For instance, for a TM-FT analysis with a relatively modest number of resolvable points $TBP \sim 10$, about 90% of the signal information is necessarily lost in the analysis. As such, the TM-FT approach is not suitable for a gap-free RT-SA of high-speed broadband signals.

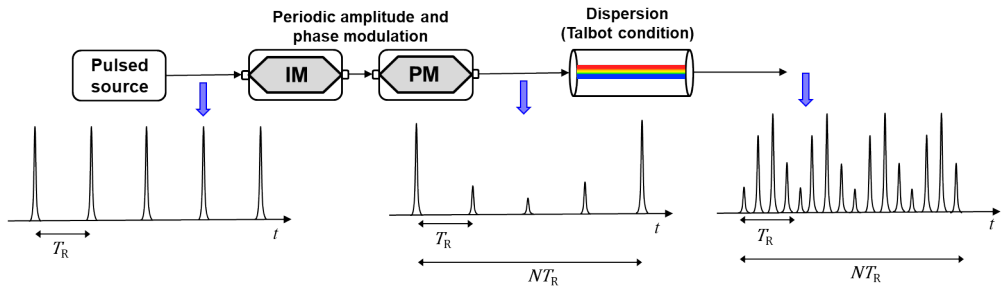

Fig. 1.6: Time-mapping the discrete Fourier transform (DFT) coefficients of a periodic waveform, by temporal modulation and dispersive propagation. The periodically modulated temporal envelope is propagated through a second-order dispersive medium under Talbot condition [82]. The output pulse train temporal envelope periodically maps the DFT coefficients of the input temporal envelope. IM: Intensity modulator; PM: phase-modulator.

1.4.2 Discrete Fourier transform using sampling and dispersion

An approach for generating the discrete Fourier transform (DFT) coefficients of a temporal envelope modulated periodically on a train of optical pulses, has been demonstrated in [82, 83]. A schematic of this approach is shown in the Fig. 1.6, involving temporal sampling and a dispersive medium. A temporal envelope is modulated periodically on a train of optical pulses using amplitude and/or phase modulators. The modulated optical pulses are then propagated through a suitably designed second order dispersive medium. The output of the dispersive element is a periodic pulse train, whose intensity repetition rate has been multiplied and whose envelope is proportional to the Discrete Fourier Transform of the modulating coefficients. Hence, this configuration offers only static spectral analysis of temporally periodic waveforms and can not be applied for dynamic real-time spectral analysis. It is important to note that the scheme proposed in this Thesis work for RT-SA involves a continuous mapping of the short-time Fourier transform (or spectrogram) of the signal under test and it is based on a design similar to the one described in [82, 83], for real-time DFT of periodic signals. Thus, this previous work represents a particular application case of the general real-time spectrogram concept that is introduced and demonstrated in this Thesis, as described in the following Section 1.5 below.

1.4.3 Real time spectral analysis using frequency shifting feedback loop

Another analog approach for the RT-SA of microwave and optical waveforms is based on a frequency-shifted feedback laser [84], whose schematic is shown in the Fig. 1.7. The frequency shifting feedback

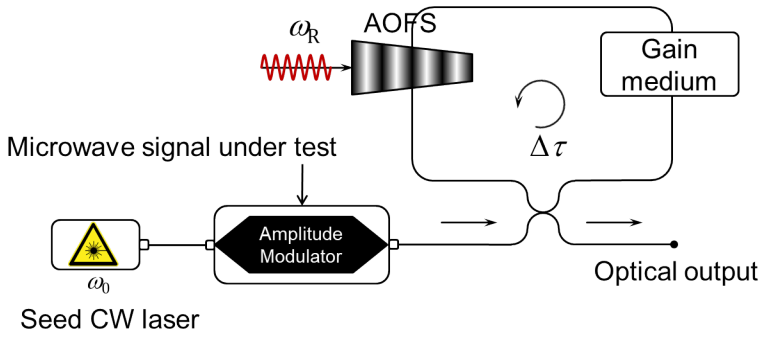

Fig. 1.7: Real-time spectral analysis of periodic waveforms by using frequency shifting feedback (FSF) laser cavity. The FSF cavity is seeded with a monochromatic wave at ω_0. An acousto-optic frequency shifter (AOFS) is driven at frequency ω_R, resulting in frequency shift per round trip equal to ω_R. $\Delta\tau$ is the cavity round trip time. The incoming signal under test is modulated on the CW seed laser. The SUT spectrum is repeatedly mapped along the output temporal domain [84].

(FSF) cavity superpose multiple signal replicas that are shifted simultaneously along the temporal and spectral domains, leading to an output temporal waveform that is proportional to the input optical spectrum. This configuration overcomes the frequency-resolution limitations of the TM-FT discussed in the Section. 1.4.1. Moreover frequency-to-time mapping of the input signal spectrum is performed with a minimum latency [84]. However, the major drawback of this configuration is that it is limited to provide a static RT-SA of periodic microwave/optical waveforms. No solution has been envisioned for implementation of the powerful concept of frequency-to-time mapping to enable a full analysis of continuous time-varying spectra.

1.5 Objectives, contributions and organization of the Thesis

The main goal of this Thesis is to design, study and experimentally demonstrate an analog signal processing approach for real-time spectral analysis of broadband waveforms, capable of providing the following target performance specifications:

- Real-time instantaneous bandwidth in the GHz range or higher,
- FT processing speeds in the GHz range,
- Temporal resolutions in the nanosecond range,
- Continuous gap-free spectral analysis to avoid missing any rare events.

Towards this aim, this Thesis proposes a new universal analog-processing scheme that enables a mapping of the full STFT of an incoming arbitrary signal along the time domain. This can be interpreted as an extension of the TM-FT concept but for a full two-dimensional T-F signal analysis and processing. The proposed approach involves temporal sampling of the incoming signal followed by a suitable amount of second-order chromatic dispersion. The principle exploits a well-designed interference among consecutively sampled and dispersed copies of the input signal. The intuition behind the proposed time-mapped STFT or the time-mapped spectrogram (TM-SP), as compared to the TM-FT approach, is illustrated in the Fig. 1.8. The full spectrogram of a continuous broadband waveform is time-mapped in the analog physical wave domain. The TM-SP effectively performs FT analysis of consecutive, virtually time-windowed sections of the incoming waveform, and maps the resulting windowed FTs (or the STFT) along the output temporal domain. The mapped spectrogram implements virtual time-windowing of the consecutive sections of the signal under test, without actually truncating the incoming waveform. Under the proper design conditions, the combination of temporal sampling followed by dispersive propagation creates a controlled interference among the delayed and frequency shifted copies of the incoming signal, resulting in a virtually windowed FT that is mapped along the output temporal domain. Moreover, this virtual windowing is implemented in a highly overlapped manner, which ensures that the real-time spectral analysis is continuous and entirely gap-free. Towards this stated goal, the central contributions of this Thesis are the following:

- The proposal and theoretical study including derivation of all main design equations for a universal analog signal processing for real-time spectral analysis, based on a time-mapped STFT. The proposed analog signal processing architecture involves two widely available signal processing units namely, temporal sampling and group-delay dispersion. The design conditions of this scheme to perform a time-mapped STFT analysis of the incoming signal will be derived and discussed in this Thesis.

- Numerical validation of the proposed time-mapped STFT concept and its main performance specifications and trade-offs. The proposed architecture is found to be particularly interesting when implemented on a photonic platform aiming at RT-SA of broadband waveforms, offering performance specifications superior to the existing solutions. Thus, without lost of

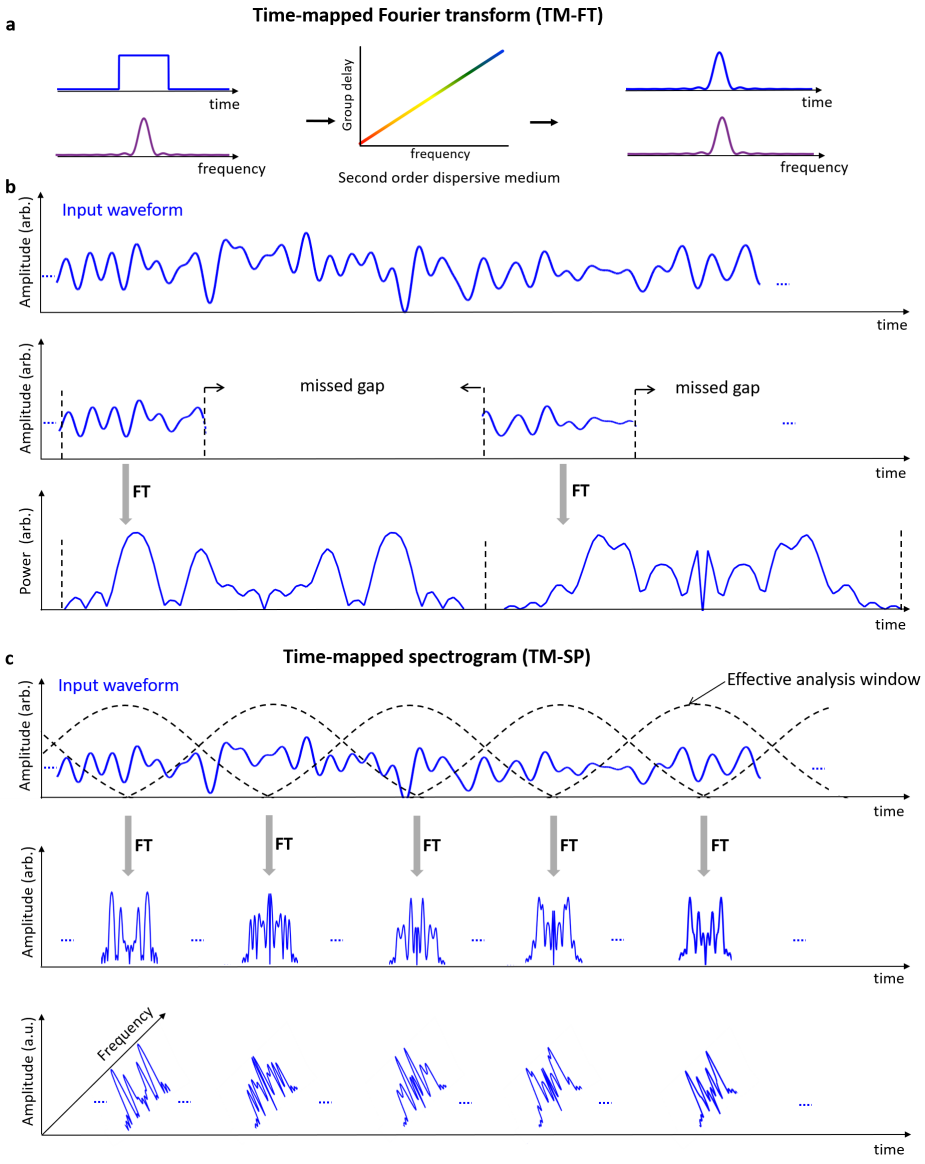

Fig. 1.8: ,Illustration of the idea of time-mapped Fourier transform (TM-FT) and the proposed time-mapped spectrogram analysis (TM-SP). (a) Analysis of a temporal pulsed waveform using the TM-FT. Here, the sinc-shaped power spectrum of the incoming square shaped temporal waveform, is mapped onto the output temporal domain after the TM-FT operation (see Appendix. B). (b) Analysis of a continuous temporal waveform using the TM-FT. The time-mapped power spectrum through TM-FT occupies a output temporal duration much longer than the input signal section duration. Hence, for a continuous time-varying signal under analysis, the signal needs to be temporally truncated and subsequently stretched along the time axis, using linear chromatic dispersion. As a result, most of the signal information, in between consecutive truncated signal sections, is simply lost in this process. (c) A conceptual illustration of the proposed time-mapped spectrogram (TM-SP) analysis applied on the same incoming time-varying waveform. In this approach, the full short-time Fourier transform (ST-FT) distribution (in amplitude and phase), or full spectrogram, of the incoming time-varying waveform is mapped along the temporal domain purely in real-time and in a continuous fashion. The TM-SP effectively performs Fourier analysis of consecutive time-windowed sections of the incoming waveform. This is achieved through a combination of short-pulse sampling and dispersive delay without using an actual truncation or windowing of the incoming waveform. The mapped spectrogram involves the analysis of time-windowed consecutive sections of the signal under test that are heavily overlapped, which ensures that the continuous real-time spectral analysis is entirely gap-free.

generality, the numerical analysis of the proposed signal processing architecture is performed on a photonic implementation aimed at RT-SA of broadband microwave signals.

- Experimental demonstration of a photonic-based time-mapped STFT for RT-SA of arbitrary broadband microwave signals, providing the following set of performance specifications 4.1:
  - Real-time instantaneous bandwidth in the GHz range or higher,
  - FT processing speeds in the GHz range, i.e., corresponding to several billions of FTs per second,
  - Temporal resolutions down to the nanosecond regime,
  - Gap-free temporal windowing to avoid missing any rare events.
- Proposal, theoretical evaluation and experimental demonstration of additional analysis and processing capabilities of the time-mapped STFT concept, including the following:
  - Time-mapped STFT of complex (amplitude and phase) optical waveforms 5.1.
  - Leveraging the band-pass sampling concept, the frequency range of operation of the time-mapped STFT is extended beyond the Nyquist sampling rate, to broadband waveforms centered at higher frequencies. Experimental results are reported on a photonic implementation of the band-pass sampling time-mapped STFT concept. 5.2
  - The capability to implement a real-time manipulation of the time-mapped STFT in the temporal domain, thus enabling real-time time-varying user-defined frequency filtering of the incoming signal, in which the filtering function can be programmed electronically. I present simulation and experimental results to validate the concept. 5.3

The outline of this Thesis is as follows: In Chapter 2, I will give a description of the central theoretical findings of this dissertation. I will first present the mathematical description of the proposed analog signal processing architecture for the RT-SA of broadband waveforms, referred to as the time-mapped STFT or the time-mapped spectrogram (TM-SP). Chapter 2 will then provide the necessary theoretical background needed for our discussions in the subsequent chapters. Chapter 3 presents numerical simulations to validate the concept as well as the main performance trade-offs of the newly proposed architecture. The proposed architecture is particularly appealing

when implemented on a photonic platform aiming at RT-SA of broadband waveforms, offering performance specifications such as instantaneous bandwidth, resolutions, and processing speed that are superior to the existing solutions. Thus, I mainly focus on this photonic implementation, aiming at RT-SA of broadband microwave signals. Some unique features of the TM-SP, which are of particular interest to interference detection application will be explored through simulations. In Chapter 4, an experimental photonic implementation of the TM-SP analog-processing system will be presented for gap-free continuous RT-SA of GHz-bandwidth microwave signals. The demonstrated experimental configuration is able to capture the full 2D T-F distribution (full SP) information of microseconds-long (ideally infinitely long - only limited by the waveform memory of the instrument used) microwave signals directly in a real-time oscilloscope, with a full instantaneous bandwidth equal to the Nyquist bandwidth of the sampling pulses, performing FT processing at the sampling rate. The proof-of-the concept experiments presented in Chapter 4 already demonstrated instantaneous bandwidth as large as ∼5 GHz, and FT processing at ∼5 billion FTs/second. The same configuration is able to offer nanoseconds temporal resolution simultaneously, enabling to capture frequency transients as short as about 2 ns. Chapter 5 presents additional capabilities of the TM-SP concept to perform real-time spectrogram analysis of complex broadband waveforms. I discuss the concept of band-pass sampling applied to the proposed TM-SP, enabling real-time spectral analysis of high-frequency waveforms. Finally, I discuss a signal-processing functionality, known as time-varying frequency filtering, where the signal's time-frequency distribution (i.e., the STFT) is modified in a user-defined manner using temporal modulation. This Thesis then concludes with Chapter 6, pointing to existing challenges and unprecedented opportunities that the TM-SP brings to real-time spectral analysis and processing.

Chapter 2

Theory of Time-mapped Spectrogram

This chapter presents the central theoretical findings of this dissertation, most importantly the concept of time-mapped spectrogram (TM-SP) [AJ1], [P1], [AC4]. I will first present the mathematical description of the TM-SP -a universal analog signal processing architecture for the RT-SA of temporal waveforms. Some important properties of the TM-SP, are discussed in detail, such as its time and frequency resolutions as well as its oversampling features and related performance improvements.

2.1 Operation principle of the time-mapped spectrogram (TM-SP) analysis

For the purpose of our theoretical analysis, let the temporal signal under test (SUT) be generally expressed as (analytical function) $s(t_1)e^{i\omega_0 t_1}$, where $s(t_1)$ is the signal's complex temporal envelope. Here, ω_0 is the signal's carrier frequency ($\omega_0 = 0$ for a base-band signal). Note t_1 is used to denote the time variable at the system input, whereas t_2 will be used for the time variable at the system output. The SUT is assumed to be band-limited with a full frequency bandwidth denoted by $\Delta\omega_s$. No constraints are imposed on the signal's time duration, so that in general, this can be infinitely long($-\infty \leq t_1 \leq +\infty$). Fig. 2.1 shows the temporal base-band SUT, $s(t_1)$ along the horizontal axis, and its spectrum, $S(\omega_1) = \mathrm{FT}(s(t_1))$ along the vertical axis, where FT stands for the Fourier transform as defined in Eq. 1.1. As illustrated in Fig. 2.1, the proposed concept for TM-SP involves processing the SUT with a cascade of two standard signal-processing units, namely 1) a

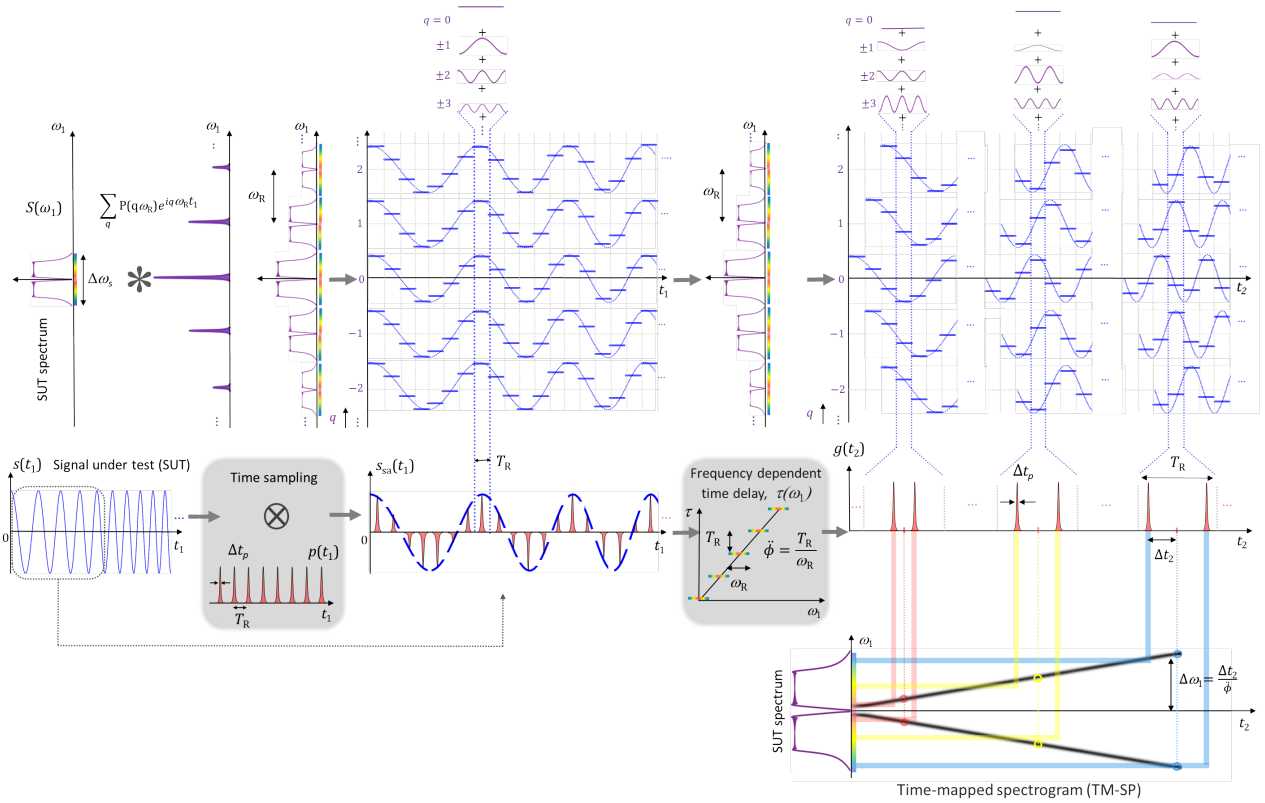

Fig. 2.1: Basic principle of the proposed TM-SP method. The scheme involves initially (1) a temporal sampling unit (first shaded box), where the signal under test (SUT), with a complex temporal envelope defined by $s(t_1)$, is modulated by a repetitive train of short pulses, with a sampling period defined by T_R. Temporal sampling generates frequency-shifted copies of the input SUT, whereas each spectral copy is shifted by $\omega_R = 2\pi/T_R$. The temporal sampling is followed by (2) a frequency-dependent (dispersive) time-delay unit (second shaded box), $\tau(\omega_1)$, where frequency shifted spectral copies (by ω_R) are delayed with respect to each other by an amount T_R. This second unit can be implemented through a dispersive element providing a linear group delay (as a function of radial frequency) with a slope defined by the parameter $\ddot{\phi} = \pm\frac{T_R}{\omega_R} = \frac{{T_R}^2}{2\pi}$ (dispersion), over the full frequency bandwidth of the sampling pulses. As illustrated in the top section of the figure, the interference between the simultaneously time delayed and frequency shifted copies of the SUT produces a temporal pattern $g(t_2)$ along each sampling-period slot T_R that is proportional to the FT of the corresponding time-windowed section of the analyzed input signal, thus implementing a continuous time mapping of the signal's STFT or full SP. In the example shown here, the SUT is a sinusoidal function with a frequency that is linearly increasing along time, so-called a linear frequency chirp signal. Thus, at the output of the proposed scheme, the FT of the corresponding time-windowed section copy of the SUT -namely two finite-duration pulses, corresponding to the double-side spectrum of a single-frequency sinusoidal function -is mapped along the time domain within each analysis period of duration T_R. The obtained FT changes period by period -i.e., with an inter-pulse separation $2 \times \Delta t_2$ (proportional to twice the corresponding sinusoidal frequency) that increases linearly period by period -as the temporal analysis window is 'virtually' shifted by this same delay (T_R).

temporal sampling unit, and 2) a frequency dependent time delay unit. The operation of each signal-processing unit on the incoming SUT is described below.

1. A conventional temporal sampling unit is used to modulate the SUT with a periodic train of short pulses [1]. In particular, the sampling pulse train $r(t_1)$ is represented as

$$r(t_1) = \sum_m p(t_1 - mT_{\mathrm{R}}), \tag{2.1}$$

where $p(t_1)$ defines the temporal shape of each individual short pulse in the sampling sequence, and T_{R} holds for the repetition period, i.e., the sampling repetition frequency is $\omega_{\mathrm{R}} = 2\pi/T_{\mathrm{R}}$. Fig. 2.1 shows the sampling pulse train inside the temporal sampling unit. We recall that for an ideal sampling process, one must ensure that the duration of the individual sampling pulses is shorter than the repetition period, i.e., $\Delta t_p < T_{\mathrm{R}}$, whereas the repetition frequency must be larger than the full frequency bandwidth of the sampled signal $s(t_1)$, i.e., $\Delta\omega_s < \omega_{\mathrm{R}}$. The latest condition is known as the Nyquist criterion discussed in the Eq. A.6. The sampled signal at the output of this unit can be mathematically expressed as follows:

$$s_{sa}(t_1) = s(t_1)\sum_m p(t_1 - mT_{\mathrm{R}}) \propto s(t_1)\sum_q P(q\omega_{\mathrm{R}})e^{iq\omega_{\mathrm{R}}t_1} = \sum_q P(q\omega_{\mathrm{R}})s(t_1)e^{iq\omega_{\mathrm{R}}t_1}, \tag{2.2}$$

where $\propto$ holds for proportionality, and $m, q = 0, \pm1, \pm2, ...$ In deriving this equation, we have used the Fourier series representation of a periodic sampling pulse train [1], where $P(\omega_1)$ is the frequency spectrum of the individual sampling pulse train, i.e., $P(\omega_1) = \mathrm{FT}(P(\omega_1))$, where FT stands for the Fourier transform as defined in Eq. 1.1. The full-width spectral extent of $P(\omega_1)$ is $\sim \Delta\omega_p$. The Fourier spectrum of the sampling pulse train, as represented by the Fourier series expansion in Eq. 2.2, is shown along the vertical frequency axis in Fig. 2.1. Notice Eq. 2.2 ignores any potential latency in the sampling unit, an effect that is considered in our analysis at a later stage. Each of the factors of the sum obtained in the Eq. 2.2, i.e., $P(q\omega_{\mathrm{R}})e^{iq\omega_{\mathrm{R}}t_1}$, corresponds to a copy of the input signal $s(t_1)$, frequency shifted by $q\omega_{\mathrm{R}}$ and weighted by the corresponding Fourier coefficient of the sampling pulse, $P(\omega_{\mathrm{R}})$. Fig. 2.1 shows the temporal sampled signal, $s_{sa}(t_1)$ at the output of the sampling unit, and its corresponding frequency spectrum, along the vertical frequency axis. The input signal's spectral copies that are frequency shifted by $q\omega_{\mathrm{R}}$, are also shown in the 2D time-frequency plot. Then, each of the sampled pulse at the output of the sampling unit can be interpreted as a coherent summation

of the input SUT's frequency shifted copies (by $q\omega_{\mathrm{R}}$), weighted by the corresponding sampling pulse Fourier coefficient $P(q\omega_{\mathrm{R}})$, as represented at the top of the 2D time-frequency plot in Fig. 2.1. The same can be interpreted from Eq. 2.2. Also recall that the Nyquist criterion ensures that each of these signal copies extend over a frequency bandwidth narrower than ω_{R}, avoiding their spectral overlapping.

2. The sampling process in the above step (1) is followed by a frequency-dependent (or dispersive) time delay unit shown in the Fig. 2.1. It can be understood as an ideal linear all-pass type filter, that alters only the phase profile of the incoming signal. Particularly, here the function of the dispersive unit is to cause a delay of $\Delta\tau$ between the frequencies that are separated by ω_{R}. As illustrated in the Fig. 2.1, the consecutive spectral copies of the sampled SUT, frequency spaced by ω_{R}, are delayed by an amount $\Delta\tau$ with respect to each other. For simplicity, in the following analysis, we assume a positive delay as a function of the frequency shift (i.e., a positive slope of the delay vs frequency curve or dispersion parameter) but similar results would be obtained for a negative dispersion parameter. Mathematically, the temporal waveform at the output of the dispersion delay unit can then be expressed as $g(t_2)e^{i\omega_0 t_2}$, where $t_2 = t_1 - \Delta t_L$ defines the time variable at the system output, simply delayed with respect to the input by a latency or overall average delay of the system (including the latency in the sampling and dispersive delay units), Δt_L. The resulting temporal complex envelope of the output waveform is then

$$\begin{aligned} g(t_2) &\propto \sum_q P(q\omega_{\mathrm{R}}) s(t_2 - q\Delta\tau) e^{iq\omega_{\mathrm{R}}(t_2 - q\Delta\tau)} \\ &= \sum_q P(q\omega_{\mathrm{R}}) s(t_2 - q\Delta\tau) e^{iq\omega_{\mathrm{R}} t_2} e^{(-iq^2\omega_{\mathrm{R}}\Delta\tau)}. \end{aligned} \tag{2.3}$$

Notice that in deriving Eq. 2.3 from Eq. 2.2 we have simply implemented the variable change: $t_1 \leftarrow t_2 - \Delta\tau$ to account for the delay that is introduced by the dispersive unit (2) on each of the spectral copies of the sampled input signal, i.e., a relative delay of $q\Delta\tau$ for the q^{th} spectral copy with respect to the original one (copy corresponding to $q = 0$, centered at $\omega_2 = 0$). Eq. 2.3 shows that the waveform at the output of the two concatenated processing units, $g(t_2)$, consists of the coherent addition of a set of copies of the input SUT that are simultaneously shifted in time (with a

relative delay between consecutive copies of $\Delta\tau$) and in frequency (with a relative frequency spacing between consecutive copies of ω_{R}), while being weighted according to the frequency spectrum of the sampling pulses, namely, following the function $P(q\omega_{\mathrm{R}})$. The output temporal waveform, $g(t_2)$ as a coherent summation of input SUT copies that are simultaneously shifted in frequency and time, is illustrated in the 2D time-frequency plot at the output of the dispersive delay unit in the Fig. 2.1.

We further assume that the relative time delay in between consecutive spectral copies of the SUT is set to be equal to the sampling period, i.e., $\Delta\tau = T_{\mathrm{R}}$. Under this condition, the quadratic phase term in the latest sum in Eq. 2.3 is equal to unity, i.e., $e^{(iq^2\omega_{\mathrm{R}}\Delta\tau)} = 1$, for all values of q. In addition, the slope of the dispersive delay process (dispersion parameter) is then defined as

$$\mid \ddot{\phi} \mid = \frac{\Delta\tau}{\omega_{\mathrm{R}}} = \frac{{T_{\mathrm{R}}}^2}{2\pi} \tag{2.4}$$

We reiterate that though the case of a positive dispersion parameter is considered in the detailed analysis presented here, similar results would be obtained for a negative dispersion parameter. To proceed further with our analysis, we will use the fact that the above-stated Nyquist criterion implies that the function $s(t_2)$ remains approximately constant over the temporal sampling period $\Delta\tau = T_{\mathrm{R}}$ [9]. It is thus convenient to evaluate the resulting waveform from Eq. 2.3 over time slots of duration T_{R}, namely, over each of the consecutive time slots defined by $nT_{\mathrm{R}} - \frac{T_{\mathrm{R}}}{2} \leq t_2 < nT_{\mathrm{R}} + \frac{T_{\mathrm{R}}}{2}$, with $n = 0, \pm 1, \pm 2, ...$ In the nth time slot, the function $s(t_2)$ can be approximated by $s(nT_{\mathrm{R}})$. The temporal waveform at the output of the dispersive delay unit along the nth time slot can then be expressed as follows:

$$\begin{aligned} g_n(t') &\propto \sum_q P(q\omega_{\mathrm{R}}) s(nT_{\mathrm{R}} - qT_{\mathrm{R}}) e^{iq\omega_{\mathrm{R}}t'} \\ &= e^{in\omega_{\mathrm{R}}t'} \sum_{q'} P([n-q']\frac{T_{\mathrm{R}}}{\ddot{\phi}}) s(q'T_{\mathrm{R}}) e^{(i\omega_1 q' T_{\mathrm{R}})}, \end{aligned} \tag{2.5}$$

where we have implemented the following variable changes: $t' = t_2 - nT_{\mathrm{R}}, q' = n - q$ (thus, $q' = 0, \pm 1, \pm 2, ..., \pm\infty$), and $\omega_1 = t'/\ddot{\phi}$. We define now the following new function:

$$h(t) = P(\omega_1 = -t'/\ddot{\phi}) \tag{2.6}$$

which will be referred to as the "temporal window function". Introducing this newly defined function in Eq. 2.5, we obtain:

$$g_n(t') \propto e^{in\omega_{\mathrm{R}}t'} \sum_{q'} h(q'T_{\mathrm{R}} - nT_{\mathrm{R}}) s(q'T_{\mathrm{R}}) e^{i\omega_1 q' T_{\mathrm{R}}} \tag{2.7}$$

The sum in the Eq. 2.7 can be interpreted as the discretized version of the corresponding continuous-time integral form, sampled at $t_1 \leftarrow q'T_{\mathrm{R}}$, and in particular, within the defined analysis temporal slot ($-T_{\mathrm{R}}/2 \leq t' \leq T_{\mathrm{R}}/2$), the expression in Eq. 2.7 is then equivalent to:

$$g_n(t') \propto \int_{-\infty}^{\infty} h(t_1 - nT_{\mathrm{R}}) s(t_1) e^{-i\omega_1 t_1} dt_1, \tag{2.8}$$

where, we recall that $\omega_1 = t'/\ddot{\phi}$. The equivalence between the discretized and continuous-time version of the same expression in Eq. 2.7 and Eq. 2.8 is based on the fact that the temporal sampling process used to establish this eqivalance, $t' \leftarrow q'T_{\mathrm{R}}$, satisfies the Nyquist critetion in regard to both the input SUT, $s(t_1)$ (as per the specification of the sampling unit (1)), and the newly defined temporal window function $h(t_1)$. Notice that following the definition in Eq. 2.6, sampling the window function $h(t_1)$ at $q'T_{\mathrm{R}}$ corresponds to sampling the pulse frequency spectrum, $P(\omega_1)$, at $q\omega_{\mathrm{R}}$, and this process strictly satisfies the related Nyquist criterion, considering that the pulse temporal width is necessarily shorter than the sampling period, $\Delta t_p < T_{\mathrm{R}}$. Finally, Eq. 2.8 involves Fourier transform (FT), as defined in Eq. 1.1, so it can be re-written as follows:

$$\begin{aligned} g_n(t_2) &\propto e^{in\omega_{\mathrm{R}}t_2} \times \mathrm{FT}(h(t_1 - nT_{\mathrm{R}}) s(t_1))_{\omega_1 = \frac{t_2 - nT_{\mathrm{R}}}{\ddot{\phi}}} \\ &= e^{in\omega_{\mathrm{R}}t_2} \times \mathrm{STFT}_s(nT_{\mathrm{R}}, \omega_1 = \frac{t_2 - nT_{\mathrm{R}}}{\ddot{\phi}}), \end{aligned} \tag{2.9}$$

where we have used the definition of the short-time Fourier transform (STFT) from Eq. 1.6. The result in Eq. 2.9 shows that except for an additional linear phase term $e^{in\omega_{\mathrm{R}}t_2}$, the temporal waveform at the output of the proposed system, $g_n(t_2)$, when evaluated at each time slot $nT_{\mathrm{R}} - \frac{T_{\mathrm{R}}}{2} \leq t_2 < nT_{\mathrm{R}} + \frac{T_{\mathrm{R}}}{2}$, is proportional to the STFT of the waveform under analysis, $s(t_1)$, namely the FT of a time-windowed version of the SUT, with the central location of the temporal analysis window, $h(t_1)$, running as nT_{R}, with $n = 0, \pm 1, \pm 2, ..., \pm\infty$.

Thus, the temporal waveform, $g(t_2)$ at the output of the proposed system that performs a coherent summation of input SUT copies, that are simultaneously shifted in frequency and time, as illustrated in the 2D time-frequency plot at the output in Fig. 2.1, provides a direct computation of the signal spectrogram (SP), evaluated at the temporal sampling points (nT_{R}). In particular, for the n^{th} sampling-period slot, the intensity of the output temporal waveform is proportional to a full SP or time-frequency distribution of the SUT, i.e., $|g_n(t_2)|^2 \propto SP_s(nT_{\mathrm{R}}, \omega_1 = \frac{t_2 - nT_{\mathrm{R}}}{\ddot{\phi}})$. Most importantly, within each of the analysis sampling-period slots, the corresponding STFT information is directly mapped along the time domain. Specifically, the output temporal waveform along the sampling-period slot centered at nT_{R} ($g_n(t_2)$) is just a time-mapped copy of the corresponding STFT of the input signal, i.e., the truncated FT computed with a temporal window centered around $t_1 = nT_{\mathrm{R}}$. In this manner, the SUT's entire dynamic spectrum is mapped on to the output temporal domain within each sampling period, nT_{R} as illustrated at the bottom of the output temporal waveform in Fig. 2.1. Here, the frequency-to-time mapping factor in the described process ($\Delta\omega_1 \rightarrow \Delta t_2$) is defined by the slope of the dispersive delay process, i.e., $\Delta t_2/\Delta\omega_1 = \ddot{\phi} = T_{\mathrm{R}}/2\pi$. As a result, the entire frequency spectrum of the truncated signal (Nyquist limited), when mapped along the time domain, is comprised within the corresponding analysis period (with a duration T_{R}), namely, $|\ddot{\phi}| \times \Delta\omega_s < T_{\mathrm{R}}$.

As illustrated in Fig. 2.1, a central assumption in the above derivations is that the consecutive spectral copies of the sampled SUT, frequency spaced by ω_{R}, undergoes a constant group delay $\Delta\tau$ with respect to each other, corresponding to a linear phase variation across the bandwidth of each of these copies. As mentioned above, the group delay increases from one spectral copy to the adjacent one by the differential delay defined in Eq. 2.4. In practice, this operation is implemented using a second-order dispersive medium, such as the one used for implementing TM-FT in Section.1.4.1. This implies that each of the frequency copies of the input SUT is affected by an additional quadratic spectral phase filtering factor of the form $\phi_{\mathrm{disp}} = \ddot{\phi}{\omega'_1}^2$, where ω_1 is the frequency variable relative to the central frequency of the corresponding SUT copy. In principle, this factor should induce a temporal distortion on the signal under analysis as per the implemented dispersion operation. However, in general, this distortion is very small, and it can be actually neglected in most practical cases. Specifically, the overall phase excursion introduced by this dispersive factor across the frequency bandwidth of the SUT ($\Delta\omega'_s$) can be estimated $\Delta\phi_{\mathrm{disp}} = |\ddot{\phi}|(\Delta\omega'_s/2)^2 = ({T_{\mathrm{R}}}^2/2\pi)(\Delta\omega'_s/2)^2$,

where we have considered the value of the dispersion parameter in Eq. 2.4. Recall that the full signal bandwidth must be smaller than the sampling frequency ω_{R} (Nyquist criterion); additionally, in most practical cases, the SUT will exhibit a spectrum with a decreasing amplitude towards the signal's edges (as the frequency relative to the signal's central frequency is increased), such that a fair estimate is that most signal energy will be comprised within a frequency bandwidth around half of the sampling frequency,$\Delta\omega_s' < \omega_{\mathrm{R}}/2$. This implies that the total phase excursion induced by the dispersive factor will be constrained to $\Delta\phi_{\mathrm{disp}} < \pi/8$, such that the overall effect of this factor is negligible.

Finally, it is also worth noting that the condition in Eq. 2.4 is in fact the so-called fundamental temporal Talbot condition for a periodic train of pulses (of period T_{R}) propagating through a linear group-velocity dispersive medium with a total second-order dispersion coefficient [85]. Recall that under this condition, the periodic pulse train propagates through the dispersive medium without undergoing any distortion in its temporal profile, except for practical passive losses in the medium; said other way, the original pulse train is exactly replicated (self-imaged) at the output of the dispersive medium. This case would correspond to the ST-FT of a uniform temporal profile (constant function), leading to a periodic set of short pulses, each with a width fixed by the time-mapped frequency resolution (width of the original sampling pulses), spaced by the temporal analysis period T_{R}. As described in Section 1.4.2, the fact that a modulated pulse train can be Fourier transformed by propagation through a linear dispersive medium under the Talbot conditions have been previously anticipated and demonstrated [82]. In this previous work, a main assumption is that the pulse train is modulated by a periodic function, leading to the implementation of a time-mapped FT of the periodic modulation; thus, the resulting FT is itself a discrete function that is also periodically repeated as mapped along the time domain. This previous scheme can be interpreted as a particular case of the general concept introduced in this thesis,involving a time-mapped STFT computation of a fully arbitrary(including, non-stationary) modulation.

2.2 Time and frequency resolutions

As discussed in Chapter 1, the time resolution in standard STFT analysis is determined by the duration of the "temporal analysis window" function $h(t)$, and the corresponding frequency resolution

is given by the frequency bandwidth of $h(t)$ [24]. As a result, the time and frequency resolutions of the TM-SP approach are respectively determined by the duration and frequency bandwidth of the virtual window function in the implemented STFT calculation, $h(t)$, which is given by Eq. 2.6. The window function, $h(t)$ is proportional to the FT of the sampling pulse, scaled along the time domain by the dispersion factor $\ddot{\phi}$, as depicted in Fig. 2.2. Thus, the "time resolution" of the proposed spectrogram analysis is dictated by the temporal duration of the window function $h(t)$, Δt_h, whereas the corresponding "frequency resolution" is simply given by the inverse of the time resolution. Mathematically, we obtain the following estimates, assuming a definition of the involved width/resolution values at the full-width at half maximum (FWHM) of the corresponding time/frequency functions:

$$\text{Time resolution: } \delta t_r \approx \delta t_h \approx |\ddot{\phi}| \times \Delta\omega_p \tag{2.10a}$$

$$\text{Frequency resolution: } \delta\omega_r \approx \Delta t_p / |\ddot{\phi}| \tag{2.10b}$$

where, $\Delta\omega_p$ is the FWHM of the individual sampling pulse frequency spectrum, $P(\omega_1)$, and Δt_p is the FWHM of the temporal sampling pulse, $p(t)$, see Fig. 2.2. In deriving these equations, we have also assumed that in a first approximation, $\Delta t_p \approx 2\pi/\Delta\omega_p$.

The estimates in Eq. 2.10 indicate that the resolution of the time-mapped spectrum is directly determined by the temporal width, Δt_p, of the pulses used in the sampling process. As a result, each windowed Fourier spectrum (mapped along a duration T_{R}) is resolved in time with a total number of features (or points) given by the ratio of the sampling period to pulse width, $M \approx T_{\mathrm{R}}/\Delta t_p$. The value of the sampling period, T_{R}, is determined by the maximum frequency bandwidth of the SUT (Nyquist criterion). Thus, in a practical setup, the number of points of the conducted spectral analysis can be modified by correspondingly adjusting the time-frequency resolution of the resulting SP, which in turn can be tailored as desired by properly tuning the sampling pulse frequency bandwidth (or time width). The effect of the sampling pulse width on the time and frequency resolutions of the TM-STFT is further discussed through numerical simulations in the Chapter 3.

The above findings indicate that in order to capture the resulting SP, one would need to utilize a detection system with a sampling rate and bandwidth higher than the inverse of the resolution of

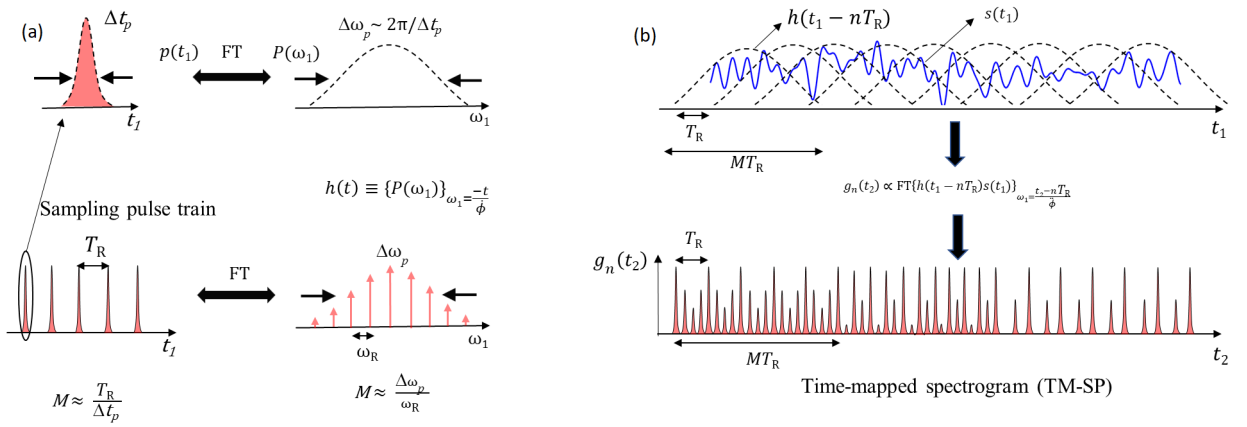

Fig. 2.2: Illustration of the "virtual temporal analysis window" implemented by the time-mapped spectrogram scheme. (a) A sampling pulse train with time bandwidth product (TBP), $M \approx \frac{T_R}{\Delta t_p} = \frac{\Delta\omega_p}{\omega_R}$ is used for temporal sampling. Here, $T_R, \Delta t_p$ are the temporal period and pulse width of the sampling pulse train respectively, and $\omega_R, \Delta\omega_p$ are repetition frequency and spectral width of the same pulse train. The implemented virtual temporal analysis window, $h(t)$ is related to the sampling pulse, $p(t_1)$ as $h(t) = \{P(\omega_1)\}_{\omega 1=\frac{-t}{\phi}}$. (b) An illustration for understanding the action of the virtual temporal analysis window, $h(t)$ on the incoming signal, $s(t)$ in the time-mapped spectrogram (TM-SP). The windowed spectrum is mapped on to the output temporal domain within each temporal period, T_R, while the position of the window moves by the same period, T_R. The virtual temporal analysis window, $h(t)$ has a duration, $\delta t_r \approx M \times T_R$ (See Eq.2.11). Hence the time-mapped spectrum keeps the same over M sampling periods, MT_R.

the time-mapped SP profile, which is determined by the duration of the individual sampling pulses, Δt_p. This may impose stringent requirements in the detection stage. Notice that the use of a detection system offering a time resolution lower than that required to capture the sampling pulses would worsen the frequency resolution of the captured SP distribution. In particular, if as a result of the insufficient time resolution of the detection system, the individual sampling pulse is captured with an increased time-width of $\Delta t_d > \Delta t_p$, then, the frequency resolution of the detected SP will be reduced to $\delta\omega_{r,d} \approx \Delta t_d/|\ddot{\phi}|$. Nonetheless it is important to mention that the time resolution of the obtained SP depends only on the features of the sampling pulse spectrum as mapped along the time domain, according to the estimate in Eq. 2.10(a), and thus, this is not affected by the detector resolution. As discussed in the following section, the detection requirements to achieve the best possible frequency resolution could be significantly relaxed by exploiting the fact that through the TM-SP analysis, the same spectral profile is mapped over many consecutive representation periods, leading to an effective "oversampling" of the mapped spectral information.

2.3 Gap-free operation and repeated STFT patterns

The time resolution implemented by the TM-SP, defined in Eq. 2.10(a), is longer than the sampling period, as it can be easily inferred from the above equations. Specifically, by introducing the main dispersion condition for STFT, Eq. 2.4, into the expression for the time resolution in Eq. 2.10(a), we obtain the following:

$$\delta t_r \approx \ddot{\phi} \times \Delta\omega_p = \frac{{T_\mathrm{R}}^2}{2\pi}\Delta\omega_p \approx \frac{T_\mathrm{R}}{\Delta t_p}T_\mathrm{R} \approx M \times T_\mathrm{R} \tag{2.11}$$

This latest equation implies that the time resolution of the conducted TM-SP is about M times longer than the sampling period, where we recall that M provides an approximate estimate of the number of points of the implemented FT analysis. This feature is illustrated in Fig. 2.2(b), where the duration of the virtual temporal analysis window, $h(t)$ is about M times longer than the sampling period, T_R, while the window is being shifted by every T_R. The windowed FT is then mapped on to the output temporal domain, every T_R. Typically, for the sake of accuracy, one is interested in computing the FT analysis with a sufficiently large number of points, let's say, $M > 10$. In a STFT analysis, the calculated spectral profile remains nearly identical over a duration fixed by the time resolution, such that in principle, variations in the frequency characteristics of the SUT shorter than the time resolution cannot be captured by the STFT analysis [24]. Recall that in the TM-SP, each time-truncated FT profile is computed with a time-window that is shifted by an amount of T_R with respect to that of the previously computed FT profile; each of these profiles is then consecutively time-mapped over a slot of duration equal to the sampling period, T_R. As such, the fact that the time resolution of the conducted analysis is M times longer than T_R, Eq. 2.11, implies that the same spectral profile is expected to be captured over a number M of consecutive periods along the output temporal waveform, as illustrated in Fig. 2.2. The simulation results demonstrating this feature are discussed in the next Chapter 3.

The implications of the above observations are twofold. On the one hand, the temporal window used for the STFT analysis (δt_r) is typically much longer than the temporal shift in between consecutive analysis windows (T_R). This implies that there is a heavy overlapping of consecutive temporal analysis windows in the TM-SP calculation, see Fig. 2.2(b), which ensures that the conducted RT-SA is gap-free, with no dead times in the acquisition or FT computation. On the

other hand, because the time-mapped windowed spectrum keeps approximately the same (i.e., repeating) over a number M of representation periods, there is an effective oversampling of the STFT information, as illustrated in the output temporal waveform in Fig. 2.2. This latest feature can be exploited to relax the specifications, e.g., sampling rate, of the detection stage aimed at capturing the obtained time-frequency distribution. In principle, to capture the resulting SP with no distortion, one would need to sample the output temporal waveform at a rate determined by the resolution of the time-mapped SP profile, namely, with a sampling period shorter than the duration of the individual sampling pulses, Δt_p. However, by exploiting the described repetition of the calculated spectra along the time domain, the obtained spectrogram could be still fully retrieved by sampling the output waveform at a rate just slightly below the original (Nyquist) sampling rate, e.g., with a period equal to $T_{\mathrm{R}} + T_{\mathrm{R}}/M$. Notice that the detection should still be performed with a time resolution better than the sampling pulse duration. Numerical simulations are shown in the Chapter 3 to illustrate these features of the TM-SP. Other strategies might be explored to relax the specifications of the detection stage in the proposed TM-SP scheme by exploiting the resulting spectral information oversampling.

2.4 Conclusions

In this chapter, I have introduced the theory of TM-SP - a universal analog signal processing framework to map the full STFT of an incoming arbitrary waveform along the time domain through a very simple design, involving two widely available, basic signal-processing units, namely temporal sampling and dispersive delay. The proposed approach could be readily used to capture the full STFT of high-speed signals (e.g., microwave to optical) in real time, entirely avoiding the need for computationally intensive fast Fourier transform algorithms. I have discussed the main design trade-offs and versatility offered by the TM-SP architecture. As a relevant example, the time and frequency resolutions of the conducted analysis can be conveniently tuned by simply varying the sampling pulse width (for instance, through a customized band-pass filtering of the sampling pulse train). On the other hand, as expected for a STFT or SP analysis, the time and frequency resolutions in the TM-SP analysis are fundamentally limited by the Fourier transform uncertainty principle [24, 29]. Finally, I have highlighted the oversampling features of the time-mapped STFT

information -a unique feature of the proposed TM-SP method, and how these oversampling features could be used to relax the detection bandwidth. In the next chapter, I present extensive numerical simulations to validate the TM-SP concept and the theoretical findings described in this chapter.

Chapter 3

Numerical Simulations of Photonics-based Time-mapped Spectrogram

This chapter presents numerical simulations to validate the central theoretical findings on the time-mapped spectrogram (TM-SP) discussed in Chapter 2. A practical photonic-based platform for TM-SP implementation is proposed and numerically simulated. The important properties of the TM-SP as discussed in Chapter 2, such as time and frequency resolutions, continuous gap-free operation, oversampling features, are all verified through extensive numerical simulations [AJ2]. Finally, we show that a well designed and realistic TM-SP photonic implementation is suitable for real-time spectral analysis (RT-SA) of broadband waveforms, and capable of providing the targeted performance specifications outlined in Chapter 1, namely

- Real-time instantaneous bandwidth in the GHz range or higher,
- FT processing speeds in the GHz range,
- Temporal resolutions in the nanosecond range,
- Continuous gap-free spectral analysis to avoid missing any rare events.

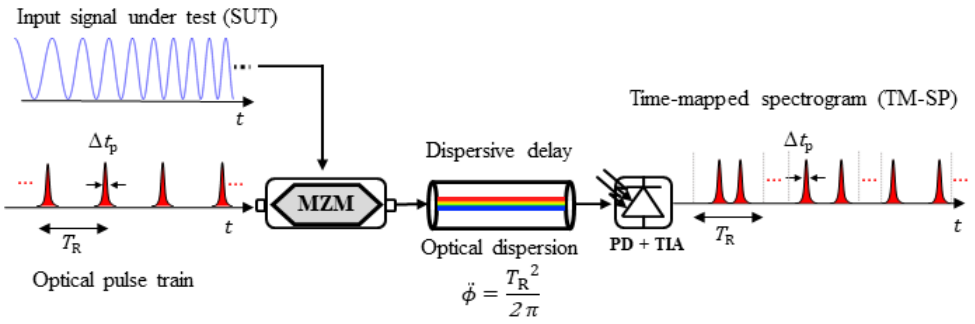

Fig. 3.1: Simulation setup for photonics-based TM-SP analysis of broadband microwave signals. The microwave SUT is modulated on short optical pulses using MZM. The sampled SUT is propagated through a dispersive line. The optical to electrical conversion is performed in a photo-detector of sufficient bandwidth, hence the output pulse width is the same as the sampling pulses. MZM: Mach-Zehnder modulator; PD: photo-detector, TIA: Transimpedence amplifier

3.1 Simulation setup

As discussed in the Chapter 2, the proposed TM-SP concept involves two standard universal signal processing units, namely 1) a temporal sampling unit, and 2) a frequency dependent time delay unit, see Fig. 2.1. In this thesis, we are particularly interested in processing broadband waveforms using a fiber-optics platform, however the same signal processing principles discussed in Chapter 2 can be implemented for waveform processing on other platforms, which are beyond the scope of this thesis.

A fiber-optics based TM-SP scheme for RT-SA of broadband waveforms is illustrated in Fig. 3.1. The temporal sampling of the incoming signal under test (SUT) is implemented by temporal modulation of the SUT with a periodic train of picosecond optical pulses, using an electro-optic Mach-Zehnder modulator (MZM) [36]. The frequency dependent time delay unit is implemented using group-velocity (or chromatic) dispersion in an optical fiber [68] (See Appendix B). The output optical waveform is then converted to electrical voltage waveform using a photo-detector followed by a transimpedence amplifier of sufficient RF bandwidth. A practical fiber-optics based TM-SP analog-processing system, such as that shown in Fig. 3.1 is then numerically simulated in Matlab [AJ2]. For the sampling optical pulse train, each individual pulse is assumed to have a Gaussian shape, with amplitude FWHM time width of $\Delta t_p \sim 2$ ps, FWHM frequency bandwidth $\Delta\omega_p \sim 2\pi \times 441$ GHz, and a repetition rate of 10 GHz ($T_{\mathrm{R}} = 100$ ps). These specifications are commensurate with available pulsed laser sources [78]. The amplitude modulation transfer function

of the MZM [68] is numerically modeled, for the temporal modulation of the SUT on the optical pulse train. The MZM is biased at the minimum transmission point, V_π, with V_π=2 V. This ensures that there is no significant carrier component at the output of the modulator due to the bias. Since the modulator is biased at the minimum transmission point, which is highly nonlinear in transfer function, the drive voltage should be chosen small enough such that there are no significant higher harmonics after modulation [86]. The peak-to-peak voltage of the SUT is chosen small enough, such that the voltage to output optical amplitude transfer function of the MZM is linear. The RF bandwidth of the MZM is not considered in the numerical simulations. The SUT modulated optical pulse train is then propagated through a second order optical dispersion. The optical dispersion is numerically modeled as an optical fiber with a linear transfer function (See Appendix B). The dispersive optical fiber introduces the dispersion amount that is required by the main design condition in Eq. 2.4, $\ddot{\phi} = \frac{T_\mathrm{R}}{\omega_\mathrm{R}} = \frac{{T_\mathrm{R}}^2}{2\pi} = 10^4/2\pi$ ps^2/rad, over the full frequency bandwidth of the sampling pulses. Such a dispersive line could be practically implemented using for instance a highly-dispersive optical fiber section or a reflective linearly chirped fiber Bragg grating [68]. In the numerical simulations aimed at validating the TM-SP concept, we assume ideal photo-detection without considering the RF bandwidth and noise associated with the photo-detection process.

3.2 Numerical validation of the time-mapped spectrogram (TM-SP)

The simulated input SUTs are specifically designed to validate the main proposal, i.e., time-mapped spectrogram (TM-SP), and to evaluate the time and frequency resolutions of the TM-SP, as well as to demonstrate some unique capabilities of the TM-SP, such as the capability to perform a real-time spectral analysis (RT-SA) of short interference and transient frequency events. Fig. 3.2(a) shows the 50-ns long microwave SUT, which is composed by a linearly increasing frequency-chirp sinusoid, with a frequency increasing from 500 MHz to 4.5 GHz, and isolated frequency interferences of equal amplitude as that of the frequency chirp component, but with varying frequency content and temporal durations. Specifically, we consider a set of interferences along the signal with durations ranging from 100 ps to 5 ns, and corresponding central frequencies ranging from of 0.5 GHz to 4 GHz, as detailed in Fig. 3.2(a). The average amplitude of the temporal waveform at the output of

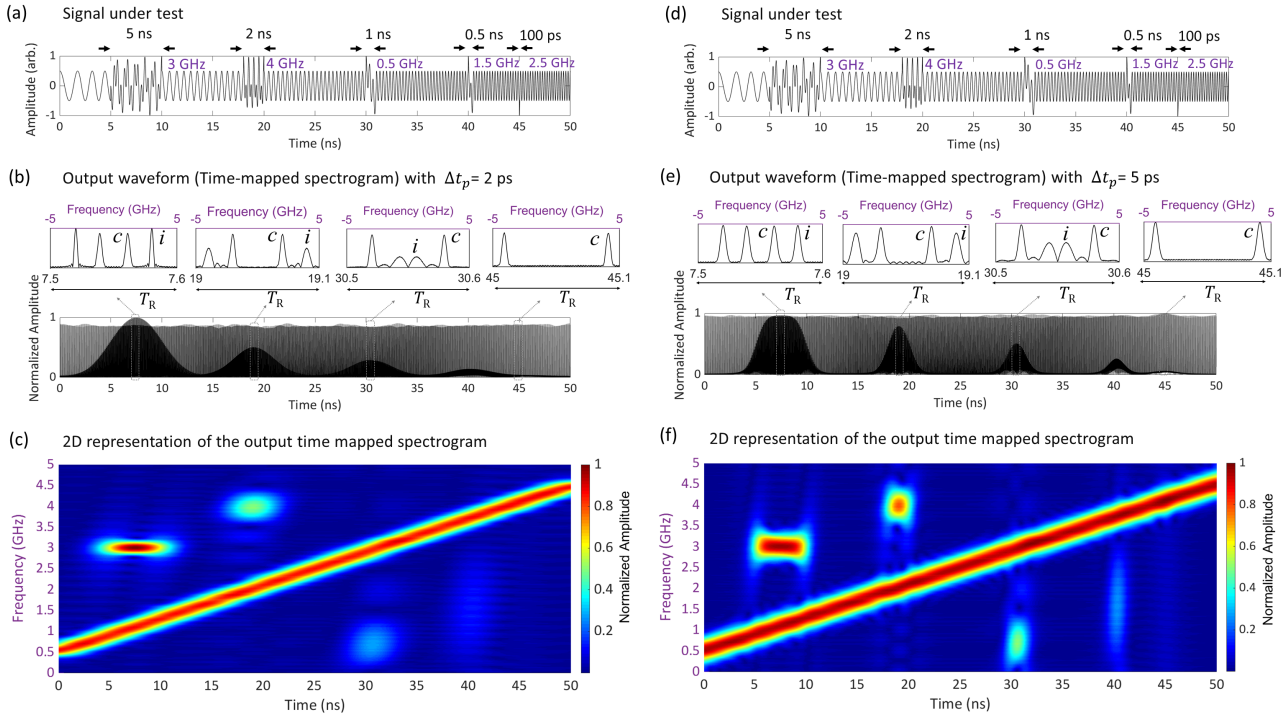

Fig. 3.2: Numerical simulations of time-mapped SP analysis of a broadband (GHz bandwidth) signal. (a) Temporal trace of a signal under test (SUT) at the input of the TM-SP system, when the sampling pulse width, $\Delta t_p = 2ps$, and sampling period, $T_R = 100$ ps. (b) Average amplitude of the temporal waveform at the output of the TM-SP system. The inset plots show a zoom of the output waveform around four different time slots, each extending over one analysis period (T_R). The corresponding frequency axis for each of the traces shown in the insets is represented in the top horizontal axis, following the mapping law $\Delta t_2 \leftarrow \Delta\omega_1 \ddot{\phi}$. (c) 2D representation of the signal joint T-F energy distribution (SP) that is recovered from the output temporal trace. To facilitate interpretation of the obtained results, only the positive axis of frequencies is represented here since the negative frequency side is just a mirrored copy of this same distribution. (d) Temporal trace of the SUT at the input of the TM-SP system when the sampling pulse width, $\Delta t_p = 5$ ps, and sampling period, $T_R = 100$ ps. (e) Average amplitude of the output temporal waveform when the sampling pulse width is increased to $\Delta t_p = 5$ ps. (f) 2D representation of the signal joint T-F energy distribution (SP) that is recovered from the output temporal trace shown in (e).

the TM-SP system (i.e., magnitude of the output complex temporal waveform), also extending over a total duration of 50 ns, is shown in Fig. 3.2(b). A main assumption in our numerical simulations is that the detection system is not bandwidth limited and it has the capability to capture the fastest temporal features in the output waveform. An infinite dynamic range is assumed for the detection process as well. Though unrealistic, these assumptions allowed us to validate the ideal time and frequency resolutions estimates provided in Eq. 2.10. A zoom over different analysis periods (each with a duration T_R) at specific interference locations along the output temporal waveform is also shown in Fig. 3.2(b). Each temporal period (T_R) is mapped onto the corresponding frequency axis according to the frequency-to-time mapping law defined in Fig. 2.1, $\frac{\Delta t_2}{\Delta\omega_1} = \ddot{\phi}$.

As predicted, and as it can be observed from the insets in Fig. 3.2(b), the temporal mapping clearly identifies the frequency components of the SUT, namely the linearly increasing frequency chirp term (denoted as $\boldsymbol{c}$) and the isolated frequency interferences (denoted as $\boldsymbol{i}$) at the expected temporal locations, except for the 100-ps duration interference term centered at 2.5 GHz that occurs at the 45-ns time location (with respect to the beginning of the chirp waveform, $t = 0$). This is anticipated because the 100 ps duration is at the limit of the Nyquist sampling period $T_{\mathrm{R}} = 100$ ps, such that the sampling process cannot capture this interference event. The detection of the other interference events is ultimately limited by the time resolution of the conducted TM-SP analysis. Recall that the time and frequency resolutions (amplitude FWHM widths) can be estimated from Eq. 2.10 as: time resolution, $\delta t_r \sim 4.4$ ns, and frequency resolution, $\delta\omega_r \sim 2\pi \times 200$ MHz, with a Gaussian shape temporal analysis window $h(t)$. From Fig. 3.2(b) inset, the instantaneous spectrum of the 5-ns-duration, 3-GHz, interference (denoted as $\boldsymbol{i}$) is clearly identified, with an almost equal amplitude to that of the chirp component (denoted as $\boldsymbol{c}$) at the corresponding temporal location. The individual temporal pulses recovered at the system output, corresponding to the individual frequency components of the continuous chirp signal ($\boldsymbol{c}$) of the SUT, exhibit about the same time width as the sampling pulses, $\Delta t_p \approx 2$ ps FWHM in amplitude. This is consistent with our theoretical prediction of a frequency resolution of $\Delta t_p/\ddot{\phi} \approx 2\pi \times 200$MHz. Moreover, from the insets of Fig. 3.2(b), we infer that the shape of each of the output pulses corresponding to the Fourier spectrum of each of the individual short interference components ($\boldsymbol{i}$) of the SUT exhibits a sinc profile, as expected for a square temporal shape (i.e., finite duration) interference, with an increasing width as the duration of the interference component under analysis is decreased. From Fig. 3.2(b), we also infer that even though the 4-GHz interference of 2 ns duration and other interferences along the SUT are shorter than the estimated time resolution of $\delta t_r \sim 4.4$ns, they can still be captured by the TM-SP system, though with the expected increased frequency-width and with amplitude levels that are lower than that of the chirp component.

Fig. 3.2(c) shows a 2D representation of the signal joint T-F energy distribution (spectrogram) that is recovered from the output temporal trace according to the time-to-frequency mapping $\frac{\Delta t_2}{\Delta\omega_1} = \ddot{\phi} = \frac{{T_{\mathrm{R}}}^2}{2\pi}$. The color code represents the relative amplitude levels at each T-F location. As expected, the recovered SP shows the T-F distributions corresponding to the linear frequency-chirp component and the frequency interferences of the SUT at the prescribed time and frequency locations, thus

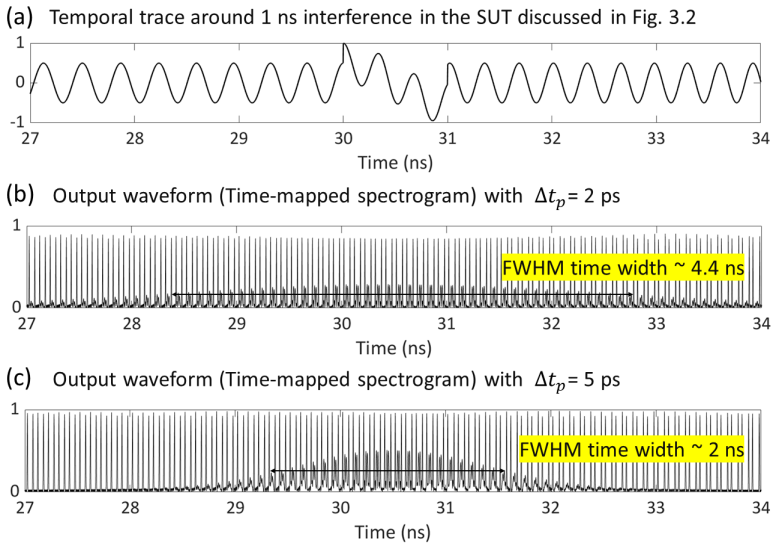

Fig. 3.3: Numerical simulations showing the effect of the virtual temporal analysis window of the TM-SP on the interference detection capability. (a) Temporal trace of the input SUT around the 1-ns-duration, 0.5 GHz interference term. (b) Average amplitude of the temporal waveform at the output of the TM-SP system with $\Delta t_p = 2$ ps, i.e., corresponding temporal resolution $\Delta t_r \sim 4.4$ ns, shown around the same analysis time slot. The windowed spectrum is mapped within each temporal period, T_{R}. The spectral amplitude of the 1-ns duration interference is maximum at the location of the interference, and reduces in amplitude away from the central location, according to the Gaussian shaped temporal analysis window of duration $\Delta t_r \sim 4.4$ ns. (c) Average amplitude of the output temporal waveform when the sampling pulse width is increased to $\Delta t_p = 5$ ps, i.e., leading to an improved temporal resolution $\Delta t_r \sim 1.7$ ns, shown around the same analysis time slot. Results for other interferences of the SUT in Fig. 2.2 are summarized in Table. 1.

validating the main theoretical operation principle of the TM-SP. The effect of the temporal analysis window on the obtained T-F patterns corresponding to the different interferences can be clearly observed in Fig. 3.2(c): as expected, the amplitude of each of these patterns is reduced for a shorter duration of the interference event (below the time-resolution level). It is important to highlight that no re scaling is applied to represent the time axis and the color mapping in the 2D T-F plot in Fig. 3.2(c). Hence, the output waveform follows the input signal SP at the exact same pace of the signal spectrum variations. Specifically, the dynamic FT spectrum of GHz bandwidth signals is calculated every 100 ps, i.e., at a speed of 10×10^9 FTs per second, with a time resolution of $\delta t_r \sim 4.4$ ns.

3.3 Time and frequency resolutions and the interference detection capability of the TM-SP

As discussed in Section 2.2, the time and frequency resolutions can be customized as desired by simply adjusting the time (or frequency) width of the sampling pulses. For instance, this can

be easily achieved by tuning the frequency bandwidth of a band-pass linear filter applied to the sampling pulses [36]. Fig. 3.2(d) shows the same input SUT as discussed above, now sampled with the sampling pulses with increased FWHM time-width, $\Delta t_p = 5$ ps. Fig. 3.2(e) shows the average amplitude of the output temporal waveform when the FWHM time-width of the sampling pulses is increased to $\Delta t_p = 5$ ps, for the same SUT. A zoom over different analysis periods (each with a duration T_{R}), around different interference locations, show the respective time-mapped spectra. The modified resolutions (amplitude FWHM widths) estimated from Eq. 2.10 are: time resolution $\delta t_r = 1.7$ ns, and corresponding frequency resolution, $\delta\omega_r = 2\pi \times 500$ MHz. Fig. 3.2(f) shows the 2D representation of the signal joint T-F energy distribution (SP) that is recovered from the output temporal trace. This analysis confirms that the reduced temporal analysis window duration can better intercept shorter interferences (i.e., with an increased amplitude value, as compared with the 4.4-ns resolution case), but with the expected related deterioration in the frequency resolution. The change in the relative amplitude of the captured interferences can be clearly observed by comparing Fig. 3.2(c) and Fig. 3.2(f), owing to the improved temporal resolution in the later case. To be more specific, from the insets Fig. 3.2(e), we observe that the 4-GHz interference ($\boldsymbol{i}$) of 2 ns duration is resolved with a sinc pulse profile, whose peak amplitude is now closer to that of the chirp component ($\boldsymbol{c}$), though with a pulse width larger than that recovered for the 4.4-ns resolution case (Fig. 3.2(b), same temporal location). This is consistent with the improved time resolution of $\delta t_r \sim 1.7$ ns and related deterioration of the frequency resolution. It is also worth noting that the 5-ns-duration, 3-GHz interference component ($\boldsymbol{i}$) from the inset around 7.5 ns in Fig. 3.2(e) is resolved with a Gaussian pulse shape, like that of the chirp component ($\boldsymbol{i}$). This is attributed to the longer duration of the interference, as compared to the temporal resolution of $\delta t_r \sim 1.7$ ns , leading to an "smoothing" effect of the interference's sinc spectral shape. The sinc shaping characteristics of the recovered spectral components are however clearly evident for interferences with durations of the order of ~ 2 ns and shorter, as can be observed from the corresponding insets in Fig. 3.2(e).

Fig. 3.3 shows a more detailed analysis of the effect of the virtual temporal analysis window implemented by the TM-SP on the interference detection capability. Fig. 3.3(a) shows the same SUT discussed in Fig. 3.2(a) around the 1-ns-duration, 0.5-GHz interference. Fig. 3.3(b) and (c) shows the output TM-SP along the corresponding time slot for the cases of 4.4-ns and 1.7-ns time resolutions, respectively (results corresponding to Fig. 3.2(b) and Fig. 3.2(e), respectively).

Estimates on interference detection from the results in Fig. 3.2								
Interference(→)	5 ns		2 ns		1 ns		0.5 ns	
$\delta t_r(\downarrow)$	$\boldsymbol{i/c}$	FWHM(ns)	$\boldsymbol{i/c}$	FWHM(ns)	$\boldsymbol{i/c}$	FWHM(ns)	$\boldsymbol{i/c}$	FWHM(ns)
4.4 ns (Fig. 3.2(b))	1	6	0.6	4.8	0.3	4.4	0.2	4.4
1.7 ns (Fig. 3.2(d))	1	5	0.8	2.4	0.5	2	0.3	2

Table 3.1: Estimates on interference detection from the results in Fig. 3.2. (1) Ratio of peak magnitude of the Fourier coefficient of the interference to that of the instantaneous chirp signal $\boldsymbol{i/c}$, and (2) the FWHM time width of the captured interferences $\boldsymbol{i/c}$, using an evaluation similar to that of the example shown in Fig. 3.3.

The time-mapped spectrum of the interference component ($\boldsymbol{i}$) is clearly shaped by the Gaussian temporal analysis window with a duration $\delta t_r \sim 4.4$ ns, Fig. 3.3(b) and $\delta t_r \sim 1.7$ ns Fig. 3.3(c), respectively. In contrast, the chirp component ($\boldsymbol{c}$) is essentially not affected by the resolution limitations. The maximum amplitude of the interference component ($\boldsymbol{i}$) is also affected by the Gaussian temporal analysis window, and hence has a reduced amplitude compared to that of the continuous chirp component ($\boldsymbol{c}$), whose amplitude is not affected by the moving temporal analysis window as discussed above. We attribute this performance to the fact that whereas the temporal analysis window is actually longer than the interference event under test, consecutive analysis windows are however shifted with respect to each other by a much shorter delay, i.e., by $T_{\mathrm{R}} = 100$ps, thus being able to capture the shorter duration interference. Nonetheless, each of the time-mapped spectra is still weighted by the shape of the temporal analysis window. As a result, a Gaussian temporal analysis window with a duration longer than that of the interference event to be analyzed may still capture the event, but the resulting peak amplitude will be smaller than that expected for an event of the same instantaneous amplitude that fulfills the entire Gaussian window (such as for the chirped component case in our reported examples). The same phenomenon has been observed for temporal events that are down to $\sim 500 -$ ps long, i.e., even nearly one order of magnitude shorter than the time resolution of the TM-SP. For example, see the TM-SP of 500-ps interference in Fig. 3.2(b), and the corresponding 2D distribution in Fig. 3.2(c). The amplitude of the interference component is smaller than the continuous chirp component. Table 3.1 reports the data estimated from the TM-SP results in Fig. 3.2(b) and Fig. 3.2(e) on the peak amplitude of the time-mapped frequency component corresponding to each analyzed interference signal relative to that of the time-mapped frequency component of the chirp signal ($\boldsymbol{i/c}$).

Additionally, Table 3.1 also reports the FWHM time-width of the TM-SP corresponding to each captured interference, evaluated following the strategy illustrated in the example shown in Fig. 3.2.

The FWHM time-width of the TM-SP of each analyzed interference is close to the interference duration when this is longer than the temporal resolution of the implemented spectrogram, and it approaches the temporal resolution as the interference duration reduces below this resolution value. The ($\boldsymbol{i/c}$) ratio is also reduced as the interference duration decreases, making it more difficult for efficient detection of the shorter interferences in a practical setup. On the other hand, as shown in the insets of Fig. 3.2(b) and as mentioned above, the temporal width of the time-mapped sinc shaped output pulses, corresponding to the frequency spectrum of each of the interference components ($\boldsymbol{i}$) of the SUT, increases as the duration of the corresponding interferences along the SUT decreases. This trend is expected because of the Fourier transform inverse relationship between the finite duration interference and the corresponding sinc shaped spectrum. The frequency widths of the interference components ($\boldsymbol{i}$) are estimated for each of the captured interferences in Fig. 3.2 and the results are summarized in Table 3.2, both for the 4.4-ns and 1.7-ns resolution cases. Note here that the temporal width between the first nulls of the sinc shaped pulse is used to estimate the corresponding frequency width.

3.4 Gap-free operation and reduced detection sampling rate of the TM-SP

As discussed in Section 2.3, and illustrated through Fig. 2.2(b), the time resolution of the implemented SP is defined by the duration of the analysis temporal window, and comprises about M periods of the original sampling pulse train. Here, recall that M (ratio of sampling period to pulse width) is the number of points of the performed FT analysis, see Eq. 2.11. In our numerical example, $M \approx 44$. This implies that the time-mapped windowed FT will keep approximately the same (i.e., repeating) over a number M of analysis periods of the calculated SP (with each analysis period having a duration T_{R}), while the window is being shifted by every T_{R} (see Fig. 2.2(b)). This ensures that the time-mapped windowed FT is computed in a highly overlapped manner, without missing any gaps in the conducted analysis, ensuring continuous gap-free operation.

This feature is confirmed through the simulation example presented in Fig. 3.4. The input SUT and the analysis parameters are the same as those defined in Section 3.2 for the short sampling pulse case, results in Fig. 3.2(a)-(c). Hence, the time and frequency resolutions also remain the

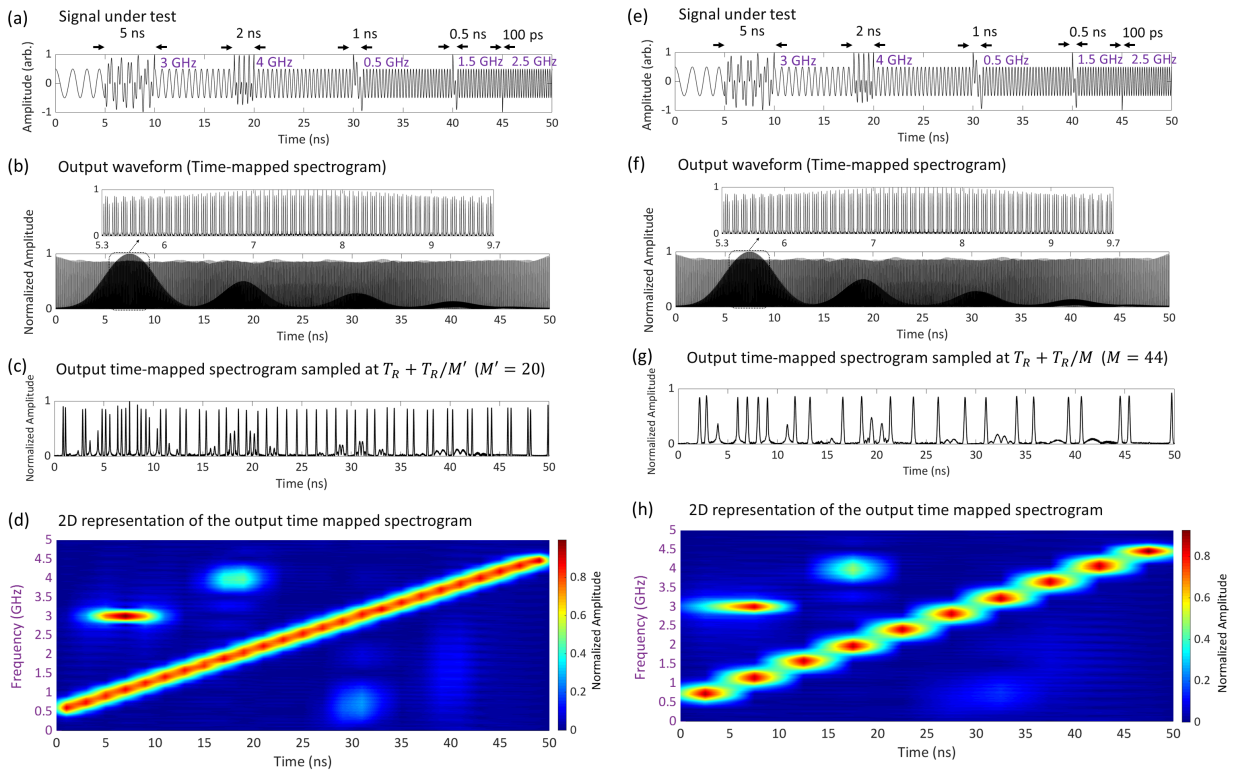

Fig. 3.4: Numerical simulation results showing the proposed strategy to relax the detection sampling rate using the oversampling features in the TM-SP method. (a) Temporal trace of the SUT at the input. (b) Average amplitude of the temporal waveform at the output of the TM-SP system (with a sampling pulse width of $\Delta t_p = 2$ ps). The inset plot shows a zoom of the output waveform over a temporal duration equal to $M = 44$ analysis periods (total of 4.4 ns duration). (c) Average amplitude of the temporal waveform at the output of the TM-SP when sampled at a reduced rate of 9.52 GHz, corresponding to a sampling period of $T_\mathrm{R} + T_\mathrm{R}/20$. (d) 2D representation of the SP that is recovered from the output temporal trace in (c), showing only the positive side of the frequency axis. (e) Temporal trace of the SUT at the input. (f) Average amplitude of the temporal waveform at the output of the TM-SP system (with a sampling pulse width of $\Delta t_p = 2$ ps). (g) Average amplitude of the temporal waveform at the output of the TM-SP when sampled at a reduced rate of 9.77 GHz, corresponding to a sampling period of $T_\mathrm{R} + T_\mathrm{R}/44$. (h) 2D representation of the SP that is recovered from the output temporal trace in (e).

same, i.e., time resolution, $\delta t_r \sim 4.4$ ns, and frequency resolution, $\delta\omega_r \sim 2\pi \times 200$ MHz. Fig. 3.4(b) shows the temporal waveform at the output of the dispersion unit. The zoomed section of the output temporal waveform in the inset of Fig. 3.4(b) shows the time-mapped spectra over a duration equal to $M = 44$ analysis periods (total duration of 4.4 ns). Each of the mapped spectra extends over a single sampling period ($T_\mathrm{R} = 100$ ps) and it consists of the spectral components of a linear frequency chirp signal and the 5-ns-long interference term at 3 GHz. While the continuous frequency chirp term is repeated over $M = 44$ analysis periods in the mapped spectra, unaffected by the shape of the temporal analysis window $h(t)$, the 5-ns duration interference component is however relatively weighted by the shape of the analysis window. From the zoom section of Fig.

Estimates on interference detection from the results in Fig. 3.3 and Fig. 3.4								
Interference(→)	5 ns		2 ns		1 ns		0.5 ns	
Down-sampling(↓)	$\boldsymbol{i/c}$	width(GHz)	$\boldsymbol{i/c}$	width(GHz)	$\boldsymbol{i/c}$	width(GHz)	$\boldsymbol{i/c}$	width(GHz)
Original TM-SP (Fig. 3.2(b))	1	0.5	0.6	1	0.3	1.5	0.2	3
Original TM-SP (Fig. 3.2(d))	1	Gauss-shape	0.8	1.3	0.5	1.5	0.3	3
M=20 (Fig. 3.4(c))	1	0.5	0.5	1	0.3	1.5	0.2	3
M=44 (Fig. 3.4(g))	1	0.5	0.5	1	0.2	1.5	0.2	3

Table 3.2: Estimates on interference detection from the results in Fig. 3.2 and Fig. 3.4. (1) Ratio of the magnitude of the Fourier coefficient of the interference to that of the instantaneous chirp $\boldsymbol{i/c}$ and (2) the modified frequency resolution width(GHz) (estimated from the time width between first nulls of the sinc shaped output pulse) of the interferences that are obtained through the TM-SP for the different interferences of the SUT analyzed in Fig. 3.2 and Fig. 3.4.

3.4(b), it can be observed that the weight function is a Gaussian shape, consistently with the shape of the temporal analysis window $h(t)$ in the implemented TM-SP. It is clearly evident from Fig. 3.4(b) that the temporal window, $h(t)$ is much longer than the temporal shift in between consecutive analysis windows (T_{R}), mapping the dynamic FT of the SUT without missing any gaps in between the consecutive TM-SP calculations. This feature ensures that the conducted RT-SA is gap-free. These repeating features in the FT computation can be interpreted as an oversampling of the recovered information, which can in turn be exploited in detecting or processing the obtained SP distribution.

One such strategy is to take advantage of these repeating features to relax the detection sampling rate requirements [AJ2]. In principle, for capturing the output TM-SP in real-time, the output waveform needs to be sampled with a sampling period shorter than at least the individual pulse width, Δt_p (detection sampling rate larger than the spectral bandwidth, to satisfy the Nyquist criterion for lossless sampling). These detection sampling rate requirements can be significantly relaxed by taking advantage of the repeating features in the output TM-SP. A sequential sampling strategy such as the one used in electrical sampling oscilloscopes is implemented here. A sequential sampling approach acquires these M samples over M consecutive replicas of the repeating waveform. Since the mapped spectrum at the output is repeating over M times, a detection scheme can be designed to acquire M sampling points over a duration of M replicas, providing the complete TM-SP information. For instance, in Fig. 3.4(c), we propose such a detection strategy, where the output

time-mapped SP is sampled with a period $T_{\mathrm{R}} + T_{\mathrm{R}}/M'$, where $M' \leq M$ (i.e., at a sampling rate slightly below the Nyquist bandwidth of the SUT), such that M' distinct samples are captured over the duration of $M' \times T_{\mathrm{R}}$ ($\leq \delta t_r = 4.4$ ns), comprising the complete SP information. Fig. 3.4(c) presents the results for a case with $M' = 20$, showing the interferences and chirp component of the down-sampled TM-SP. Fig. 3.4(d) shows the retrieved SP, clearly mapping the expected frequency components of the SUT with the predicted time-frequency resolution. As compared with the T-F distribution retrieved in Fig. 3.2(c), we observe that the down-sampled TM-SP in Fig. 3.4(d) still enables capturing fast events with durations even an order of magnitude shorter than the time resolution of the SP analysis (down to 500 ps vs. the time resolution of 5 ns). The relative interference ($\boldsymbol{i/c}$) ratio after down-sampling, and the frequency resolution of the interferences as a function of interference duration, summarized in Table 3.2, shows that the down-sampled TM-SP can still analyze the shorter interferences with similar amplitude levels and frequency resolutions as those of the original TM-SP in Fig. 3.2(b). Finally, Fig. 3.4(f) shows the output TM-SP for $M' = 44$ (i.e., at a sampling rate 9.77 GHz, slightly below the Nyquist bandwidth of the SUT), such that 44 distinct samples are captured over the duration of a time resolution, comprising the complete SP information. The interference ratio ($\boldsymbol{i/c}$) and the frequency resolution of the interferences in this case, as observed in Fig. 3.4(f) and summarized in Table 3.2, shows that the TM-SP is again capable of capturing the shorter isolated interferences with similar frequency resolutions, though with amplitude levels just slightly lower than those obtained for the original (over-sampled) TM-SP case. These results confirm that the proposed down-sampling strategy of the TM-SP does not hinder the gap-free operation of the implemented real-time Fourier analysis.

3.5 Conclusions

In this chapter, I have presented the numerical simulations to validate the theory of the time-mapped spectrogram (TM-SP) proposed in Chapter 2. A practical photonic-based platform for TM-SP implementation is numerically simulated, aiming at real-time spectral analysis (RT-SA) of broadband waveforms. All properties of the TM-SP discussed in Chapter 2, such as time and frequency resolutions, continuous gap-free operation, oversampling features, are verified through numerical simulations. These simulations confirm that the photonic implementation of TM-SP is

particularly attractive for continuous gap-free RT-SA of GHz bandwidth microwave signals, offering GHz rate FT processing speeds, and nanosecond temporal resolutions. In the next chapter, I present experimental results from a photonics-based TM-SP scheme for RT-SA of GHz bandwidth microwave signals. The key features of the TM-SP discussed in Chapter 2 and Chapter 3 will be experimentally validated.

Chapter 4

Experimental Evaluation of Photonics-based Time-mapped Spectrogram

This chapter presents experimental results on demonstration of a photonic-based TM-SP for real-time spectral analysis (RT-SA) of arbitrary broadband microwave signals, aimed at the following set of performance specifications [AJ1, AJ3]:

- Real-time instantaneous bandwidth in the GHz range or higher,
- FT processing speeds in the GHz range,
- Temporal resolutions in the nanosecond range,
- Continuous gap-free spectral analysis to avoid missing any rare events.

4.1 Time-mapped spectrogram of non-stationary microwave signals

In order to experimentally verify the proposed TM-SP concept, a simple photonic-based platform is designed for gap-free RT-SA of GHz-bandwidth microwave signals, using widely available off-the-shelf photonics components [AJ1], [AC5, AC6]. The experimental setup is shown in Fig. 4.1.

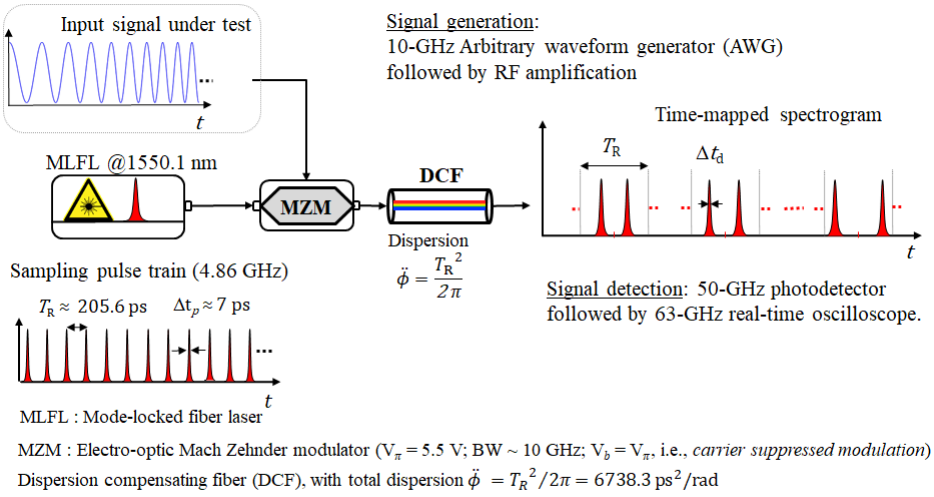

Fig. 4.1: Schematic of the experimental setup for gap-free RT-SA of GHz-bandwidth microwave signals based on the time-mapped spectrogram analysis. The microwave signal under test (SUT) is sampled with a picosecond optical pulse train generated from a mode-locked fiber laser, in a Mach-Zehnder modulator (MZM). The optical samples are propagated through dispersion compensating fiber (DCF) with a total dispersion $\ddot{\phi}$, and the output TM-SP is captured in a real-time oscilloscope after photo-detection.

Customized high-speed microwave waveforms were generated using an electronic arbitrary waveform generator (AWG). The experimental setup follows the same general schematic used for simulations in Chapter.3, see Fig. 3.1, and is shown in Fig. 4.2(a). The user-defined microwave signal under tests (SUTs) used for testing the photonic-based TM-SP setup are all generated from an electronic AWG (Tektronix AWG7122C) with an analog bandwidth of 10 GHz and a sampling rate of 24 GS/s. The optical sampling pulses used for sampling the microwave SUTs are generated from an actively mode-locked fiber laser (Pritel - Ultrafast Optical Clock) , with each individual pulse having a Gaussian-like temporal shape with an intensity FWHM time width of $\Delta t_p \approx 7$ ps (corresponding transform limited FWHM frequency bandwidth $\Delta\omega_p \approx 2\pi \times 60$ GHz), and a repetition period $T_\mathrm{R} \approx 205.76$ps (sampling rate = 4.86 GHz). Temporal sampling of the microwave SUTs is performed with a 40-GHz electro-optic Mach-Zehnder modulator (MZM) biased at minimum transmission point. An optical polarization controller is used before the MZM to optimize the electro-optic modulation process. The MZM performs carrier-suppressed amplitude modulation of the microwave SUT within its linear region of operation, for SUTs with peak-to-peak voltage amplitude (V_{p-p}) up to 0.4 V. The sampling rate of 4.86 GHz enables the analysis of microwave SUTs with a full frequency bandwidth up to $\sim$ 4.86 GHz (Nyquist criterion). Subsequently, the modulated optical pulses are

linearly propagated through a dispersion compensating fiber (DCF), which provides a second-order dispersion amount of ~ 6825 ps^{2}rad^{-1}, about 1.3% off the ideal amount of dispersion from Eq. 2.4, $\ddot{\phi} = {T_\mathrm{R}}^2/2\pi = 6738.2$ ps^{2}rad^{-1}, over the full frequency bandwidth of the sampling pulses. The total loss of the DCF used in the experiments is ~ 28 dB, which is compensated for using an optical pulse amplifier (Pritel EDFA). The amplified spontaneous emission (ASE) noise associated with the optical amplification is filtered out using a tunable optical bandpass filter before photo-detection. The output non-repetitive waveform is captured with a 50-GHz bandwidth photo-detector attached to a 63-GHz bandwidth real-time oscilloscope (Keysight DSAZ634A), with no averaging. The

The proposed TM-SP concept does not impose any fundamental limitation on the signal duration: the signal Fourier content is inherently time mapped in a continuous fashion as it propagates through the TM-SP system. The duration of each of the studied waveforms in our experimental examples was limited by the available memory of the instruments used for generation (AWG) and measurement (real-time scope) of waveforms. Additionally, in this way, the entire output signal could be captured with the real-time scope for subsequent off-line analysis and representation of the detected data (e.g., for the 2D time-frequency graphs). The real-time oscilloscope is triggered with a marker from the electronic AWG that coincides with the beginning of the microwave modulation signal. No synchronization is needed between the optical pulses and microwave signal in the modulation process. Further processing of the captured temporal traces, namely re-sampling, re-timing, and re-scaling to the frequency domain, is performed numerically offline, using Matlab in a personal computer. Note that the measured output waveform is sampled in the real-time scope at a rate of 160 GS/s or with a sampling period of 6.25 ps. This translates into a non-integer number of samples, i.e., 32.922 samples, per analysis period ($T_\mathrm{R} \approx 205.76$ ps) along the corresponding time-mapped frequency axis, and could result in vertical frame displacements in the 2D spectrogram representations. Re-sampling of the captured temporal waveforms is performed to ensure an integer number of samples (100) per analysis period to facilitate the 2D representations.

Fig. 4.2 presents the analysis of a 2-μs long microwave signal with an instantaneous frequency $\omega_{RF}(t_1)$, linearly increasing from 500 MHz to 2 GHz, Fig. 4.2(b). The plot in Fig. 4.2(c) shows the voltage of the output electrical temporal waveform that is directly captured on the real-time scope. The measured output temporal waveform along each slot of duration T_R (sampling period) is mapped into the equivalent frequency axis using the defined mapping law, $\Delta t_2 \leftarrow \Delta\omega_1\ddot{\phi}$. The

instantaneous spectrum of the input SUT at any given instant of time consists of 2 individual pulses, corresponding to the instantaneous frequency of the signal, $\pm\omega_{RF}(t_1)$ linearly increasing with time. Fig. 4.2(d) shows the 2D representation of the signal joint time-frequency energy distribution (spectrogram) that is directly recovered from the output temporal trace.

As expected, the experimentally recovered spectrogram follows the theoretical linear frequency chirp of the input SUT (dashed grey lines). The deviations of the 2D distribution along the vertical frequency axis, with respect to the theoretical linear frequency chirp, that are observed in Fig. 4.2(d) are attributed to the finite timing jitter in the picosecond optical pulses used for temporal sampling. It is important to highlight that no re-scaling was applied to represent the time axis in the 2D time-frequency plot in Fig. 4.2(d), which indicates that the output waveform delivers the spectrogram of the input signal purely in real time. Specifically, the changing signal FT is calculated every $T_{\mathrm{R}} \approx 205.76$ ps, i.e., at a speed of 4.86×10^9 FTs per second, significantly outperforming present instrumentation. For a comparative reference, a state-of-the-art real-time RF spectrum analyzer based on DSP, the Keysight N9040B-RT2 provides a maximum of 292,969 discrete Fourier transforms per second. .The results in Fig. 4.2 confirm the capability of the demonstrated setup to provide a gap-free RT-SA of waveforms with an instantaneous frequency bandwidth approaching 5-GHz, beyond the capabilities of current electronic DSP-based platforms.

Fig. 4.3 report the results of gap-free RT-SA of two additional, more complex GHz-bandwidth microwave signals using the described photonics platform: a signal composed by two superimposed sinusoidal waveforms with exact opposite quadratic frequency chirps (left plots), and a sinusoidally frequency-modulated carrier (right plots) [AJ1], [AC7]. For each of these testing cases, the top plot (a, d) shows the measured input temporal waveform; the plot at the center (b, e) shows the numerically computed spectrogram of the digital version of the input SUT, using a temporal analysis window that matches the one implemented by the real-time photonics platform, i.e., a 2.54-ns (FWHM) Gaussian pulse; and the plot at the bottom (c, f) shows the 2D spectrogram representation that is directly recovered from the measured output temporal trace. As expected, in all cases, there is an excellent agreement between the measured real-time spectrogram and the numerically calculated one. The simulated spectrogram distributions shown in Fig. 4.3 are computed using a numerical algorithm in Matlab. The plots in Fig. 4.3(b) and (e) show the numerical spectrogram (squared magnitude of the STFT) of the corresponding digitized measured input SUT. The sampling period

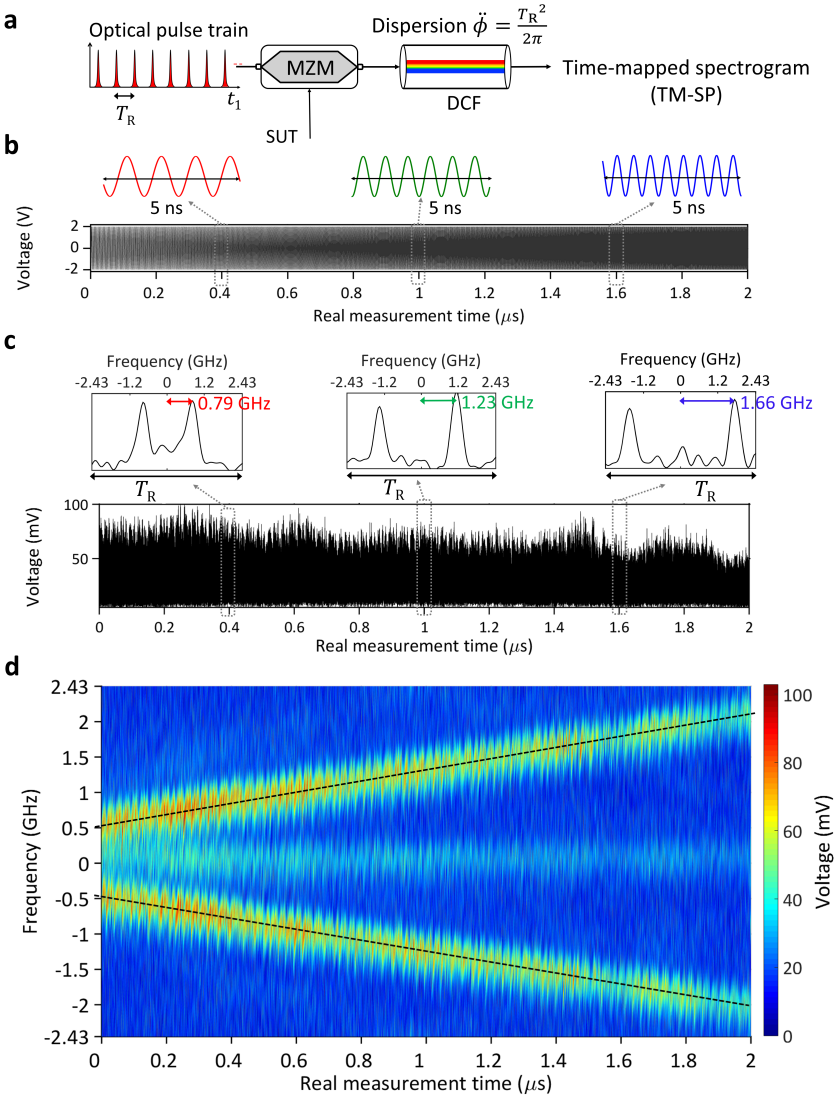

Fig. 4.2: Experimental results on time-mapped spectrogram analysis of a linearly chirped RF waveform using photonic sampling and dispersion. (a) shows a schematic of the photonics-based TM-SP experimental setup for real-time spectral analysis of broadband microwave signals. The microwave signal under test (SUT) is sampled with a picosecond optical pulse train generated from a mode-locked fiber laser, in a Mach-Zehnder modulator (MZM). The optical samples are propagated through dispersion compensating fiber (DCF) with a total dispersion $\ddot{\phi}$, and the output TM-SP is captured in a real-time oscilloscope after photo-detection. (b) shows the temporal trace of the microwave signal under test (SUT), with a linearly increasing frequency, from 500 MHz to 2 GHz, along a duration of 2 μs. (c) shows the photo-detected output temporal waveform (voltage signal) that is directly captured in a real-time oscilloscope, over the same 2 μs duration. The inset plots show a zoom of the output waveform around three different time slots, each extending over one analysis period ($T_R = 205.6$ ps). The temporal trace along each consecutive analysis period, T_R, is a time-mapped copy of the FT of the input SUT, effectively windowed around the corresponding time of analysis. The top horizontal axis follows the frequency scale that is obtained using the mapping law $\Delta t_2 \leftarrow \Delta\omega_1\ddot{\phi}$. The instantaneous spectrum of the input signal at any given instant of time consists of 2 individual pulses, corresponding to the frequency of the signal, $\pm\omega_{RF}(t_1)$ linearly increasing with time. The observed signal background (including at the location corresponding to DC) is attributed to unwanted variations in the bias condition of the electro-optic modulation process with respect to the optimal design. (d) shows a 2D representation of the signal joint time-frequency energy distribution (spectrogram) that is directly recovered from the output temporal trace.

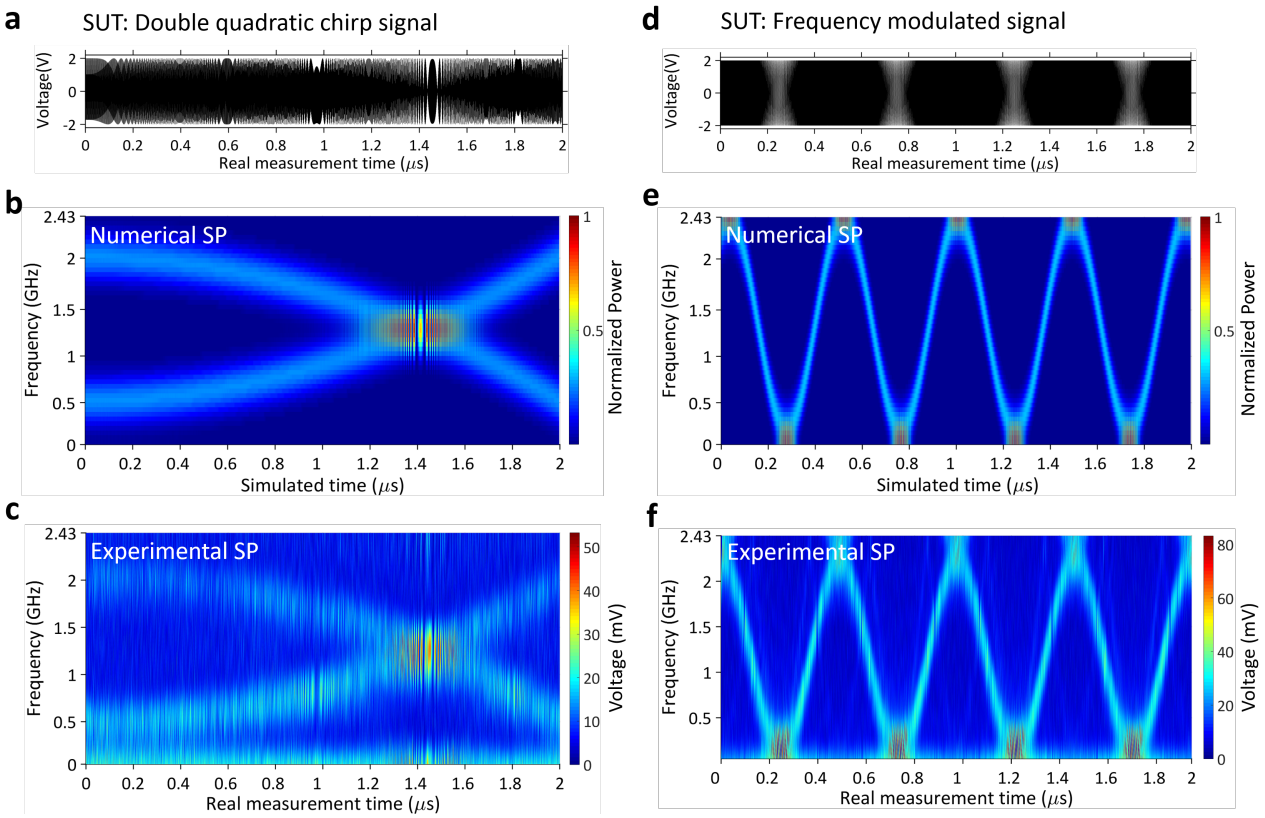

Fig. 4.3: Experimental results on time-mapped spectrogram analysis of two complex high-speed microwave signals using photonic sampling and dispersion. (a)-(c) show the results corresponding to the analysis of a $2-\mu$s long microwave signal under test (SUT), which is composed by two superimposed frequency-chirped sinusoids, namely a sinusoid with an increasing quadratic frequency chirp, from 500 MHz to 2 GHz, and a sinusoid with the same but opposite frequency chirp. The signal exhibits two separate frequency bands at each instant of time. (d)-(f) show the results corresponding to the analysis of a 2-MHz tone that is frequency modulated on a 1.215-GHz microwave carrier with a maximum frequency deviation of ± 1.215 GHz. For each of the analyzed signals, the top plot, (a) and (d), respectively, shows the measured temporal waveform (voltage) of the input microwave SUT; the plot in the middle, (b) and (e), respectively, shows the numerically computed spectrogram (SP) distribution of the measured input signal, calculated using a 2.54-ns Gaussian pulse as the analysis temporal window; and the bottom plot shows the 2D TM-SP distribution that is directly recovered from the measured temporal trace at the output of the experimental photonic sampling and dispersion scheme. To facilitate interpretation of the obtained results, in each spectrogram representation, only the positive axis of frequencies is represented.

of the discretization used in simulations is fixed to be the same as the sampling period of the optical pulses ($T_{\mathrm{R}} \approx 205.76$ ps) used in the experiments. Hence, the number of samples along the time and frequency axis are identical for all the 2D distributions (numerical and experimental) shown in Fig. 4.3. The analysis temporal window, $h(t)$, in the proposed TM-SP method is given by the time-mapped version of the sampling pulse spectrum. The sampling optical pulses in the demonstrated experimental setup have a Gaussian-like shape; therefore, the corresponding pulse spectrum is also Gaussian in shape, with an estimated time-mapped intensity FWHM of ~ 2.54 ns.

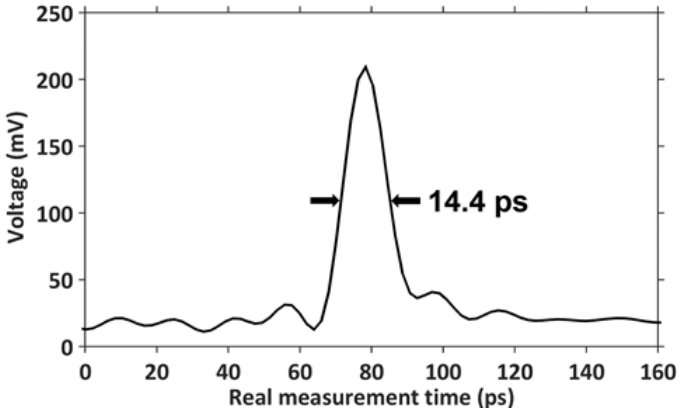

Fig. 4.4: The measured output pulse width detected with a 50-GHz photodetector. The intensity FWHM of the detected pulses is $\Delta t_d \sim 14.4$ ps. This is the value used to estimate the frequency resolution of the implemented real-time SP analysis

Consistently, for the numerical SP calculations, a Gaussian temporal analysis window with an intensity FWHM time-width of ~ 2.54 ns is also used. The speed of calculation of each simulated spectrogram is quantified as the number of fast Fourier transforms (FFTs) that are computed per second, which is 6 FFT/s with available computation power on a general purpose computer running Matlab. All the simulations were performed in Matlab 2015a running on a Windows 10, 64-bit operating system. The numerical SP required a heavy digital computation based on fast-Fourier transform (FFT) algorithms and in particular, considering the specifications of the general-purpose computing platform used for these calculations. In sharp contrast, the reported photonic-based analysis platform provides the spectrogram distribution purely in real time, at nearly $\sim 5 \times 10^9$ FTs/second.

4.2 Evaluation of time and frequency resolutions

The frequency resolution estimates of the TM-SP discussed in Chapter 2 are valid, assuming that the detection bandwidth is high enough to resolve the sampling pulses; otherwise, one should rather consider the temporal width of the detected pulses for this estimate ($\Delta t_d \leftarrow \Delta t_p$). In our particular experimental realization, the intensity full-width at half-maximum (FWHM) of the sampling pulses was $\Delta t_p \approx 7$ ps, whereas the FWHM after photo-detection was measured to be about twice this value, $\Delta t_d \approx 14.4$ ps, see Fig. 4.4. This corresponds with a theoretical frequency resolution $\Delta\omega_r \approx \Delta t_d/|\ddot{\phi}| \sim 2\pi \times 340.3$ MHz. Note that the limited detection bandwidth does not modify

the time resolution of the calculated spectrogram, which is given by $\delta t_r \approx |\ddot{\phi}| \times \Delta\omega_p \sim 2.54$ ns. Thus, a longer time resolution can be obtained by use of a sampling pulse with a broader frequency bandwidth, practically limited only by the operation bandwidth of the dispersive line used in the system. As mentioned, the frequency resolution will however remain limited by the detection bandwidth. The highest frequency resolution offered by the system (inverse of the SP time resolution) can be exploited only if a detection stage is available with a sufficiently large bandwidth to capture the sampling pulse time width (with no distortion).

The experimental results reported in Fig. 4.5 validate further the derived time-frequency resolution estimates. The SUTs in Fig. 4.5 are designed to test weather the TM-SP setup could follow sharp frequency transitions, according to the estimated time resolution of ~ 2.54 ns, and with a frequency resolution of 340 MHz. Fig. 4.5(a) and (d) show SUTs consisting of a high-frequency (1.7-GHz) sinusoid in between two low-frequency (500 MHz) sinusoids, the difference being in that the 1.7-GHz sinusoid in Fig. 4.5(a) exhibits a shorter duration (1 ns) than that of the SUT in Fig. 4.5(d). Fig. 4.5(b) and (e) show the 2D spectrogram distributions of the two analyzed signals that are recovered from the measured output temporal waveforms shown in Fig. 4.5(c) and (f) respectively. As clearly evident from the two test cases in Fig. 4.5(b), (e), the TM-SP system is able to capture the 3-ns duration transition, whereas it is not able to capture the shorter 1-ns duration transition, as it is shorter than the time resolution. In both the cases, the 500 MHz tone is clearly captured by the TM-SP system, with the expected frequency resolution of 340 MHz.

4.3 Application for short-event (nanosecond-duration) tracking

The demonstrated TM-SP based gap-free continuous RT-SA of broadband waveforms is particularly attractive for real-time tracking of short nanosecond-duration events within the broadband spectrum. This capability of the TM-SP is demonstrated through the experimental results presented in Fig. 4.6 [AJ1], [AC8]. The SUTs analyzed here include fast random or isolated events and frequency transients with durations down to 5 ns. This capability is beyond the performance of present DSP-based RT-SA schemes, which are typically limited to provide 100 %-probability interception of signal features with durations at least in the microsecond range [43]. Fig. 4.6(a) shows the temporal trace of a fast microwave frequency hopping sequence that is purposely designed to test the

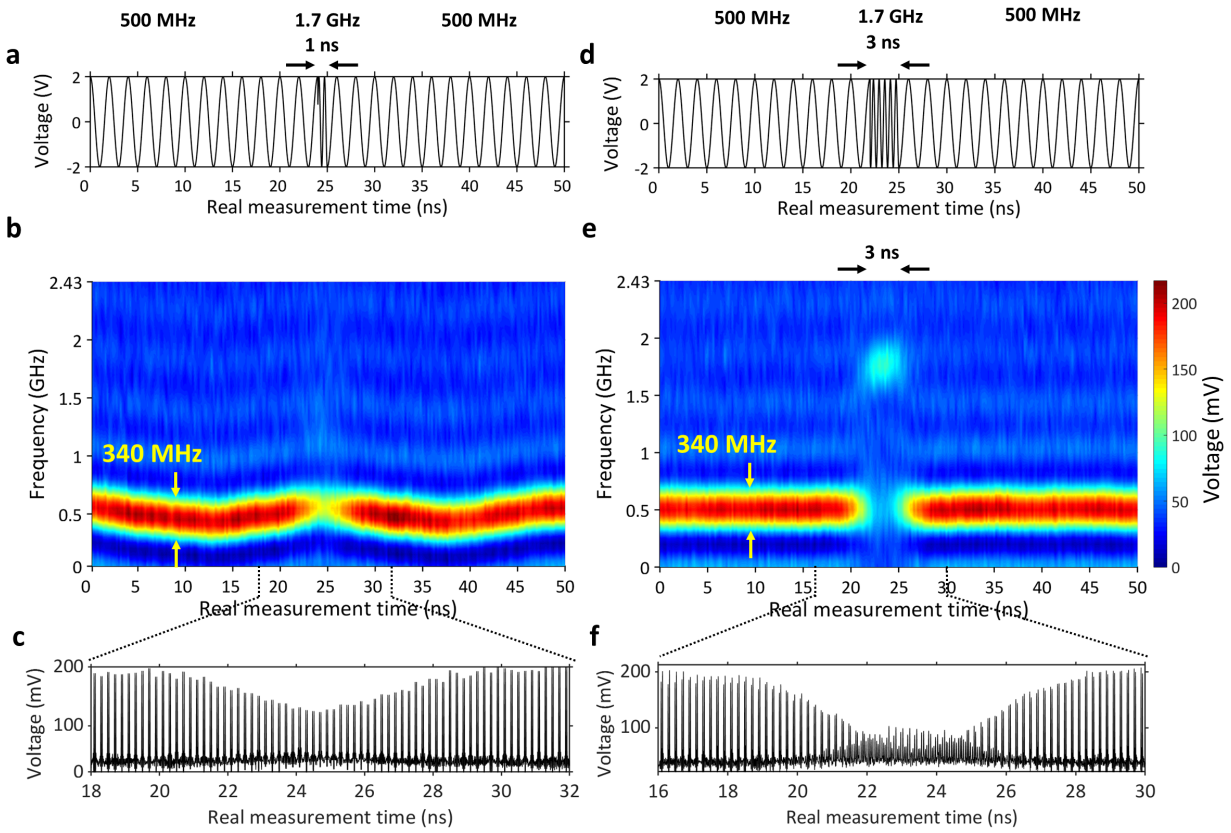

Fig. 4.5: Experimental results for evaluation of joint time-frequency resolutions of the time-mapped spectrogram analysis. The photonic sampling and delay system with the specifications described in the text is used for spectrogram analysis of the microwave signals shown in the top plots. Each of the analyzed signals, (a) and (d), consists of a high-frequency (1.7-GHz) sinusoid in between two low-frequency (500 MHz) sinusoid, the difference being in that the 1.7-GHz sinusoid in the left signal, (a), exhibits a shorter duration (1 ns) than that of the signal to the right (3 ns), (d). The middle plots, (b) and (e), respectively, show the 2D spectrogram distributions of the two analyzed signals that are recovered from the measured temporal waveforms (bottom plots (c) and (f)) at the output of the sampling and delay system. A time resolution of 2.54 ns is estimated for the photonic sampling and dispersion configuration under test. As expected, this configuration is unable to resolve the 1-ns-long high-frequency event of the first signal, (b), but it can clearly resolve the longer (3-ns) high-frequency event in the second signal, (e), consistently with the theoretical time resolution limitations

TM-SP setup performance. In particular, the SUT consists of 5-ns-long segments with a linearly increasing frequency, from 0.4 GHz to 2 GHz. Fig. 4.6(b) shows the 2D spectrogram distribution that is directly recovered from the measured temporal trace at the output of the TM-SP setup, revealing the designed hopping sequence in the time-frequency plane. Fig. 4.6(c) shows a zoom of the output temporal waveform over the 5-ns temporal window corresponding to the presence of the 0.4-GHz tone. This plot reveals that the time-mapped spectrum of this event is produced repetitively over this 5-ns window at every sampling period (i.e., about 25 times), ensuring that the event is intercepted with 100% probability.

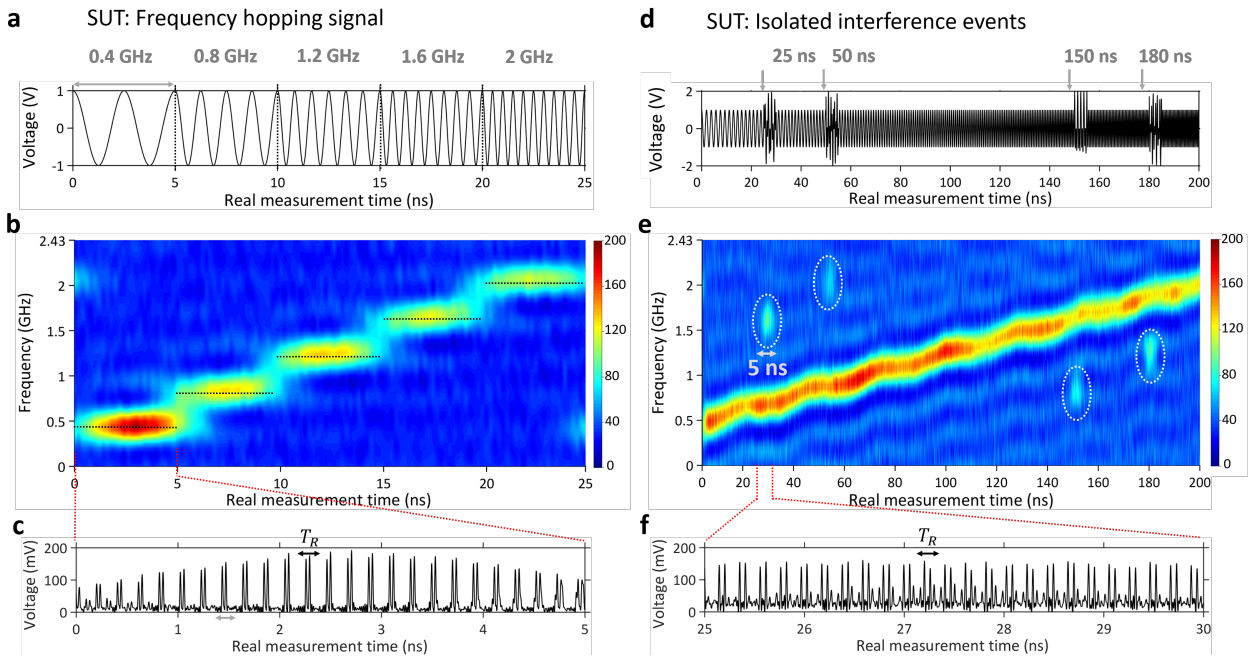

Fig. 4.6: Experimental results on the capability of the photonics-based TM-SP method to capture nanosecond-duration frequency transients. (a) shows the temporal trace of a microwave signal under test (SUT) consisting of a fast frequency hopping sequence, designed to test the time-mapped spectrogram (TM-SP) method performance. The sequence is composed by consecutive 5-ns-long tones with linearly increasing hopping frequencies, i.e., 0.4 GHz, 0.8 GHz, 1.2 GHz, 1.6 GHz, and 2 GHz. (b) shows the 2D spectrogram distribution that is directly recovered from the measured temporal trace at the output of the TM-SP setup, involving photonic sampling and dispersion with the parameters given in the text. The hopping frequency speed that can be captured with this setup is only limited by the time resolution of the calculated TM-SP, which is 2.54 ns in these experiments. The frequency fading at high-frequencies observed in (b) is attributed to the roll-off of arbitrary waveform generator used for generating SUTs. (c) shows a zoom of the output temporal waveform over the 5-ns temporal window corresponding to the presence of the 0.4-GHz tone, confirming that the resultant time-mapped spectral shape is recovered repeatedly at every T_{R}(=205.6 ps) along this analysis window. (d) shows the temporal trace of a microwave SUT composed by (i) a linearly increasing frequency chirp waveform, from 500 MHz to 2 GHz, and (ii) isolated interfering frequency transients with the same amplitude as that of the frequency chirp signal, each having a duration of 5 ns. The interfering frequency transients are centered at 1.6 GHz, 2 GHz, 0.8 GHz and 1.2 GHz, occurring at the relative times of 25 ns, 50 ns, 150 ns and 180 ns, respectively. (e) shows the 2D spectrogram distribution that is directly recovered from the measured temporal trace at the output of the TM-SP setup. The TM-SP method is clearly able to capture and analyze the 5 ns duration isolated interfering frequency transients, consistently with the predicted temporal resolution of analysis in these experiments. (f) also shows a zoom of the output temporal trace over the 5-ns temporal window corresponding to the 1.6-GHz interference event. To facilitate interpretation of the obtained results, in each 2D spectrogram representation, only the positive axis of frequencies is represented.

As another example, Fig. 4.6(d) and (e) show the results (input temporal trace and recovered spectrogram, respectively) of the analysis of a microwave signal composed by a linearly increasing frequency chirp, along with random isolated interfering frequency transients, each having a duration of 5 ns. Fig. 4.6(f) also shows a zoom of the output temporal trace over the 5-ns temporal window corresponding to the 1.6-GHz interference event, revealing again the oversampling features of the conducted RT-SA. These results clearly confirm that the photonic-based TM-SP platform allows

one to intercept the frequency content of any random or isolated signal event in a real-time fashion as long as this occurs over a duration close to the time resolution of the conducted spectrogram analysis, ~ 2.54 ns in the reported experimental configuration.

4.4 Demonstration of undersampled time-mapped spectrogram

As discussed in Section 3.4, there is a heavy overlapping between consecutive virtual temporal analysis windows, as inherently implemented by the TM-SP process. As a result, the time-mapped windowed spectrum keeps nearly identical over a number of about M consecutive representation periods, each with a duration T_{R}, where we recall that $M \approx T_{\mathrm{R}}/\Delta t_p$ ($M \sim 12$ in our experimental design). Using this property, the obtained spectrogram could be fully retrieved by sampling the output waveform at a significantly relaxed rate, just slightly below the original sampling rate, e.g., with a period equal to $T_{\mathrm{R}} + T_{\mathrm{R}}/M$.

This interesting property has been confirmed through numerical down-sampling of the output waveforms captured with the real-time scope in the reported experiments, see examples shown in Fig. 4.7 [AC9]. The temporal output waveform corresponding to the TM-SP of the input frequency modulated SUT is shown in Fig. 4.7(b). The repeated identical time-mapped windowed spectrum is also shown in the insets in Fig. 4.7(b). The corresponding 2D T-F representation is shown in Fig. 4.7(c). The output waveform is then sampled slightly below the sampling rate, at 4.48 GS/s, i.e., with a period equal to $T_{\mathrm{R}} + T_{\mathrm{R}}/M \sim$222.9 ps. Note that the proposed sampling strategy could be implemented directly in the optical domain, through all optical sampling in a nonlinear medium [87], significantly relaxing the detection sampling rate requirements. In the current example, we have implemented the sampling strategy on the digitally captured waveform. Fig. 4.7(e) shows the 2D spectrogram distribution mapped from the down-sampled output temporal trace, in excellent agreement with the 2D spectrogram distribution that is directly retrieved from the over-sampled output trace.

4.5 Conclusions

The photonic-based TM-SP reported here has enabled gap-free RT-SA of GHz-bandwidth waveforms, including the capability of intercepting random fast signals with duration down to the

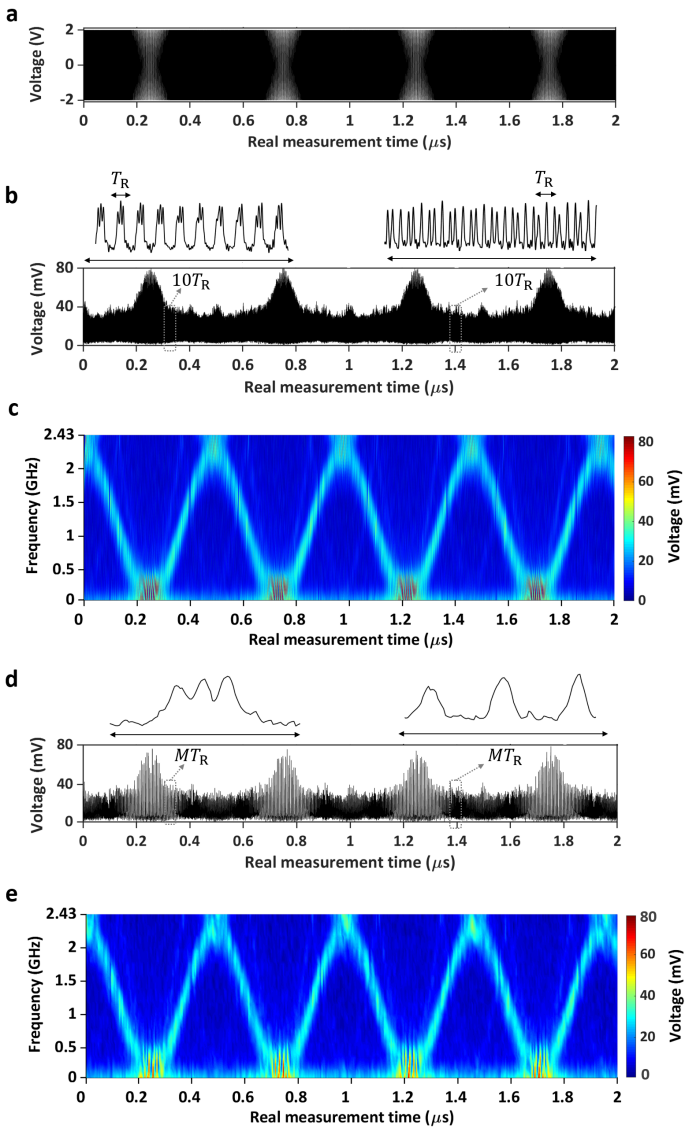

Fig. 4.7: Experimental results showing the oversampling features in the time-mapped spectrogram analysis method. (a) shows the input SUT: a 2 MHz tone that is frequency modulated on a 1.215-GHz carrier with a maximum deviation of ±1.215 GHz. (b) shows the temporal waveform at the output of the TM-SP system, showing the mapping of the input frequency spectrum along each time slot of duration T_R (sampling period), repeating over M consecutive slots, where M is the sampling period to pulse width ration, given by $M = T_R/\Delta t_p \sim 12$ in the present experimental design. (c) shows the 2D spectrogram distribution that is directly mapped from the measured temporal trace at the system output. Only the positive frequency side is shown here to facilitate interpretation. (d): The effective oversampling of the spectrogram information shown in (b) is advantageous in designing the detection stage of the obtained time-frequency distribution. Using this property, the obtained spectrogram could be fully retrieved by sampling the output waveform at a significantly relaxed rate, just slightly below the original sampling rate of 4.48 GS/s, i.e., with a period equal to $T_R + T_R/M \sim 222.9$ ps. (e) shows the 2D spectrogram distribution mapped from the down-sampled output temporal trace, in excellent agreement with the 2D spectrogram distribution that is directly retrieved from the over-sampled output trace.

nanosecond regime. This performance fulfills critical requirements of RT-SA for a wide range of applications, in communications, radar, radio astronomy, biomedical instrumentation and others. The proposed design for TM-SP is universal in that it is suited for analysis and processing of waveforms across any frequency region, provided the availability of technologies for temporal sampling and dispersive delay.

The photonics-based TM-SP configuration has the potential to offer performance specifications beyond those reported in the proof-of-the-concept experiments presented in this chapter. For example, recent developments on mode-locked lasers with hundreds of GHz repetition rates [88], matched by temporal modulation technologies with similar bandwidth performance [89] and all-optical temporal sampling techniques for output waveform measurements [87], offer the potential to enable sub-THz bandwidth RT-SA with THz-speed FT processing speeds, using the proposed method.

Chapter 5

Demonstration of Additional Features of the Time-mapped Spectrogram

This chapter presents some additional important features of the time-mapped spectrogram (TM-SP) that are particularly advantageous for real-time spectral analysis (RT-SA) and processing of broadband waveforms. The following properties of the TM-SP will be demonstrated in this chapter:

- The TM-SP concept for RT-SA of "complex" (amplitude and phase) optical waveforms will be demonstrated. In particular, I present experimental results in which the TM-SP is used for real-time observation of the complex field dynamic spectrum evolution in a GHz-bandwidth electro-optic phase-modulation process [AC1].

- The TM-SP scheme in the previous Chapter 4 has been demonstrated for the RT-SA of base-band waveforms, i.e., whose central frequency is around zero. In this chapter, an strategy is proposed and experimentally demonstrated for applications of the TM-SP on more general band-pass waveforms, having central frequencies even significantly higher than the signal's bandwidth, without the need to increase the Nyquist sampling rate [AC2]. This is achieved by employing the band-pass sampling concept [90] within the TM-SP scheme.

- The TM-SP approach provides access to the complex Fourier coefficients of the incoming non-stationary broadband signal of interest, in the analog temporal wave domain. This enables to process/filter these Fourier coefficients directly in the temporal domain, i.e., in a real-time manner. In this Chapter, a TM-SP based approach for continuous time-varying frequency

filtering of broadband microwave signals is proposed and experimentally demonstrated. This study provides a relevant example of the unique capabilities of the TM-SP concept for the analog processing and synthesis of GHz-bandwidth non-stationary signals [AC3].

5.1 Real-time spectrogram analysis of complex optical waveforms

Real-time optical spectral analysis is a fundamental tool for observation of complex spectral dynamics in ultra-fast lasers [91], soliton studies [92], spectroscopy [93], bio-imaging [94] etc. Conventional optical spectrum analyzers, relying on spatial dispersion (e.g., diffraction gratings), capture spectral information averaged over a relatively long time duration, such that they are not suitable to follow the dynamics of rapidly changing spectra. The time-mapped Fourier transform (TM-FT) based on temporal stretching by chromatic dispersion [64] enables mapping the energy frequency spectrum of the signal of interest along the time domain, i.e., frequency-to-time mapping, so that this can be captured at a very high speed (at refreshing rates above the MHz range), see detailed discussions in Section 1.4.1. The TM-FT concept has enabled many breakthroughs towards the analysis of changing events or processes [52]. However, as illustrated in Fig.1.5, TM-FT relies on "temporal stretching" and thus, it is fundamentally limited to provide static spectral information of time-limited (e.g., pulsed) waveforms repeating at a relatively low speed. In the most general case of a continuously varying signal, the TM-FT can only be applied on truncated and delayed sections of the signal, inherently losing most of the signal's information.

The time-mapped spectrogram (TM-SP) approach extends the frequency-to-time mapping concept to the analysis of continuous-time signals (not limited to pulsed waveforms) and this Thesis has confirmed that it is well suited for application on high-speed optical wave-fields. As per the theory presented in Chapter 2, the TM-SP concept is applicable to general complex temporal waveforms, with arbitrary amplitude and phase temporal profiles, within the performance specifications of the practical scheme. Nonetheless, the numerical and experimental results reported in the previous chapters of this Thesis (Chapter 3 and 4) were restricted to the analysis of amplitude signals, such as microwave signals mapped into an optical carrier. To demonstrate the capability of the TM-SP for the analysis of complex waveforms, we present here experimental results on application of this concept for real-time observation of the dynamic spectral evolution of a rapidly changing

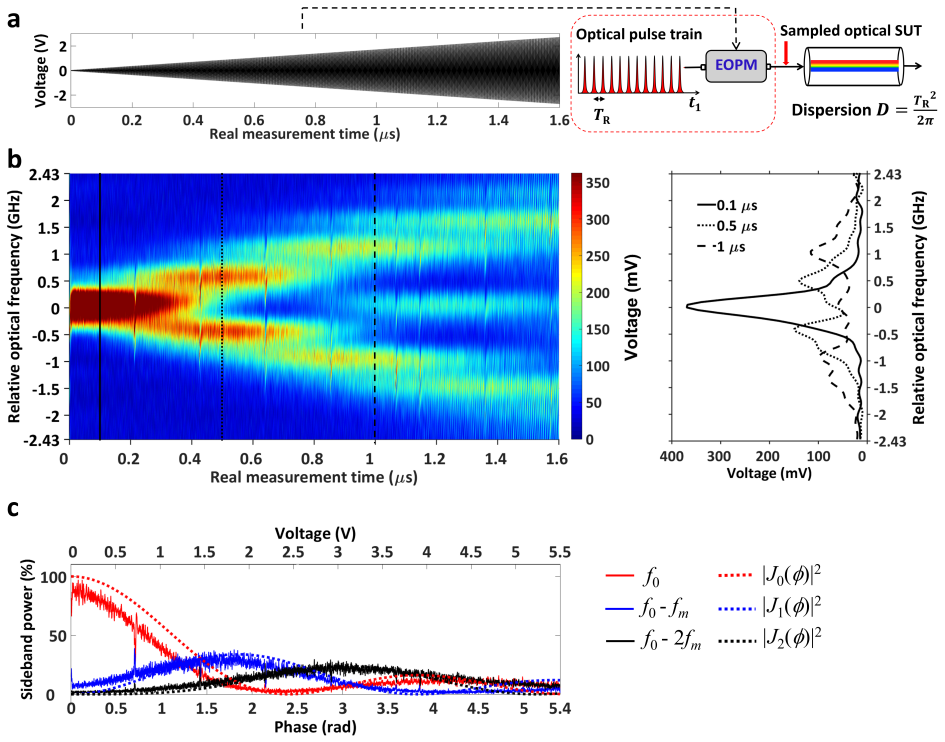

Fig. 5.1: Experimental results on real-time SP analysis of a phase-modulated optical signal. (a) Test modulation signal, with a linearly increasing amplitude, applied to an optical field through an electro-optic phase modulator. (b) 2D representation of the signal joint time-frequency energy distribution (SP) that is directly recovered from the measured output temporal trace. (c) Relative power of each of the 3 main measured spectral sidebands as a function of the linearly increasing peak-to-peak modulation voltage (and corresponding electro-optic phase shift).

phase-modulated optical field [AC1]. The reported frequency-spectrum evolution is observed with a frequency resolution of ~ 425 MHz (~ 3.4 picometer at an operating wavelength of 1550.1 nm), well beyond the performance of a conventional optical spectrum analyzer, and at an unprecedented analysis speed of nearly 5×10^9 spectra/second [AC1].

5.1.1 Experimental results

The experimental setup for the RT-SA of complex (specifically, phase-modulated) optical waveforms based on the TM-SP concept is shown in Fig. 5.1(a). This experiment is designed to follow the dynamic spectrum evolution of a rapidly-changing phase-modulated optical field. We recall that the TM-SP scheme involves short-pulse temporal sampling of the signal under test (SUT) followed by second-order chromatic dispersion. In the conducted experiment, the optical SUT is generated by phase modulation of mode-locked optical pulses (having intensity FWHM $\Delta t_p \sim 7$

ps, repetition (sampling) rate of 4.86 GHz and central optical frequency = 193.5 THz), using an electro-optic phase modulator (V_π = 3.2 V) driven by a 1.6-μs long sinusoidal signal, of frequency f_m = 500 MHz, with peak-to-peak amplitude increasing from 0 to 5.5 V (modulation signal shown in Fig. 5.1(a)). The signal at the phase modulator output can be interpreted as an optical phase-modulated uniform-amplitude waveform (SUT) that is sampled by the mode-locked pulse train, with a sampling period $T_{\rm R}$ = 205.6 ps. The sampled signal is then subsequently propagated through a dispersion compensating fiber (DCF), with a total dispersion $\ddot{\phi} = {T_{\rm R}}^2/2\pi$ = 6738.3 ps^{2}rad^{-1}. The output single-shot waveform is captured with a 50 GHz photo-detector attached to a real-time oscilloscope, with no averaging. The measured output temporal waveform along each slot of duration $T_{\rm R}$(sampling period) is simply mapped into the equivalent frequency axis using the defined mapping law , $\Delta\omega_1 \rightarrow \Delta t_2/\ddot{\phi}$; this produces the 2D representation of the signal joint time-frequency energy distribution (SP) that is shown in Fig. 5.1(b). The recovered SP reveals the evolution of the optical spectral sidebands that are induced by the electro-optic phase modulation process, purely in real time. The time-mapped optical spectrum at different time locations is also plotted on the right side of Fig. 5.1(b).

In particular, the linearly increasing voltage applied to the electro-optic phase modulator generates rapidly-changing new sidebands at the output of the phase modulator at $f_0 \pm f_m$, $f_0 \pm 2f_m$...etc. [95], around the carrier frequency of the input optical pulses, f_0. The following dispersive line maps the generated instantaneous optical spectra along the time-axis in a real time fashion, following the theory of time-mapped spectrogram analysis. The changing spectrum of the modulated optical waveform is captured at every sampling period, $T_{\rm R}$ = 205.7 ps, i.e., at a speed of 4.86×10^9 spectra per second, orders of magnitude beyond the capabilities of present optical spectrum analysis methods. Moreover, the changing spectra are each measured with a high resolution of ~425 MHz, in agreement with the theoretical estimates, $\delta\omega \approx \Delta t_d/\ddot{\phi}$, where we recall that $\Delta t_d \approx$ 18 ps is the temporal resolution of the detection system. The evolution of the optical spectral side-bands of the phase-modulated waveform follows very closely the theoretical predictions: This is confirmed through the results shown in Fig. 5.1(c), where the relative side-band power is plotted as a function of the linearly increasing applied modulation voltage (and corresponding electro-optic phase shift). The relative side-band powers are indeed following the Bessel functions that govern the modulation process of an electro-optic phase modulator [95]. The conducted analysis provides a direct experi-

mental observation of the dynamical performance of the evaluated electro-optic phase modulator, in a way that would not be possible otherwise. These results show that the TM-SP concept in general can be applied for RT-SA of complex waveforms. This capability opens additional important possibilities towards real-time spectral analysis and processing of optical fields.

5.2 Real-time spectral analysis of high-frequency waveforms through bandpass sampling

Real-time Fourier spectral analysis (RT-SA) of high-frequency broadband waveforms is required in many important applications. This includes the case of waveforms whose central frequency may be even much higher than the signal's spectral bandwidth, such as those often found in a variety of important RF applications [53, 54]. In Chapter 4, the TM-SP based design has been successfully demonstrated for the RT-SA of base-band microwave signals, in which the time-varying spectral content of the input SUT is directly captured by a real-time oscilloscope, with unprecedented performance, namely with instantaneous bandwidth in the GHz range and nanosecond resolutions. In the TM-SP scheme, the maximum frequency extension of the SUT is limited by the repetition rate of the short-pulse sampling unit, as per the Nyquist criterion [2]. As the carrier (or central) frequency of the SUT increases, the Nyquist criterion may lead to impractically high sampling rate requirements. Conventional digital RT-SA methods rely on down-converting these high-frequency waveforms to baseband for their detection and employ cumbersome multi-stage mixers and tunable local oscillators [43].

However, RT-SA of high-frequency waveforms based on the TM-SP design presents new opportunities to avoid the down-conversion stages that use mixers and local oscillators [AC2]. As discussed in Chapter 2, the front end of the TM-SP scheme consists of a basic temporal sampling unit; hence, the band-pass sampling theory [90] can then be employed to directly sample the high-frequency waveforms below the Nyquist rate without losing any of the input signal information, while avoiding the need for dedicated down-conversion stages. Bandpass sampling is a special form of under sampling, in which the spectrum of an arbitrary high-frequency bandpass signal is shifted to center it around lower frequencies, enabling direct access to the baseband spectral content of the SUT. By appropriately choosing the sampling frequency, the TM-SP of the high-frequency signal

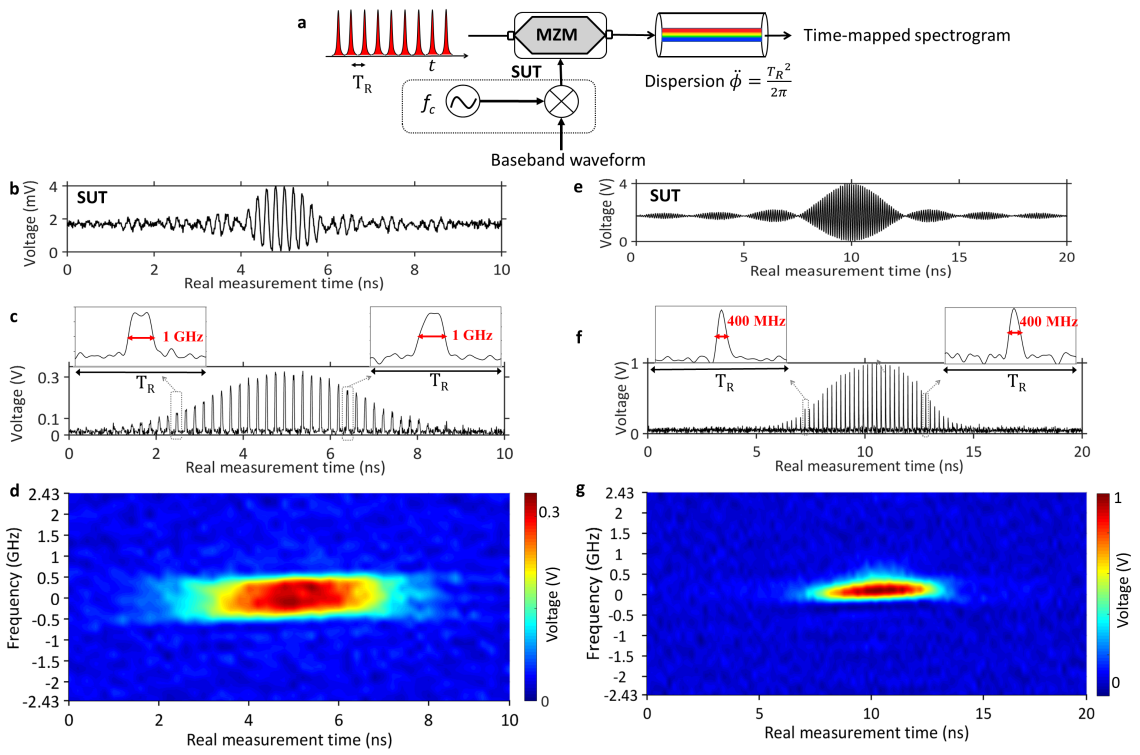

Fig. 5.2: The RT-SA of high-frequency waveforms using the TM-SP concept and bandpass sampling. (a) Experimental setup. (b) Signal under test (SUT): A 2-ns long sinc pulse modulated on a 4.86-GHz tone. (c) A single-shot real-time scope trace at the output, showing the mapping of the square-shaped baseband spectrum of the SUT, along each time slot of duration TR (205.7 ps) (d) The 2D joint T-F representation of the baseband signal SP, recovered by re-scaling the output temporal trace along each consecutive analysis period into the corresponding frequency axis (vertical axis), only showing the positive side of frequencies. (e) SUT: A 5-ns long sinc pulse modulated on 9.72 GHz (f) Output temporal waveform showing the mapping of the resolution-limited baseband spectra of the SUT. (g) The 2D joint TF representation of the SP.

can be obtained simply by propagating the bandpass sampled waveform through an adequately designed second-order dispersive medium. In the proof-of-concept experiments reported here, I have demonstrated the RT-SA of nanosecond-long microwave pulses with spectral content up to 10 GHz, corresponding to an overall bandwidth ∼20 GHz, by band-pass sampling at a significantly lower Nyquist rate (< 5 GHz).

5.2.1 Operation principle and experimental results

Fig. 5.2(a) shows the experimental setup for RT-SA of high-frequency waveforms using the TM-SP concept combined with bandpass sampling. The SUT is a sinc-shaped temporal pulse, corresponding to a square-like spectrum, of 3dB full-width bandwidth B ∼1 GHz, Fig. 5.2(b), generated from an electronic arbitrary waveform generator (AWG) and up-converted to a carrier frequency $f_c = 4.86$

GHz by mixing with an RF tone generated by a RF synthesizer. The highest frequency of the up-converted signal in this first example is then f_{max} 4.86+0.5 = 5.36 GHz. The SUT is sampled using optical pulses from a mode-locked laser (intensity FWHM pulse width $\Delta t_p \sim 7$ ps) in an electro-optic Mach-Zehnder modulator (MZM). The Nyquist criterion establishes a minimum required sampling rate of $2f_{max} = 10.72$ GHz. However, according to the band-pass sampling theory, if properly designed, the sampling rate can be as low as $B = 1$ GHz (i.e., information bandwidth), for complete reconstruction of the base-band waveform. Nonetheless, it is also important to recall that the sampling rate also fixes the temporal resolution and the amount of dispersion needed in the TM-SP scheme, i.e., a lower sampling rate translates into a longer temporal resolution and it requires a higher amount of dispersion, as described in the previous chapters. Hence, the chosen sampling rate is then fixed to $f_R = 4.86$ GHz (corresponding sampling period $T_{\mathrm{R}} = 205.6$ ps). According to the TM-SP design equations [AJ1], a group velocity dispersion (implemented here by dispersion-compensating fiber, DCF) of $\ddot{\phi} = {T_{\mathrm{R}}}^2/2\pi = 6738.3$ ps^{2}rad^{-1} is required. At the system output, the delayed and frequency-shifted copies of the input SUT interfere with each other, leading to a temporal waveform that follows the windowed Fourier transform, i.e., the spectrogram, of the SUT at every consecutive sampling period (with a duration of $T_{\mathrm{R}} = 205.6$ ps). The output temporal waveform, Fig. 5.2(c), is captured with a 50-GHz photo-detector connected to a 63-GHz bandwidth real-time oscilloscope and mapped into the equivalent frequency axis, along each slot of duration T_{R}, using the mapping law: $\Delta t_2 \leftarrow \Delta\omega_1\ddot{\phi}$.

A zoom-in over different analysis periods (each with a duration T_{R}), as shown in the insets of Fig. 5.2(c), reveals the predicted time mapping of the down-converted square-shaped base-band spectral content of the SUT, around the zero frequency. Fig. 5.2(d) shows the two-dimensional (2D) representation of the SUT's time-frequency (T-F) energy distribution (the spectrogram) that is directly mapped from the measured real-time scope trace. In this experimental configuration the time resolution of the TM-SP is ~ 2.54 ns, and the frequency resolution is ~ 340 MHz. Moreover, it can also be observed from Fig. 5.2(c) that the mapped spectra repeat over consecutive analysis periods (each of duration T_{R}), a property that we have exploited to relax the detection specifications of the TM-SP scheme (see Section 3.4). Fig. 5.2(e) shows another analysis example of a high-frequency SUT, a 400-MHz full bandwidth, 5-ns duration sinc pulse modulated on a 9.72-GHz tone. In this case, the maximum frequency content of the SUT approaches 10 GHz, corresponding to a full

spectral bandwidth of 20 GHz, whereas the sampling rate remains below 5 GHz. As expected, the output TM-SP trace in Fig. 5.2(f) shows a successful time-mapping of the 400 MHz full spectrum of the baseband waveform. Note that, in this case the time-mapped spectral shape is affected by the TM-SP frequency resolution limit of 340 MHz. The above results demonstrate a method to avoid the need for down-conversion stages before performing RT-SA, using the TM-SP approach combined with band-pass sampling. This method should prove highly useful for RT-SA applications of broadband microwave signals with high carrier frequencies, such as those found in real-life wireless environments.

5.3 Time-varying frequency filtering of broadband waveforms

Time-varying frequency filtering is an essential tool in processing and synthesis of non-stationary signals i.e., signals whose frequency content is varying with time. This functionality is desired for a wide range of applications, particularly for non-stationary interference mitigation in radar [96, 97], cognitive radio [98,99] and spread spectrum communication applications [100–102]. Conventionally, time-varying frequency filtering is performed by representing the non-stationary signal of interest in the two-dimensional (2D) time-frequency (T-F) domain, using T-F energy distributions such as the short-time Fourier transform (STFT) or spectrogram, in the digital domain, and manipulating the obtained distributions using appropriate digital filtering techniques [30, 96]. This strategy requires analog-to-digital conversion of the SUT and subsequent digital-to-analog conversion of the processed signal. However, as the signal bandwidth exceeds a few GHz, such as in the above-mentioned applications, the digital computation requirements that are needed for the 2D T-F analysis and processing of the involved broadband non-stationary microwave signals may become very inefficient or even entirely impractical, particularly in a real-time manned, mainly owing to the need for computationally intensive fast Fourier transform (FFT) algorithms, requiring large processing delays and computation power.

The TM-SP provides real-time access to the evolving Fourier coefficients of a non-stationary signal in the analog wave domain, enabling to process/filter these Fourier coefficients directly through temporal modulation. This is an inherently efficient and real-time processing approach. Specifically, the TM-SP scheme maps the 2D T-F distribution (short-time Fourier transform) of the incoming

SUT along the 1D temporal domain. A suitably designed temporal modulation function can then be used on the TM-SP waveform to process the 2D T-F energy distribution, e.g., to implement a desired time-varying frequency filter [AC3]. The processed signal is finally recovered by passing through another chromatic dispersive delay line with the exact opposite dispersion of the input one followed by a low-pass filter. Simulation results and a proof-of-concept experimental demonstration of the TM-SP based time-varying filtering principle is demonstrated.

5.3.1 Operation Principle

Fig. 5.3 illustrates the concept of the proposed on-the-fly time-varying frequency filtering of non-stationary microwave signals. The microwave signal under test (SUT) is first sampled with short pulses (individual pulse width Δt_p, and repetition frequency $\omega_{\mathrm{R}} = 2\pi/T_{\mathrm{R}}$), followed by second order chromatic (group delay) dispersion ($\ddot{\phi}$). At the output of the dispersive element $\ddot{\phi}$, the short-time Fourier transform (STFT) of the SUT is mapped along the temporal axis at the signal speed, with each consecutive Fourier spectrum mapped within each analysis period of duration T_{R}, when the dispersive delay satisfies $\ddot{\phi} = {T_{\mathrm{R}}}^2/2\pi$ $\mathrm{ps^2 rad^{-1}}$. The 2D T-F energy distribution of the SUT depicted in Fig. 5.3 is simply obtained by re-scaling the temporal trace along each T_{R} into the corresponding frequency axis according to the defined frequency-to-time mapping law (determined by the dispersion coefficient). The time resolution of the generated time-mapped spectrogram is $\delta t_r \approx \ddot{\phi} \times \Delta\omega_p$, whereas the frequency resolution is the inverse of this time resolution, given by $\delta\omega_r \approx \Delta t_p/\ddot{\phi}$; these resolutions are then only constrained by the Fourier transform uncertainty principle. A predefined temporal modulation pattern is generated and used to modulate the output time-mapped spectrogram after the first dispersive element, implementing the desired time-varying frequency filter. The modulation pattern can be designed to implement the user-defined desired filtering operation on the T-F energy distribution. Since the T-F distribution is now accessible with a time resolution of δt_r, the temporal modulation pattern can modify the signal T-F distribution at a corresponding maximum tuning speed of $1/\delta t_r$. The T-F filtered signal is recovered by propagation through a dispersive delay line with the exact opposite dispersion of the input one, $-\ddot{\phi}$. Finally, a low-pass filtering, acting as an envelope detector, may be used to extract the T-F filtered signal envelope.

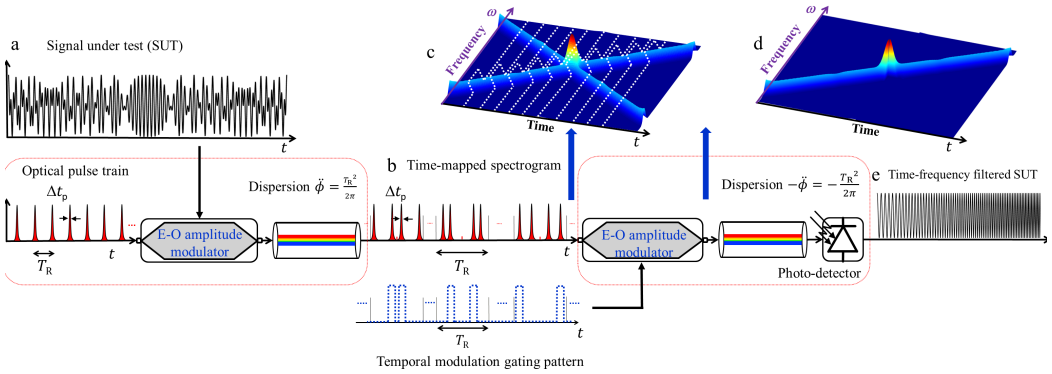

Fig. 5.3: On-the-fly continuous time-varying frequency filtering of broadband microwave signals using the TM-SP approach. (a) Microwave signal under test, composed of two linear chirp components. (b) Time-mapped STFT or the full spectrogram (c) The T-F energy distribution. Note that only the positive frequencies are shown. The dashed lines show the temporal modulation gating pattern designed to filter one of the chirp component in the time-frequency domain. (d) The T-F energy distribution after applying the temporal modulation gating pattern. (e) The output filtered signal consisting of only a single chirp component.

5.3.2 Simulation Results

A practical system based on the proposed design in Fig. 5.3 for on-the-fly time-varying frequency filtering of GHz-bandwidth microwave signals is first validated through the numerical simulation example shown in Fig. 5.4. The input SUT consists of a 100-ns long microwave signal, shown in Fig. 5.4(a), which is composed by two temporally superimposed frequency-chirped sinusoidal waveforms, $\omega_{\mathrm{RF},1}(t)$ from 500 MHz to 2 GHz, and $\omega_{\mathrm{RF},2}(t)$, from 2 GHz to 500 MHz. An electro-optic Mach-Zehnder is used to modulate the SUT with a periodic train of optical pulses having an intensity FWHM time width of $\Delta t_p \approx 7$ps (FWHM frequency bandwidth $\Delta\omega_p \approx 2\pi \times 60$ GHz), at a repetition rate 4.86 GHz, thus satisfying the Nyquist criterion for microwave signals with frequency content up to 2.43 GHz. The following dispersive line introduces total dispersion $\ddot{\phi} = {T_\mathrm{R}}^2/2\pi \approx 6738.3\ \mathrm{ps}^2\mathrm{rad}^{-1}$ over the full frequency bandwidth of the sampling pulses. Fig. 5.4(b) shows the average intensity of the output temporal waveform, also extending over a total duration of 100 ns. Fig. 5.4(b) also shows a zoom along different time instances, each of duration T_R, showing the time-mapped instantaneous spectra of two different frequency components of the SUT, $\pm\omega_{\mathrm{RF},1}(t)$ and $\pm\omega_{\mathrm{RF},2}(t)$, linearly increasing and decreasing with time, respectively. The dashed line shows the temporal modulation gating pattern applied to filter the T-F energy distribution. The temporal modulation gating pattern is chosen such that only the chirp component $\omega_{\mathrm{RF},1}(t)$ is selected in every analysis period T_R. Fig. 5.4(c) shows a 2D representation of the signal joint T-F energy distribution (SP)

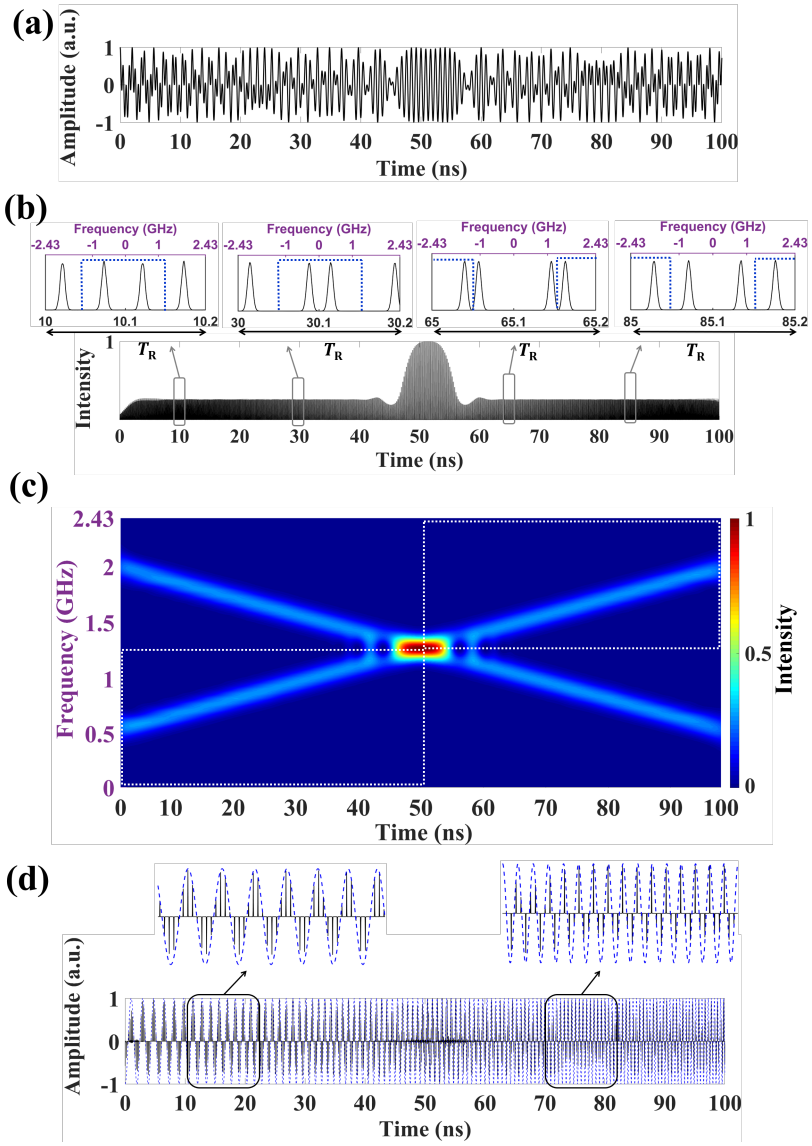

Fig. 5.4: Numerical evaluation of time-varying frequency filtering using the TM-SP approach. (a) Input signal composed by two superimposed linearly frequency-chirped sinusoidal waveforms (b) The average intensity of the temporal waveform at the output of the first dispersive line $\ddot{\phi}$, showing the time-mapped spectrogram, along with the temporal gating waveform (dashed) used to manipulate (i.e., custom filter) the time-mapped spectrum within each analysis period. (c) 2D representation of the signal joint T-F energy distribution of the time-mapped spectrogram along with time-domain filtering process. (d) The recovered chirp component of the SUT, $\omega_{\mathrm{RF},1}(t)$ after second dispersive element $-\ddot{\phi}$.

that is recovered from the output temporal trace according to the defined time-to-frequency mapping law. Note that negative frequencies are not shown in Fig. 5.4(c). The temporal modulation gating pattern along each T_{R} is also shown with dashed lines. The T-F filtered, sampled SUT is further propagated through a dispersive line with a total dispersion $\ddot{\phi} = -{T_{\mathrm{R}}}^2/2\pi \approx -6738.3$ ps^{2}rad^{-1} for signal retrieval. Finally, a low pass filter having a bandwidth of 5 GHz is used for envelope

detection. Fig. 5.4(d) shows the recovered sampled SUT after the second dispersive line. The dotted lines show the ideal chirp component $\omega_{\mathrm{RF},1}(t)$ which matches very closely the envelope of the recovered sampled version.

5.3.3 Experimental Results

A proof-of-concept experiment is also performed to demonstrate the time-varying filtering scheme based on the design illustrated in Fig. 5.3, results presented in Fig. 5.5. A linearly chirped microwave signal $\omega_{\mathrm{RF,a}}(t)$ is generated from an AWG, with frequencies increasing from 500 MHz to 1 GHz within the time interval from 0 to 1 μs, and frequencies decreasing from 1 GHz to 500 MHz within the 1 μs to 2 μs interval. This microwave signal is modulated by a periodic train of picosecond optical pulses ($\Delta t_p \sim 7$ps) at a repetition (sampling) rate of 4.86 GHz using an electro-optic Mach-Zehnder modulator biased at the quadrature bias point. The voltage of the microwave SUT is chosen such that the electro-optic modulation process generates in addition to $\omega_{\mathrm{RF,a}}(t)$, the third harmonic of the microwave chirp i.e., $\omega_{\mathrm{RF,3a}}(t)$, having a frequency chirp from 1.5 GHz to 3 GHz within the 0 to 1 μs interval and from 3 GHz to 1.5 GHz within the 1 μs to 2 μs interval. The sampled SUT after the modulation is shown in Fig. 5.5(a), as captured in a 23 GHz real-time scope (without averaging) after photo-detection. The envelope (red) of the sampled SUT after modulation is obtained by low pass filtering the sampled SUT within the Nyquist bandwidth (-2.43 GHz, +2.43 GHz). Fig. 5.5(b) shows the spectrogram of the envelope of the sampled SUT, obtained digitally. It shows the two defined chirp components $\omega_{\mathrm{RF,a}}(t)$, and $\omega_{\mathrm{RF,3a}}(t)$, over a the SUT duration. Note that $\omega_{\mathrm{RF,3a}}(t)$, is exceeding the Nyquist bandwidth, and as a result, the frequency content greater than 2.43 GHz is wrapped and folded within the Nyquist bandwidth. The sampled SUT is propagated through a suitable dispersive line, implemented using a dispersion compensating fiber (DCF), with a total dispersion $\ddot{\phi} = {T_{\mathrm{R}}}^2/2\pi \approx 6738.3$ ps^{2}rad^{-1}.

At the output of the dispersive line, the T-F distribution (STFT) of the sampled SUT is continuously mapped onto the temporal domain with a time resolution $\delta t_r \approx 6$ns. Hence, we can manipulate the T-F distribution at this time scale, i.e., corresponding to a tuning rate of the implemented frequency filtering operation of ~ 167 MHz. The temporal modulation or gating pattern is generated from a 24 GS/s AWG with an analog bandwidth of 10 GHz and imposed on the optical signal after the first dispersive line(time-mapped spectrogram waveform) using another MZ modu-

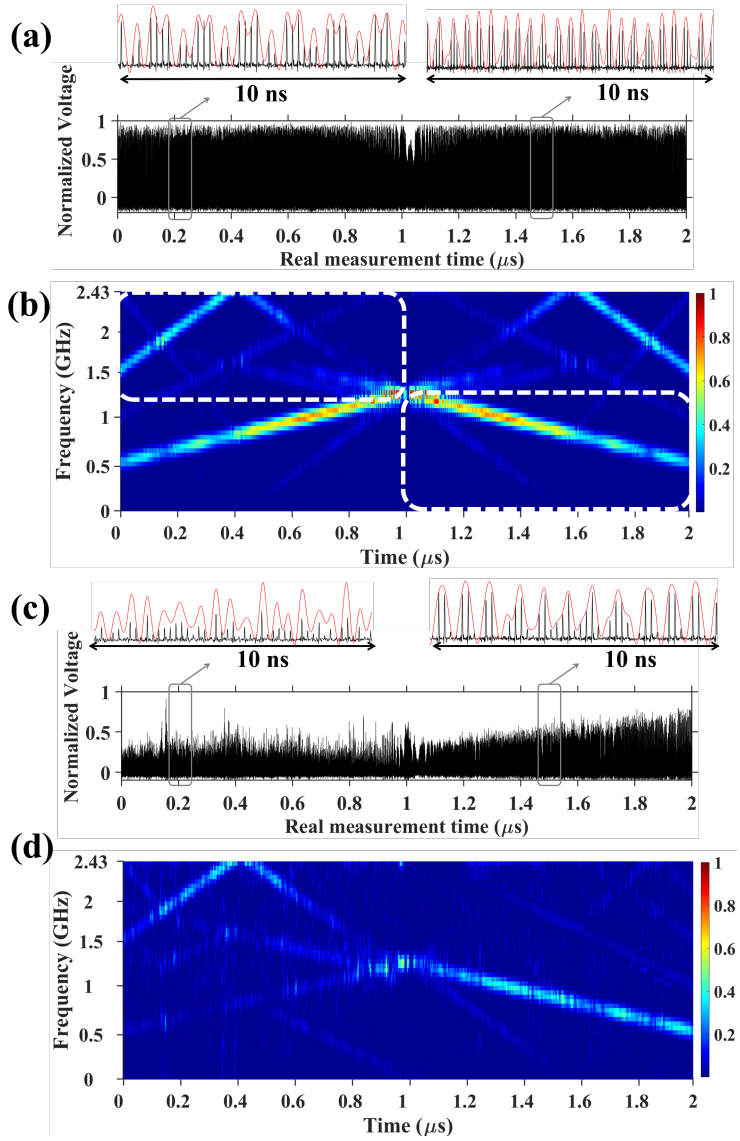

Fig. 5.5: Experimental evaluation of the time-varying frequency filtering using the TM-SP approach. Experimental results (a) Sampled SUT composed by two frequency-chirped sinusoidal waveforms (b) Digitally generated spectrogram. It also shows temporal gating filter (dashed lines) (c) The T-F filtered, sampled SUT after second dispersive line. (d) Digitally generated spectrogram of the envelope of the T-F filtered output.

lator. The temporal gating pattern is also shown in Fig. 5.5(b). Ideally, the gating pattern must be designed such that it can select the desired frequency components at every $T_{\mathrm{R}} = 205.76$ ps, as described with the simulation example in the previous section. In the most general case, we need to generate a temporal gating pattern each gating pulse having a width equal to the individual optical sampling pulses i.e., $\Delta t_p \sim$7 ps, which would require the use of a very high-speed AWG for generation of such a short-gating width. However, with the available AWG, we could generate a gating

pulse width of $\sim$ 100 ps, which corresponds to half of the Nyquist bandwidth, as can be observed in Fig. 5.5(b). Hence, the gating pulses are generated such that the signal component $\omega_{\mathrm{RF,3a}}(t)$ is selected within the 0 to 1 μs interval, whereas the $\omega_{\mathrm{RF,a}}(t)$ component is selected within the second half of the signal (1 to 2 μs). The T-F filtered SUT is recovered after the second dispersive line, $-\ddot{\phi} = -{T_{\mathrm{R}}}^2/2\pi \approx -6738.3$ ps^{2}rad^{-1}. Fig. 5.5(c) shows the filtered sampled SUT, captured in a 23 GHz real-time scope after photo-detection. The envelope is obtained by low pass filtering with a 5 GHz bandwidth. Fig. 5.5(d) shows the corresponding digitally generated spectrogram of the envelope. It is evident that as designed, the component $\omega_{\mathrm{RF,3a}}(t)$ is recovered within the first half of the signal (0 to 1 μs) and the component $\omega_{\mathrm{RF,a}}(t)$ is recovered within the second half of the signal (1 µs to 2 μs). This example provides a preliminary first proof of the interesting potential of the TM-SP concept for the analysis, processing and synthesis of the joint TF distribution of arbitrary high-speed signals in a real-time manner and directly in the analog wave domain.

5.4 Conclusions

In this chapter, I have discussed some important features of the TM-SP that are particularly found advantageous for RT-SA and processing of broadband waveforms. The proposed TM-SP based RT-SA of complex optical wave-fields could be highly useful in studying complex ultra-fast phenomenon in laser systems [52,91–93]. The bandpass sampling concept employed in the TM-SP eliminates the need for cumbersome mixing stages while down-converting high-frequency waveforms to base-band, thereby greatly simplifying the RT-SA architecture. Finally, the proposed on-the-fly time-frequency filtering of broadband waveforms based on the TM-SP enables real-time, ultra-high-speed user-defined time-frequency manipulation of broadband waveforms in the native analog wave domain.

Chapter 6

Conclusions and Future Work

A summary of the findings on the analog signal processing framework for the real-time spectral analysis (RT-SA) of broadband waveforms, that have been reported in this Thesis is presented. Real-time digital signal processing functionalities that could be directly implemented in the analog domain, by using the analog signal processing framework proposed in this Thesis is envisioned.

6.1 Summary

Chapter 2 introduced the theory of time-mapped spectrogram (TM-SP) - a universal analog signal processing framework to map the full short-time Fourier transform (STFT) of an incoming arbitrary waveform along the time domain through temporal sampling and dispersive delay. The TM-SP captures the full STFT of high-speed signals (e.g., microwave to optical) in real time and directly in the analog wave domain, avoiding the need for computationally intensive fast Fourier transform (FFT) algorithms. The main design trade-offs, performance specifications, and some unique features offered by the TM-SP architecture have been discussed. For example, the time and frequency resolutions of the conducted STFT analysis were found to be related to the sampling pulse width, and hence conveniently tuned by changing the sampling pulse width. The repeated time-mapping of the STFT information - a unique feature of the TM-SP has been also found out and studied in detail.

In Chapter 3, a practical photonic-based platform for the TM-SP implementation was numerically simulated, aiming at continuous gap-free RT-SA of broadband waveforms. The design

trade-offs such as time and frequency resolutions, and unique features such as continuous gap-free operation, and repeated mapping of the STFT information, were all verified through numerical simulations. The photonic implementation of the TM-SP is particularly attractive for continuous gap-free RT-SA of GHz bandwidth microwave signals, offering GHz rate Fourier transform (FT) processing speeds, and nanosecond temporal resolutions.

A photonic-based TM-SP was then experimentally demonstrated in Chapter 4 by using off-the-shelf components, enabling continuous gap-free RT-SA of GHz-bandwidth microwave waveforms. The demonstrated photonic-based TM-SP has achieved unprecedented RT-SA performance specifications 4.1, namely

- Real-time instantaneous bandwidth ~ 5 GHz,
- FT processing speeds of $\sim 5 \times 10^9$ FT per second,
- Temporal resolutions ~ 2 ns,
- Intercepting random fast signals with durations down to the nanosecond regime, by performing continuous gap-free spectral analysis

These performance specifications fulfill critical requirements of the RT-SA for a wide range of applications, in communications, radar, radio astronomy, biomedical instrumentation and others. Most importantly, the universal TM-SP architecture is well suited for the analysis and processing of waveforms across other frequency regions in the electromagnetic spectrum as well. Moreover, the performance specifications of the photonic-based TM-SP achieved in this doctoral project can easily be upgraded by using the latest developments on mode-locked lasers having hundreds of GHz repetition rates [88], matched by temporal modulation technologies with similar bandwidth performance [89, 103] and all-optical temporal sampling techniques for output waveform measurements [87], offering the potential for sub-THz bandwidth RT-SA with THz-speed FT processing speeds.

Finally, some important features of the TM-SP that are particularly found advantageous for RT-SA and processing of broadband waveforms were presented in Chapter 5. The TM-SP based RT-SA of complex optical wave-fields could be highly useful in studying complex ultra-fast phenomenon in laser systems [52]. The bandpass sampling concept employed in the TM-SP eliminates the need for

cumbersome mixing stages while down-converting high-frequency waveforms to base-band, thereby greatly simplifying the RT-SA architecture. The on-the-fly time-frequency filtering of broadband waveforms based on the TM-SP enables real-time, ultra-high-speed user-defined time-frequency manipulation of broadband waveforms in the native analog wave domain.

An important challenge in the proposed photonic implementation of the TM-SP is the requirement of a large detection bandwidth, higher than the spectral bandwidth of the SUT. Ideally, the detection bandwidth should be sufficiently high to capture the short sampling optical pulses. Otherwise, a deterioration of the theoretical frequency resolution is expected, as discussed in Section. 4.2. Additional strategies might be useful for efficient detection of the time-mapped spectrograms within practical performance specifications. One such detection strategy, which relaxes the detection sampling rate requirements, has been proposed in Section. 3.4, and demonstrated in Fig. 4.7. However, there is clearly scope for improving the TM-SP architecture for relaxing further the detection bandwidth requirements. For instance, I anticipate that the use of time-lens based waveform processing configurations, such as temporal microscopy schemes [104–107], may provide a path towards this aim.

6.2 Future work

The TM-SP analysis proposed in this Thesis time-maps the full STFT of the incoming analog waveform, while the output processed waveform remains in the original physical wave domain. This provides additional important capabilities to process the entire signal's time-frequency distribution in an efficient and direct fashion using well-established time-domain waveform manipulation methods. Many important joint time-frequency signal processing functionalities [30, 34, 41], such as time-variant frequency filtering, re-shaping a waveform to provide a prescribed time-frequency distribution (so-called time-frequency synthesis), or pattern identification in the joint time-frequency plane, could be all implemented on the fly through standard time-domain processing methods. For instance, customized filtering of the input signal in the time-frequency plane, i.e., time-varying frequency filtering has been demonstrated for a relatively simple time domain filter configuration scenario in Section 5.3. More complex rapidly tunable time-domain filter configurations could be designed using such a design. These prospects are particularly interesting for broadband waveforms,

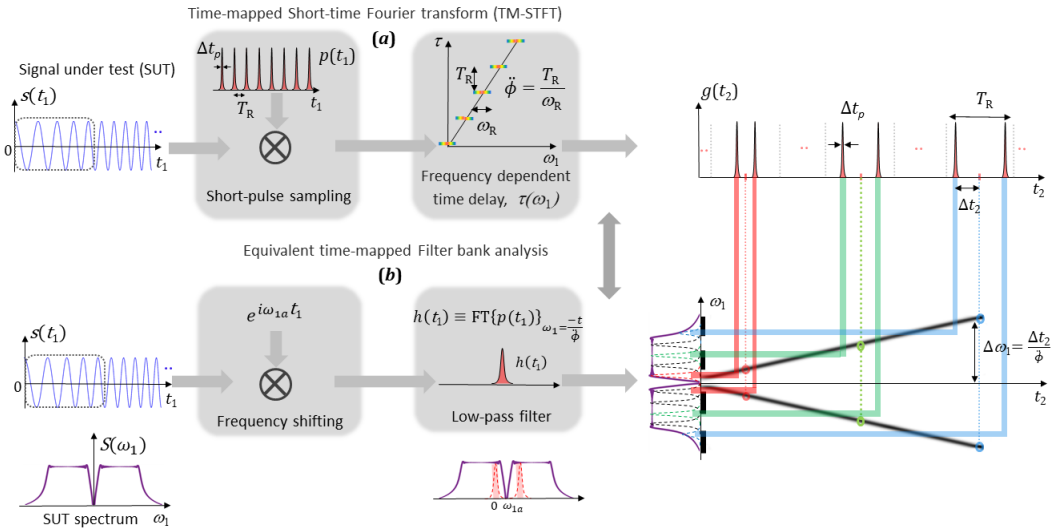

Fig. 6.1: Real-time analog filter-bank interpretation of the time-mapped STFT. (a) Schematic of TM-STFT concept. (b) The equivalent time-mapped filter-bank interpretation of the TM-STFT.

i.e., with bandwidths in the GHz regime and above, from the microwave to the optical domain, for which real-time dynamic Fourier analysis and processing tools remain challenging.

To give a few examples, the following real-time digital signal processing concepts could be directly implemented in the analog domain by using the TM-SP concept.

6.2.1 Real-time analog filter banks

Owing to the filter-bank interpretation of the general short-time Fourier transform definition [109, 110], the newly proposed time-mapped STFT in Fig. 6.1(a) can be interpreted as an equivalent analog real-time filter bank implementation, as illustrated in Fig. 6.1(b). The filter-bank interpretation positions the time-mapped spectrogram in the general context of a broader real-time filter bank theory, and could offer new opportunities for analog real-time implementation of signal processing functionalities enabled by the filter bank techniques, such as sampling rate conversion, compression, expansion etc. [109, 110].

6.2.2 Real-time ultra-fast convolution

The convolution is a key signal processing operation in linear system theory. Convolution of two signals is often computed efficiently in the frequency domain, using FFT algorithms, referred to as the

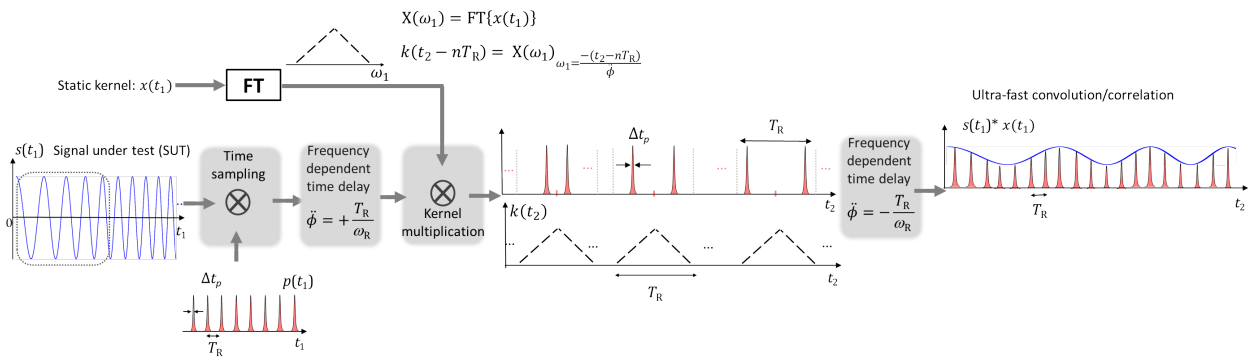

Fig. 6.2: Real-time fast convolution using time-mapped STFT. The time-mapped STFT maps the incoming SUT's Fourier transform (FT) on to the temporal domain. The FT of the static kernel is generated digitally and multiplied with the time-mapped STFT in time domian, within the each temporal period, T_{R}. After the frequency domain multiplication of the SUT's FT with kernel's FT, the resulting waveform is further propagated through another dispersive medium of same magnitude of dispersion but opposite sign, $-\ddot{\phi}$ to perform inverse FT. The resulting output temporal waveform envelope gives convolution of the SUT with the kernel.

fast-convolution [9]. The fast-convolution relies on the property that the time-domain convolution between two signals is equivalent to point wise multiplication of their corresponding FT spectra. Real-time fast-convolution is a work-horse in real-time DSP applications such as filtering, correlation, matched-filtering etc. [9,10]. Moreover, real-time convolutional filtering is increasingly desired in image processing tasks, convolutional neural networks and other related applications [111,112].

As illustrated in Fig. 6.2, for real-time filtering application scenario, one of the signals to be convolved is often a long duration signal (e.g., infinitely long), acquired continuously in real-time, while the other signal is a known sequence of finite duration, referred to as the kernel. In the conventional DSP implementation, the incoming signal of interest is transformed into the frequency domain by computing the successive FFTs at the signal speed (i.e. in real time), the static (convolution filter) kernel is multiplied in the frequency domain, and then converted back to the time domain by another real-time FFT operation. Since the TM-SP approach proposed in this Thesis computes the incoming signal FTs efficiently and at ultra-high-speeds, the TM-SP based architecture could be useful in performing the real-time fast convolutional filtering at speeds that are beyond the potential of digital platforms. The proposed schematic is illustrated in Fig. 6.2. The time-mapped spectra of the incoming SUT is temporally modulated with the digitally generated Fourier transform of the kernel, within each temporal period, T_{R}. Once the FT of the static kernel is multiplied with the dynamic FT of the incoming SUT, the resulting waveform is further propagated through another

dispersive medium with same magnitude and opposite sign to perform inverse Fourier transform. The resulting output should give the convolution of the kernel with SUT.

6.2.3 Real-time spectral analysis of multiple frequency bands

As discussed in Section 5.2, the TM-SP design has enabled RT-SA of high-frequency pass-band waveforms, without dedicated down-conversion stages in the front end, by employing the band-pass sampling theory [AC2] . In this demonstration, real band-pass sampling has been employed, which translated the real double sided spectrum of the high-frequency waveforms to the base-band. However, the TM-SP concept in general can be applied to complex temporal envelope sampling, see Section 2.1 and demonstration in Section 5.1. This feature implies that complex band-pass sampling [108] could also be employed with the TM-SP, enabling direct down-conversion RT-SA of high-frequency complex waveforms. Moreover, by properly choosing the sampling frequency, multiple bands of complex waveforms (e.g., single side-band waveforms) with different center frequencies could be simultaneously down-converted, thereby enabling multi-band RT-SA.

Associated Publications in Journals

[AJ1] S. R. Konatham, R. Maram, L. Romero Cortés *et al.*, "Real-time gap-free dynamic waveform spectral analysis with nanosecond resolutions through analog signal processing," Nature Communications **11**, 3309 (2020). [**Featured as one of the most relevant scientific achievements within Optics during 2020 by the OSA OPN magazine**].

[AJ2] S. R. Konatham, H. G. de Chatellus, and J. Azaña, "Photonics-based real-time spectrogram analysis of broadband waveforms," J. Lightwave Technol. **38**, 5356–5367 (2020). [**Invited**].

[AJ3] S. R. Konatham, R. Maram, L. R. Cortés *et al.*, "Ultra-high-speed time-frequency signal processing," Opt. Photon. News **31**, 37–37 (2020).

Associated Publications in International Conferences

[AC1] S. R. Konatham, R. Maram, and J. Azaña, "Real-time spectrogram analysis of continuous optical wavefields," in *2018 IEEE Photonics Conference (IPC)* (2018), 1–2. [**Post-deadline**].

[AC2] S. R. Konatham, L. R. Cortés, J. H. Chang *et al.*, "Downconversion-free real-time spectral analysis of high- frequency broadband waveforms," in *Conference on Lasers and Electro-Optics* (Optical Society of America, 2020), JW2C.3. [**OSA Incubic/Milton Chang Travel Award**].

[AC3] S. R. Konatham, B. Crockett, L. R. Cortés, and J. Azaña, "On-the-fly continuous time varying frequency filtering of broadband microwave signals," in *2019 European Conference on Optical Communication (ECOC)* (2019), 1–4.

[AC4] J. Azaña, S. R. Konatham, R. Maram, and H. G. de Chatellus, "Real-time analog time-frequency signal analysis," in *2019 IEEE Pacific Rim Conference on Communications, Computers and Signal Processing (PACRIM)* (2019), 1–6.

[AC5] S. Reddy, R. Maram, and J. Azaña, "On-the-fly time mapped full spectrogram analysis of high-speed non-stationary microwave signals," in *2018 European Conference on Optical Communication (ECOC)* (2018), 1–3.

[AC6] J. Azaña, S. R. Konatham, R. Maram, and H. G. d. Chatellus, "Photonics-based real-time 2d (time-frequency) broadband signal analysis and processing," in *2019 International Topical Meeting on Microwave Photonics (MWP)* (2019), 1–4. [**Invited**].

[AC7] S. R. Konatham, R. Maram, and J. Azaña, "Ghz-speed tracking of the frequency spectrum of complex continuous waveforms through photonic analog processing," in *OSA Advanced Photonics Congress (AP) 2019 (IPR, Networks, NOMA, SPPCom, PVLED)* (Optical Society of America, 2019), SpM3E.1. [**Best paper award: upgraded to invited**].

[AC8] S. R. Konatham, L. R. Cortés, J. H. Chang *et al.*, "Photonic-enabled real-time frequency-spectrum tracking of broadband microwave signals at a nanosecond scale," in *2020 Optical Fiber Communications Conference and Exhibition (OFC)* (2020), 1–3. [**Corning outstanding student paper finalist**].

[AC9] S. R. Konatham and J. Azaña, "Time-mapped spectrogram analysis with relaxed detection sampling rate," in *2019 IEEE Photonics Conference (IPC)* (2019), 1–2.

[AC10] S. R. Konatham, R. Maram, and J. Azana, "On-the-fly dynamic fourier transform analysis of non-stationary microwave signals," in *2019 Photonics North (PN)* (2019), 1–1.

Other Contributed Publications

[OC1] B. Crockett, L. Romero Cortés, S. R. Konatham, and J. Azaña, "Full recovery of ultrafast waveforms lost under noise," Nature Communications **12**, 2402 (2021). [**Editors highlight**].

[OC2] M. P. Fernández, L. R. Cortés, S. R. Konatham *et al.*, "Nonlinear time-lens with improved power efficiency through a discrete multilevel pump," Opt. Lett. **45**, 3557–3560 (2020).

[OC3] B. Crockett, L. R. Cortés, S. R. Konatham, and J. Azaña, "Phase preserving passive spectral enhancement of short optical pulses," in *OSA Advanced Photonics Congress 2021 (Signal Processing in Photonic Communication)* (Optical Society of America, 2021), SpF1E.5.

[OC4] B. Crockett, S. R. Konatham, and J. Azaña, "Asynchronous recovery of broadband signals corrupted by in-band noise," in *2021 IEEE Photonics Society Summer Topicals Meeting Series (SUM)* (2021), TuA3.1. [**Invited**].

[OC5] B. Crockett, L. R. Cortés, S. R. Konatham, and J. Azaña, "Real-time and single-shot recovery of arbitrary subnoise signals," in *2020 IEEE Photonics Society Summer Topicals Meeting Series (SUM)* (2020), 1–2.

[OC6] B. Crockett, L. R. Cortés, S. R. Konatham, and J. Azaña, "Single-shot subnoise signal recovery by coherent spectral energy redistribution," in *Conference on Lasers and Electro-Optics* (Optical Society of America, 2019), JW2A.71.

[OC7] B. Crockett, L. R. Cortes, S. R. Konatham, and J. Azana, "On-the-fly spectral noise mitigation through passive amplification and sampling," in *2019 Photonics North (PN)* (2019), 1–1.

Patent

[P1] J. Azaña, S. R. Konatham, R. Maram, , and H. G. De Chatellus, "Method and system for generating time-frequency representation of a continuous signal," US Patent App. 16/583,736.

References

[1] A. V. Oppenheim, A. S. Willsky, and S. Hamid, *Signals and Systems* (Prentice Hall, 1996), 2nd ed.

[2] A. V. Oppenheim and G. C. Verghese, *Signals, Systems and Inference*, Prentice Hall Signal Processing Series (Prentice Hall, 2015), 1st ed.

[3] J.-B.-J. Fourier, *Théorie Analytique de la Chaleur* (Paris: F. Didot, 1822).

[4] A. Domínguez, "Highlights in the history of the Fourier transform [retrospectroscope]," IEEE Pulse **7**, 53–61 (2016).

[5] R. Bracewell, "The Fourier transform," Scientific American 62–69 (1989).

[6] J. Gaskill, *Linear Systems, Fourier Transforms, and Optics* (Wiley, USA, 1978).

[7] R. Bracewell, *The Fourier Transform and Its Applications* (McGraw-Hill, USA, 1999).

[8] J. G. Proakis and D. G. Manolakis, *Digital signal processing : principles, algorithms, and applications*, Prentice Hall international editions (Prentice-Hall, 2006), 4th ed.

[9] A. V. Oppenheim and R. W. Schafer, *Discrete-Time Signal Processing* (Pearson Education, 2014), 3rd ed.

[10] J. G. Proakis and D. K. Manolakis, *Digital Signal Processing: Pearson New International Edition* (Pearson Education Limited, 2014), 4th ed.

[11] J. Cooley and J. Tukey, "An algorithm for the machine calculation of complex Fourier series," Mathematics of Computation **19**, 297–301 (1965).

[12] G. D. Bergland, "A guided tour of the fast Fourier transform," IEEE Spectrum **6**, 41–52 (1969).

[13] M. Heideman, D. Johnson, and C. Burrus, "Gauss and the history of the Fast Fourier Transform," IEEE ASSP Magazine **1**, 14–21 (1984).

[14] J. Cooley, P. Lewis, and P. Welch, "Historical notes on the Fast Fourier Transform," IEEE Transactions on Audio and Electroacoustics **15**, 76–79 (1967).

[15] J. G. Proakis and M. Salehi, *Digital communications*, McGraw-Hill higher education (McGraw-Hill, 2008), 5th ed.

[16] E. O. Brigham, *The Fast Fourier Transform* (Prentice Hall PTR, 1974).

[17] E. O. Brigham, *The Fast Fourier Transform and Its Applications* (Prentice-Hall, Inc., USA, 1988).

[18] H. J. Nussbaumer, *Fast Fourier Transform and Convolution Algorithms*, Springer Series in Information Sciences 2 (Springer-Verlag Berlin Heidelberg, 1982), 2nd ed.

[19] K. Rao, D. Kim, and J. Hwang, *Fast Fourier Transform - Algorithms and Applications*, Signals and Communication Technology (Springer Netherlands, 2010), 1st ed.

[20] D. Takahashi, *Fast Fourier Transform Algorithms for Parallel Computers*, High-Performance Computing Series 2 (Springer Singapore, 2019), 1st ed.

[21] E. Chu and A. George, *Inside the FFT Black Box: Serial and Parallel Fast Fourier Transform Algorithms*, Computational Mathematics (CRC Press, 1999), 1st ed.

[22] G. Strang, "Wavelets," American Scientist **82**, 250–255 (1994).

[23] J. M. Perkel, "Ten computer codes that transformed science," Nature **589**, 344–348 (2021).

[24] L. Cohen, "Time-frequency distributions-a review," Proceedings of the IEEE **77**, 941–981 (1989).

[25] L. Cohen, *Time frequency analysis: Theory and applications*, Prentice-Hall signal processing series (Prentice Hall PTR, 1995), 1st ed.

[26] L. R. Rabiner and R. W. Schafer, *Introduction to Digital Speech Processing (Foundations and Trends in Signal Processing)* (NOW, 2007).

[27] S. Qian and D. Chen, "Joint time-frequency analysis," IEEE Signal Processing Magazine **16**, 52–67 (1999).

[28] D. Gabor, "Theory of communication. part 1: The analysis of information," Journal of the Institution of Electrical Engineers - Part III: Radio and Communication Engineering **93**, 429–441(12) (1946).

[29] P. C. J. Hill, "Dennis Gabor - contributions to communication theory signal processing," in *EUROCON 2007 - The International Conference on "Computer as a Tool"* (2007), 2632–2637.

[30] B. Boashash, *Time-Frequency Signal Analysis and Processing (Second Edition)* (Academic Press, Oxford, 2016).

[31] P. Flandrin, M. Amin, S. McLaughlin, and B. Torrésani, "Time-frequency analysis and applications [from the guest editors]," IEEE Signal Processing Magazine **30**, 19–150 (2013).

[32] M. Daković, L. Stanković, and T. Thayaparan, *Time-frequency signal analysis with applications*, Artech House radar library. (Artech House, 2013).

[33] L. R. Rabiner and R. W. Schafer, *Theory and Applications of Digital Speech Processing* (Pearson, 2010), 1st ed.

[34] V. C. Chen and Hao Ling, "Joint time-frequency analysis for radar signal and image processing," IEEE Signal Processing Magazine **16**, 81–93 (1999).

[35] R. Trebino, *Frequency-Resolved Optical Gating: The Measurement of Ultrashort Laser Pulses* (Springer, USA, 2000).

[36] A. Weiner, *Ultrafast Optics* (Wiley Publishing, 2009).

[37] C. Dorrer and I. Kang, "Simultaneous temporal characterization of telecommunication optical pulses and modulators by use of spectrograms," Opt. Lett. **27**, 1315–1317 (2002).

[38] R. M. Monroe, "Gigahertz bandwidth and nanosecond timescales: New frontiers in radio astronomy through peak performance signal processing," Dissertation (Ph.D.), California Institute of Technology.

[39] B. P. Abbott and et al, "Observation of gravitational waves from a binary black hole merger," Phys. Rev. Lett. **116**, 061102 (2016).

[40] J. Allen, "Short term spectral analysis, synthesis, and modification by discrete Fourier transform," IEEE Transactions on Acoustics, Speech, and Signal Processing **25**, 235–238 (1977).

[41] J. B. Allen and L. R. Rabiner, "A unified approach to short-time Fourier analysis and synthesis," Proceedings of the IEEE **65**, 1558–1564 (1977).

[42] A. Papoulis, *Fourier integral and applications*, Classic Textbook Reissue Series (McGraw-Hill Companies, 1962), first edition ed.

[43] "Tektronix, "fundamentals of real-time spectrum analysis," 2020. [online]," https://www.tek.com/primer/fundamentals-real-time-spectrum-analysis.

[44] C. Dorrer and D. N. Maywar, "Rf spectrum analysis of optical signals using nonlinear optics," Journal of Lightwave Technology **22**, 266–274 (2004).

[45] M. Pelusi, F. Luan, T. D. Vo *et al.*, "Photonic-chip-based radio-frequency spectrum analyser with terahertz bandwidth," Nature Photonics **3**, 139–143 (2009).

[46] M. Ma, R. Adams, and L. R. Chen, "Integrated photonic chip enabled simultaneous multichannel wideband radio frequency spectrum analyzer," Journal of Lightwave Technology **35**, 2622–2628 (2017).

[47] P. Berger, Y. Attal, M. Schwarz *et al.*, "RF spectrum analyzer for pulsed signals: Ultrawide instantaneous bandwidth, high sensitivity, and high time-resolution," Journal of Lightwave Technology **34**, 4658–4663 (2016).

[48] D. J. Esman, V. Ataie, B. P. Kuo *et al.*, "Comb-assisted cyclostationary analysis of wideband rf signals," Journal of Lightwave Technology **35**, 3705–3712 (2017).

[49] M. Burla, X. Wang, M. Li, L. Chrostowski, and J. Azaña, "Wideband dynamic microwave frequency identification system using a low-power ultracompact silicon photonic chip," Nature Communications **7**, 13004 (2016).

[50] Tektronix, "Real-time spectrum analyzers RSA7100A/B, 2020. [online] available:," https://www.tek.com/spectrum-analyzer/rsa7100b-realtime-spectrum-analyzer.

[51] G. J. e. Golio M., *RF and Microwave Applications and Systems* (CRC, 2008), 1st ed.

[52] A. Mahjoubfar, D. V. Churkin, S. Barland *et al.*, "Time stretch and its applications," Nature Photonics **11**, 341–351 (2017).

[53] J. B.-Y. Cheng, Chi-Hao; Tsui, *Digital Techniques for Wideband Receivers*, IET Radar Sonar Navigation and Avionics Series (SciTech Publishing, 2016), 3rd ed.

[54] X. Zou, B. Lu, W. Pan *et al.*, "Photonics for microwave measurements," Laser & Photonics Reviews **10**, 711–734 (2016).

[55] M. A. Richards, *Fundamentals of Radar Signal Processing* (McGraw-Hill Education, 2014), 2nd ed.

[56] A. De Martino, *Introduction to modern EW systems*, Electronic warfare library (Artech House, 2018), second edition ed.

[57] H. Sun, A. Nallanathan, C. Wang, and Y. Chen, "Wideband spectrum sensing for cognitive radio networks: a survey," IEEE Wireless Communications **20**, 74–81 (2013).

[58] R. C. Nicholas D. Sidiropoulos, Fulvio Gini and S. T. (Eds.), *Communications and Radar Signal Processing*, Academic Press Library in Signal Processing 2 (Academic Press, 2014), 1st ed.

[59] D. C. Price, J. Kocz, M. Bailes, and L. J. Greenhill, "Introduction to the special issue on digital signal processing in radio astronomy," Journal of Astronomical Instrumentation **05**, 1602002 (2016).

[60] B. Murmann, "ADC performance survey 1997-2020, 2020. [online] available:," http://web.stanford.edu/murmann/adcsurvey.html.

[61] U. Meye-Baese, *Fourier Transforms, in Digital Signal Processing with Field Programmable Gate Arrays* (Springer Berlin Heidelberg, 2014).

[62] L. Liu and C. Calozand T. Itoh, "Dominant mode leaky-wave antenna with backfire-to-endfire scanning capability," Electronics Letters **38**, 1414–1416(2) (2002).

[63] S. Gupta, S. Abielmona, and C. Caloz, "Microwave analog real-time spectrum analyzer (rtsa) based on the spectral–spatial decomposition property of leaky-wave structures," IEEE Transactions on Microwave Theory and Techniques **57**, 2989–2999 (2009).

[64] J. Azana and M. A. Muriel, "Real-time optical spectrum analysis based on the time-space duality in chirped fiber gratings," IEEE Journal of Quantum Electronics **36**, 517–526 (2000).

[65] T. Jannson, "Real-time Fourier transformation in dispersive optical fibers," Opt. Lett. **8**, 232–234 (1983).

[66] M. A. Jack, P. M. Grant, and J. H. Collins, "The theory, design, and applications of surface acoustic wave Fourier-transform processors," Proceedings of the IEEE **68**, 450–468 (1980).

[67] J. D. Schwartz, J. Azana, and D. V. Plant, "Experimental demonstration of real-time spectrum analysis using dispersive microstrip," IEEE Microwave and Wireless Components Letters **16**, 215–217 (2006).

[68] G. A. Agrawal, *Nonlinear Fiber Optics* (Academic Press, 2013), 5th ed.

[69] D. R. Solli, J. Chou, and B. Jalali, "Amplified wavelength–time transformation for real-time spectroscopy," Nature Photonics **2**, 48–51 (2008).

[70] C. Zhang, X. Wei, M. E. Marhic, and K. K. Y. Wong, "Ultrafast and versatile spectroscopy by temporal Fourier transform," Scientific Reports **4**, 5351 (2014).

[71] M. H. Asghari, Y. Park, and J. Azaña, "Complex-field measurement of ultrafast dynamic optical waveforms based on real-time spectral interferometry," Opt. Express **18**, 16526–16538 (2010).

[72] T. Ahn, Y. Park, and J. Azaña, "Ultrarapid optical frequency-domain reflectometry based upon dispersion-induced time stretching: Principle and applications," IEEE Journal of Selected Topics in Quantum Electronics **18**, 148–165 (2012).

[73] K. Goda, K. K. Tsia, and B. Jalali, "Serial time-encoded amplified imaging for real-time observation of fast dynamic phenomena," Nature **458**, 1145–1149 (2009).

[74] J.-L. Wu, Y.-Q. Xu, J.-J. Xu *et al.*, "Ultrafast laser-scanning time-stretch imaging at visible wavelengths," Light: Science & Applications **6**, e16196–e16196 (2017).

[75] J. D. Schwartz, J. Azana, and D. V. Plant, "A fully electronic system for the time magnification of ultra-wideband signals," IEEE Transactions on Microwave Theory and Techniques **55**, 327–334 (2007).

[76] Y. Han and B. Jalali, "Photonic time-stretched analog-to-digital converter: fundamental concepts and practical considerations," Journal of Lightwave Technology **21**, 3085–3103 (2003).

[77] J. Zhang and J. Yao, "Time-stretched sampling of a fast microwave waveform based on the repetitive use of a linearly chirped fiber bragg grating in a dispersive loop," Optica **1**, 64–69 (2014).

[78] A. Dezfooliyan and A. M. Weiner, "Photonic synthesis of high fidelity microwave arbitrary waveforms using near field frequency to time mapping," Opt. Express **21**, 22974–22987 (2013).

[79] R. Salem, M. A. Foster, and A. L. Gaeta, "Application of space-time duality to ultrahigh-speed optical signal processing," Adv. Opt. Photon. **5**, 274–317 (2013).

[80] A. Nuruzzaman, O. Boyraz, and B. Jalali, "Time-stretched short-time Fourier transform," IEEE Transactions on Instrumentation and Measurement **55**, 598–602 (2006).

[81] A. Mahjoubfar, D. V. Churkin, S. Barland *et al.*, "Time stretch and its applications," Nature Photonics **11**, 341–351 (2017).

[82] S. Tainta, M. J. Erro, M. J. Garde, and M. A. Muriel, "Temporal self-imaging effect for periodically modulated trains of pulses," Opt. Express **22**, 15251–15266 (2014).

[83] Q. Xie and C. Shu, "Reconfigurable envelope generation of optical pulse train based on discrete Fourier transform," IEEE Photonics Technology Letters **30**, 242–245 (2018).

[84] H. G. de Chatellus, L. R. Cortés, and J. Azaña, "Optical real-time Fourier transformation with Kilohertz resolutions," Optica **3**, 1–8 (2016).

[85] J. Azana and M. Muriel, "Temporal self-imaging effects: theory and application for multiplying pulse repetition rates," IEEE Journal of Selected Topics in Quantum Electronics **7**, 728–744 (2001).

[86] R. E. Saperstein, D. Panasenko, and Y. Fainman, "Demonstration of a microwave spectrum analyzer based on time-domain optical processing in fiber," Opt. Lett. **29**, 501–503 (2004).

[87] P. Andrekson and M. Westlund, "Nonlinear optical fiber based high resolution all-optical waveform sampling," Laser & Photonics Reviews **1**, 231–248 (2007).

[88] A. L. Gaeta, M. Lipson, and T. J. Kippenberg, "Photonic-chip-based frequency combs," Nature Photonics **13**, 158–169 (2019).

[89] M. Burla, C. Hoessbacher, W. Heni *et al.*, "500 GHz plasmonic mach-zehnder modulator enabling sub-THz microwave photonics," APL Photonics **4**, 056106 (2019).

[90] R. Vaughan, N. Scott, and D. White, "The theory of bandpass sampling," IEEE Transactions on Signal Processing **39**, 1973–1984 (1991).

[91] G. herink, B. jalali, C. Ropers, and D. R. Solli, "Resolving the build-up of femtosecond mode-locking with single-shot specroscopy at 90 mhz frame rate," Nature Photonics **10**, 321–326 (2016).

[92] P. Ryczkowski, M. Närhi, C. Billet *et al.*, "Real-time full-field characterization of transient dissipative soliton dynamics in a mode-locked laser," Nature Photonics **12**, 221–227 (2018).

[93] C. Zhang, B. Li, and K. K.-Y. Wong, "Ultrafast spectroscopy based on temporal focusing and its applications," IEEE Journal of Selected Topics in Quantum Electronics **22**, 295–306 (2016).

[94] K. Goda, K. K. Tsia, and B. Jalali, "Serial time-encoded amplified imaging for real-time observation of fast dynamic phenomena," Nature **458**, 1145–1149 (2009).

[95] A. Yariv and P. Yeh, *Photonics: Optical Electronics in Modern Communications* (Oxford University Press, 2007), 6th ed.

[96] V. C. Chen, *Time-Frequency Transforms for Radar Imaging and Signal Analysis*, Artech House radar library (Artech House, 2002), 1st ed.

[97] S. Neemat, O. Krasnov, and A. Yarovoy, "An interference mitigation technique for FMCW radar using beat-frequencies interpolation in the STFT domain," IEEE Transactions on Microwave Theory and Techniques **67**, 1207–1220 (2019).

[98] S. Haykin, "Cognitive radio: Brain-empowered wireless communications," IEEE Journal on Selected Areas in Communications **23**, 201–220 (2005).

[99] S. Lach, M. Amin, and A. Lindsey, "Broadband interference excision for software-radio spread-spectrum communications using time-frequency distribution synthesis," IEEE Journal on Selected Areas in Communications **17**, 704–714 (1999).

[100] M. Amin, "Interference mitigation in spread spectrum communication systems using time-frequency distributions," IEEE Transactions on Signal Processing **45**, 90–101 (1997).

[101] S. Barbarossa and A. Scaglione, "Adaptive time-varying cancellation of wideband interferences in spread-spectrum communications based on time-frequency distributions," IEEE Transactions on Signal Processing **47**, 957–965 (1999).

[102] X. Ouyang and M. Amin, "Short-time Fourier transform receiver for nonstationary interference excision in direct sequence spread spectrum communications," IEEE Transactions on Signal Processing **49**, 851–863 (2001).

[103] C. Wang, M. Zhang, X. Chen *et al.*, "Integrated lithium niobate electro-optic modulators operating at CMOS-compatible voltages," Nature **562**, 101–104 (2018).

[104] C. V. Bennett and B. H. Kolner, "Upconversion time microscope demonstrating 103× magnification of femtosecond waveforms," Opt. Lett. **24**, 783–785 (1999).

[105] C. Bennett and B. Kolner, "Principles of parametric temporal imaging. i. system configurations," IEEE Journal of Quantum Electronics **36**, 430–437 (2000).

[106] J. Azaña and L. R. Chen, "General temporal self-imaging phenomena," J. Opt. Soc. Am. B **20**, 1447–1458 (2003).

[107] V. J. Hernandez, C. V. Bennett, B. D. Moran *et al.*, "104 MHz rate single-shot recording with subpicosecond resolution using temporal imaging," Opt. Express **21**, 196–203 (2013).

[108] J.-C. Liu, "Complex bandpass sampling and direct downconversion of multiband analytic signals," Signal Processing **90**, 504–512 (2010).

[109] R. E. Crochiere and L. R. Rabiner, *Multirate Digital Signal Processing* (Prentice-Hall, Inc., USA, 1983).

[110] P. P. Vaidyanathan, *Multirate Systems and Filter Banks* (Prentice-Hall, Inc., USA, 1993).

[111] P. Yao, H. Wu, B. Gao *et al.*, "Fully hardware-implemented memristor convolutional neural network," Nature **577**, 641–646 (2020).

[112] X. Xu, M. Tan, B. Corcoran *et al.*, "11 TOPS photonic convolutional accelerator for optical neural networks," Nature **589**, 44–51 (2021).

[113] H. Nyquist, "Certain topics in telegraph transmission theory," Transactions of the American Institute of Electrical Engineers **47**, 617–644 (1928).

[114] C. E. Shannon, "Communication in the presence of noise," Proceedings of the IRE **37**, 10–21 (1949).

[115] H. D. Luke, "The origins of the sampling theorem," IEEE Communications Magazine **37**, 106–108 (1999).

Appendix A

Temporal sampling and the Fourier transform

Temporal sampling of band-limited signals is a very useful and practical operation that we encounter often in signal analysis, such as in the process of discretization of a continuous-time waveform. Let us assume that a continuous-time signal $s(t_1)$ with band-limited FT, $S(\omega)$, with full a bandwidth $\Delta\omega_s$, is temporally sampled with a temporal periodic function of time $r_1(t_1)$. The Fourier spectral information in such a scenario renders extremely useful in formulating the so-called Nyquist-Shannon sampling theorem [1,113–115]. A simple case of temporal sampling is when a continuous-time signal $s(t_1)$ is multiplied with a temporal periodic impulse train with a temporal period of T_R.
The temporal periodic impulse train is represented as

$$r_1(t_1) = \sum_{-\infty}^{+\infty} \delta(t - nT_R), \tag{A.1}$$

and its FT can be obtained as

$$R_1(\omega) = \frac{2\pi}{T_R} \sum_{k=-\infty}^{+\infty} \delta(\omega - k\omega_R) \tag{A.2}$$

This is again a periodic impulse train in the frequency domain with a period $\omega_R = 2\pi/T_R$. The temporal impulse sampling of $s(t_1)$ with $r_1(t_1)$ can be mathematically expressed as follows:

$$s_{ip}(t_1) = s(t_1)r_1(t_1) = \sum_{n=-\infty}^{+\infty} s(nT_R)\delta(t - nT_R) = s(nT_R) \tag{A.3}$$

From the convolution theorem, multiplication of two signals in the time domain equals convolution of their FTs [1]. Then, the sampling operation in Eq.A.3 can be expressed in the Fourier domain as

$$S_{ip}(\omega) = S(\omega) * R_1(\omega) = \frac{1}{2\pi}\int_{n=-\infty}^{+\infty} S(\theta)R_1(\omega - \theta)\, d\theta \tag{A.4}$$

Here $*$ holds for the convolution operation. Substituting Eq.A.2 in the above equation Eq.A.4, and by using the shifting property of the FT: $S(\omega) * \delta(\omega - \omega_0) = S(\omega - \omega_0)$ [1], the impulse sampled spectrum $S_{ip}(\omega)$ can be expressed as

$$S_{ip}(\omega) = \frac{1}{T_{\mathrm{R}}}\sum_{k=-\infty}^{+\infty} S(\omega - k\omega_{\mathrm{R}}) \tag{A.5}$$

Convolution with a periodic impulse train simply shifts the signal spectrum to center at integer multiples of the sampling frequency $k\omega_R$. Thus, the sampled spectrum $S_{ip}(\omega)$ is a periodic function of ω consisting of a superposition of the replicas of the signal spectrum $S(\omega)$, spaced by $2\pi/T_{\mathrm{R}}$. The replicas of the signal spectrum $S(\omega)$ are spaced by the sampling frequency ω_{R}, and hence to avoid overlapping of the spectral replicas (aliasing), the sampling frequency ω_{R} must be greater than the full bandwidth of the signal spectrum $S(\omega)$, i.e.,

$$\omega_{\mathrm{R}} \geq \Delta\omega_s \tag{A.6}$$

This is the well-known Nyquist criterion for sampling band-limited continuous-time signals, and $\omega_{\mathrm{R}} = \Delta\omega_s$ is the Nyquist rate of sampling.

In practice, sampling pulses which approximate the ideal temporal impulses, as described in Eq.A.1, are relatively difficult to generate and transmit, and it is often more convenient to sample the temporal signal $s(t_1)$ using a train of pulses with finite duration, as illustrated in Fig.A.1. Let the temporal shape of the individual sampling pulses be $p(t_1)$, and its Fourier transform, $P(\omega)$.

Mathematically it is convenient to express the sampling pulse train $r(t_1)$ as a convolution of the individual pulse shape $p(t_1)$ with an impulse train, $r_1(t)$ from Eq.A.1, then

$$r(t_1) = p(t_1) * r_1(t_1) = \sum_{-\infty}^{+\infty} p(t_1 - nT_R) \tag{A.7}$$

From the convolution theorem, a time domain convolution is equivalent to a multiplication in the FT domain [1]. Then the FT of the sampling pulse train $r(t_1)$ can be obtained as

$$R(\omega) = P(\omega)R_1(\omega) = \frac{2\pi}{T_\mathrm{R}} \sum_{k=-\infty}^{+\infty} P(k\omega_\mathrm{R})\delta(\omega - k\omega_\mathrm{R}) \tag{A.8}$$

The sampled spectrum $R(\omega)$ is then composed by a discrete set of frequencies that are equally spaced by $\omega_\mathrm{R} = 2\pi/T_\mathrm{R}$, as shown in Fig.A.1(b). Note that $R(\omega)$ has finite spectral width that is dictated by the individual pulse spectrum $P(\omega)$.

The temporal sampling of $s(t_1)$ with the sampling pulse train $r(t_1)$ can be mathematically expressed as a temporal multiplication

$$s_{sp}(t_1) = s(t_1)r(t_1) = \sum_{n=-\infty}^{+\infty} s(nT_\mathrm{R})p(t_1 - nT_\mathrm{R}) \tag{A.9}$$

It is shown in Fig.A.1(c). Again, from the convolution theorem, multiplication of two signals in the time domain corresponds with a convolution of their FTs [1]. Then, the sampling operation in Eq.A.9 can be expressed in the Fourier domain as

$$S_{sp}(\omega) = S(\omega) * R(\omega) = \frac{1}{2\pi} \int_{n=-\infty}^{+\infty} S(\theta)R(\omega - \theta)\, d\theta \tag{A.10}$$

Substituting Eq.A.8 in the above equation Eq.A.10, the sampled spectrum $S_{sp}(\omega)$ can be expressed as

$$S_{sp}(\omega) = S(\omega) * R(\omega) = S(\omega) * (P(\omega)R_1(\omega)) = \frac{1}{T_\mathrm{R}} \sum_{k=-\infty}^{+\infty} P(k\omega_\mathrm{R})S(\omega - k\omega_\mathrm{R}) \tag{A.11}$$

Comparing the sampled spectrum $S_{sp}(\omega)$ from the above Eq.A.11 with the impulse sampled spectrum $S_{ip}(\omega)$ form Eq.A.5, we can observe that the impulse sampled spectrum is weighted by the sampling pulse spectrum $P(\omega)$, as a result of the finite sampling pulse duration.

We can uniquely reconstruct the original continuous-time signal $s(t_1)$ from the sampled version

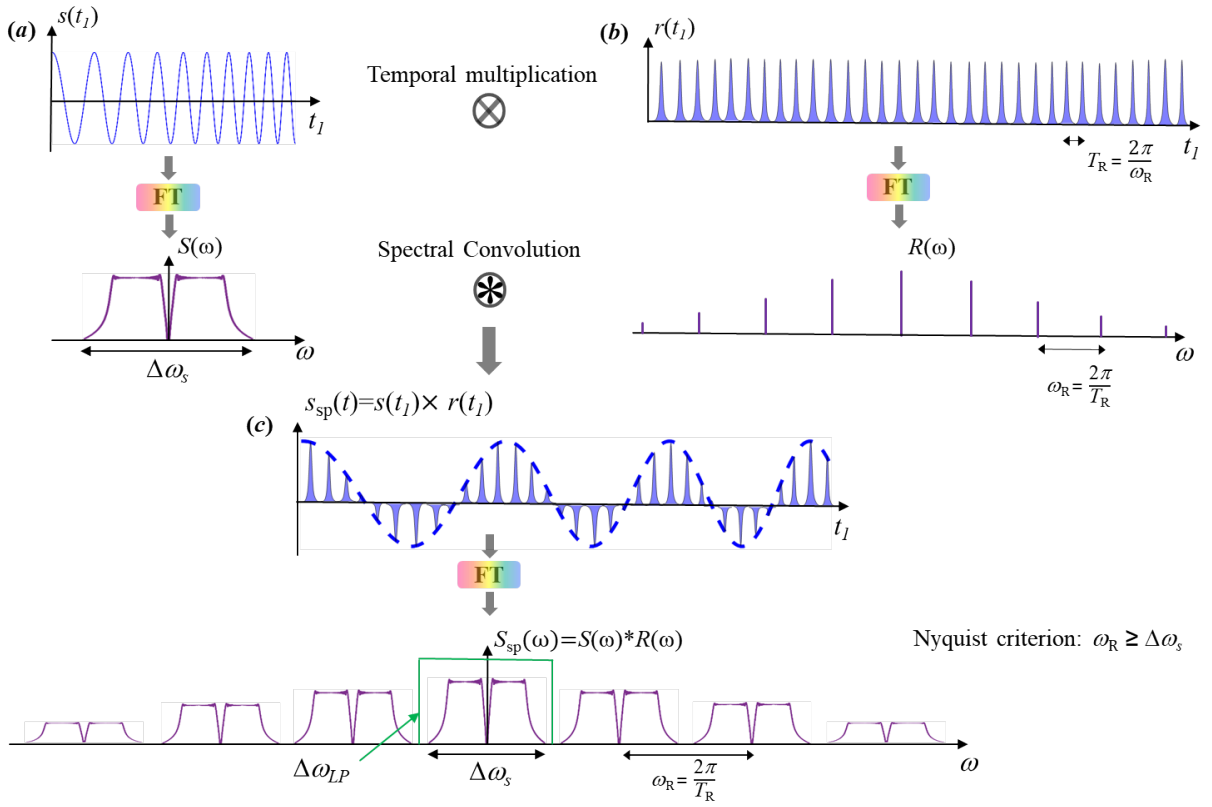

Fig. A.1: Sampling of a temporal signal and its Fourier spectrum. (a) A band limited signal and its Fourier transform. (b) Temporal sampling pulse and its Fourier transform. (c) The sampled signal in the time domain and its Fourier transform in the frequency domain.

$s_{sp}(t_1)$, by processing it through an ideal low-pass filter having a full bandwidth $\Delta\omega_{LP}$. For unambiguous reconstruction of the original $s(t_1)$, $\Delta\omega_{LP}$ must be wide enough to include the full signal bandwidth, $\Delta\omega_s$ ($\Delta\omega_{LP} > \Delta\omega_s$) and must be narrower than the Nyquist rate, ω_R ($\Delta\omega_{LP} < \omega_R$). This is very important and elegant result in the sampling of continuous-time signals, and is very useful in converting analog signals to the digital domain [28, 113, 114].

Appendix B

Time-mapped Fourier transform (TM-FT)

Let the temporal signal under test (SUT) be generally expressed as (analytical function) $a_1(t_1) = \hat{a_1}(t_1)e^{i\omega_0 t_1}$, where $\hat{a_1}(t_1)$ is the signal's complex temporal envelope, t_1 stands for the time variable (system input),ω_0 is the signal's carrier frequency ($\omega_0 = 0$ for a base-band signal). The SUT is assumed to be band-limited with a full frequency bandwidth denoted by $\Delta\omega_s$. To understand the operation of the TM-FT, dispersive media in the linear regime can be characterized as a linear transfer function [64]

$$H(\omega) = |H(\omega)|e^{-i\phi(\omega)} \tag{B.1}$$

In general, it is practical and convenient to model the dispersive media as an all-pass filter whose transfer function has constant magnitude $H(\omega) = H_0$ and quadratic phase response (linear group delay) over the spectral bandwidth of the incoming waveform, $a_1(t_1)$. Then, the transfer function for complex envelope $\hat{H(\omega')} = H(\omega_0 + \omega')$, over the pulse bandwidth, can be expressed as

$$\hat{H(\omega)} = H(\omega_0 + \omega') = H_0 e^{-i\phi_0} e^{-i\dot{\phi_0}\omega'} e^{-i\ddot{\phi_0}\omega'^2} \tag{B.2}$$

after taylor series expansion of the phase function, $\phi(\omega)$, around ω_0. Here, $\phi_0 = \phi(\omega_0)$, $\dot{\phi_0} = \partial\phi/\partial\omega|_{\omega=\omega_0}$, and $\ddot{\phi_0} = \partial^2\phi/\partial\omega^2|_{\omega=\omega_0}$. The impulse response $\hat{h(t)}$ can be obtained by taking the

inverse Fourier transform of $\hat{H(\omega)}$

$$\hat{h(t_2)} = h_t e^{i{t_2}^2/2\ddot{\phi_0}} \tag{B.3}$$

where, $t_2 = t_1 - \dot{\phi_0}$, and $h_t = H_0 e^{-i\phi_0}(1/\sqrt{i2\pi\ddot{\phi_0}})$. Here, the constant, $\dot{\phi_0}$ is the average delay (group delay), and the constant, $\ddot{\phi_0}$ is first order dispersion coefficient, responsible for waveform distortion.

From the linear system theory, the complex envelope at the output $\hat{a_2(t_2)}$ is expressed as the convolution of complex envelope at the input, $\hat{a_1(t_1)}$ and the impulse response of the dispersive medium, $\hat{h(t_2)}$.

$$\hat{a_2(t_2)} = h_t \int_{-\infty}^{\infty} \hat{a_1(t')} e^{i\frac{(t_2-t')^2}{2\ddot{\phi_0}}} dt' = h_t e^{i{t_2}^2/2\ddot{\phi_0}} \int_{-\infty}^{\infty} \hat{a_1(t')} e^{i{t'}^2/2\ddot{\phi_0}} e^{-it_2t'/\ddot{\phi_0}} dt' \tag{B.4}$$

If $\hat{a_1(t_1)}$ has temporal duration, Δt_s, and the dispersion coefficient $\ddot{\phi_0}$ is sufficiently large, so that

$$\frac{{\Delta t_s}^2}{2\pi\ddot{\phi_0}} \ll 1 \tag{B.5}$$

then the phase factor $\frac{{t'}^2}{2\ddot{\phi_0}} \leq \frac{{\Delta t_s}^2}{2\ddot{\phi_0}}$ is negligible in the Eq.B.4 and can be expressed as

$$\hat{a_2(t_2)} = h_t e^{i{t_2}^2/2\ddot{\phi_0}} \int_{-\infty}^{\infty} \hat{a_1(t')} e^{-it_2t'/\ddot{\phi_0}} dt' = h_t e^{i{t_2}^2/2\ddot{\phi_0}} FT(\hat{a_1(t_1)})_{\omega=t_2/\ddot{\phi_0}} \tag{B.6}$$

where FT stands for Fourier transform. Hence, under the condition in Eq.B.5, i.e., dispersion coefficient $\ddot{\phi_0}_{\text{TM-FT}} = \ddot{\phi_0}$ is much larger than the square of the input temporal waveform duration, Δt_s, the output temporal envelope, within a phase factor, is proportional to the FT of the input waveform, evaluated at angular frequencies $\omega = t_2/\ddot{\phi_0}$. The additional phase factor in Eq.B.6 distorts the phase of the output waveform, hence it is important to note that only magnitude of the FT of input waveform is recovered. The average ouput power, $P_2(t_2) = |\hat{a_2(t_2)}|^2$ is then proportional to the energy density spectrum (squared magnitude of the signal Fourier transform) of the input complex envelope $\hat{a_1(t_1)}$. The Eq.B.5 is a time domain equivalent of the spatial Fraunhofer condition, within a more general time-space duality framework that establishes the equivalence between free-space Fresnel diffraction of monochromatic wave and narrow-band dispersion of temporal wave in first-order dispersion [64].

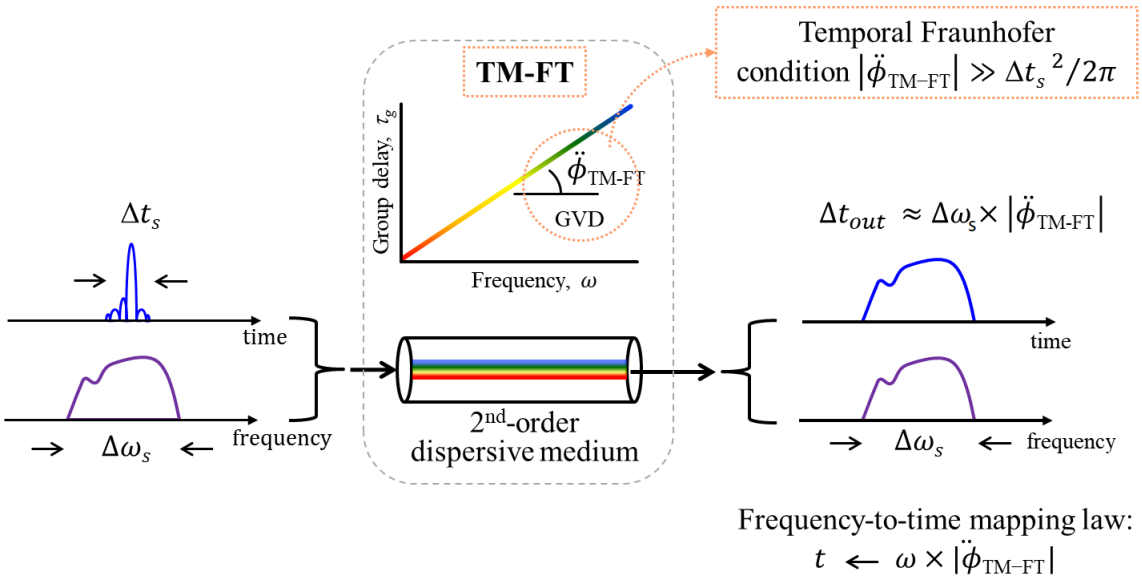

Fig. B.1: The concept of Time-mapped Fourier transform (TM-FT). The TM-FT is based on the use of linear chromatic (or group-velocity) dispersion to directly map the incoming wave spectrum along the output time axis (frequency-to-time mapping).

The concept of the TM-FT is illustrated through an example input SUT in Fig. B.1. The energy density spectrum of the input pulse is mapped along the output temporal domain, with a frequency-to-time mapping law discussed above. In Fig. B.1, the mapped energy density spectrum occupies a temporal duration, $\Delta t_{out} = \Delta\omega_s \times |\ddot{\phi}_{\text{TM-FT}}|$, much longer than the duration of the SUT at the input, Δt_s.